The Formation of New Asphaltenes during Visbreaking of Vacuum Residue Deasphalted Oil and the Storage Stability of Product from Visbreaking

by

Yuwei Yan

A thesis submitted in partial fulfillment of the requirements for the degree of

Master of Science

in

Chemical Engineering

Department of Chemical and Materials Engineering University of Alberta

Abstract

Mild thermal cracking by visbreaking emerged as an important partial upgrading technology for reducing the viscosity of Canadian oilsands bitumen to enable pipeline transport. Under typical visbreaking conditions, the conversion of bitumen is described by first-order kinetics, which forms the basis of the equivalent residence time (ERT) concept. The implication of this description is that various reaction temperature and residence time combinations can be selected that result in the same conversion. The objective of this study was to investigate if different process conditions that result in the same conversion, would also lead to the same amount of *n*-pentane insoluble material (asphaltenes) with the same properties in the final product. This study employed vacuum residue deasphalted oil (VR DAO) that was obtained from an industrial bitumen upgrader as feed material. During thermal conversion in the temperature range 417–438 °C at different residence times, new asphaltenes were formed. The kinetics of vacuum residue conversion was different compared to the kinetic of asphaltenes formation, which implied that visbreaker design based on equivalent residence time did not account for all of the important product characteristics. This was an important contribution, since visbreakers are usually designed using equivalent residence time. Based on the analysis of asphaltenes fraction before and after reaction, there was evidence that asphaltenes were participating in hydrogen transfer reactions. The visbroken product was found to be reactive during storage and after 210 days of storage under nitrogen, the amount of asphaltenes in visbroken product increased by 9 wt%. This observation led to a systematic study to determine how the visbroken product changed over time. A fresh visbroken product was prepared, which was characterized after reaction and then after 2, 4, 8, and 12 weeks storage under nitrogen. The nature of hydrogen transfer during storage was also evaluated. It was found that as the storage time increased, density, viscosity, asphaltenes content, refractive index, H:C of the asphaltenes, and the micro carbon residue all increased.

Keywords: Visbreaking, equivalent resident time (ERT), storage stability, asphaltenes

Preface

Part of the research work in this thesis were performed in collaboration, led by Dr. Glaucia Helena Carvalho do Prado at the University of Alberta. The data analysis in chapter 3 and chapter 4 were performed with the assistance of Khally Banh. The data analysis in chapter 5 are my original work, as well as the literature review in chapter 2.

Chapter 3 of this thesis has been published as Yan, Y., De Klerk, A & Prado, G.H. (2019). Visbreaking of vacuum residue deasphalted oil: new asphaltenes formation. Energy & Fuels. I was responsible for the data collection and analysis as well as the manuscript composition. Glaucia Helena Carvalho do Prado was the author and she was involved with concept formation and manuscript composition.

Dedication

To my mom, dad and uncle for all their support and love.

Acknowledgements

First, I would like to thank Dr. Arno de Klerk for giving me the opportunity to join his research group. During these two years I learned a lot from him. His patience and encouragement help me become more confident than before.

I would like also to thank Dr. Glaucia Carvalho Do Prado. This work would not have been done without her support, patience, and valuable advices.

I also want to thank my lab mates for their help and advices specially to Joy Tannous, Sowmya Turaga, Shruthi, Felipe, and Cibele. Special thanks to two of my best friends, Joanna He and Mushroom Xu for always been there when I need help and support.

Finally, I want to thank for the financial support from Nexen energy (now CNOOC International).

TABLE OF CONTENTS

LIST OF TABLES

LIST OF FIGURES

Introduction

1.1 Overview

Canada is the world leader in bitumen production, it has one of the largest oil reserves in the in the world. Around 90% of the reserves are oil sands. Bitumen present in oilsands is a type of heavy oil. Bitumen is a very heavy petroleum material; it has viscosity larger than 10^5 and density around 990 $kg \cdot m^{-3}$ [1]. It contains around 83 wt% of carbon, 10 wt% of hydrogen, 4.6 wt% of sulfur and 0.4 wt% of nitrogen [1].

Due to the poor fluidity and high viscosity of bitumen, transportation of the recovered bitumen by pipeline is nearly impossible. Therefore, dilution or treatment is required before the transportation. Visbreaking is one of the cheapest process that is used to reduce the viscosity of bitumen [2]. It is a mild thermal creaking process, which the main purpose is to decrease the viscosity of bitumen and therefore produce a material that can be transported by pipeline. It is conducted typically at 430 °C to 490 °C to avoid the formation of coke [3]. In industries, there are two types of visbreaking process available, one is coil visbreaking and the other is soaker visbreaking. Coil visbreaking is operated under high temperature (i.e. closer to 490 °C) with shorter residence time and soaker visbreaking is operated under low temperature (i.e. closer to 430 °C) with longer residence time [4].

In visbreaking, based on the equivalent residence time theory (ERT) [5], temperature and time combination can be varied to achieve the same conversion. In the BituMax™ process, *n*-pentane insoluble materials (asphaltenes) will be rejected first from the process to increase the stability of visbroken product and increase conversion of bitumen. However, it was observed that during visbreaking undesirable new asphaltenes was produced in the product. Therefore, it would be interest to investigate if process conditions that in principle lead to the same conversion, also lead to the same asphaltenes content in the visbroken product.

The stability of the visbroken product is one of the main limitations of visbreaking technology, both during reaction and after reaction. The storage stability usually refers to the resistance to changes in properties during long time storage. As it has been mentioned above, during visbreaking new asphaltenes were formed. The formation of new *n*-pentane insoluble material

will not only reduce the conversion that can be achieved by visbreaking, but it will also affect the storage stability of visbroken product.

From previous work it was known that bitumen has persistent free radicals and generally *n*-pentane insoluble materials has a higher content of free radicals [6]. Therefore, it would be valuable to investigate the changes of free radicals and other properties of visbroken product during long-time storage.

1.2 Objective

The objective of this study was to investigate if visbreaking conditions, which in principle would lead to the same conversion, would also result in the same *n*-pentane insoluble content. In addition, the changes in free radical concentration and other properties of visbroken product after reaction and during the storage will also be evaluated.

1.3 Scope of work

To understand the results and discuss the work, it is necessary to learn about and read the literature that relate to this study. Chapter 2 introduces the composition, and fundamental characteristics of bitumen, which is the feed material. This is followed by introducing the conversion processes, thermal conversion chemistry and analytical methods used for bitumen characterization. Chapter 3-5 are the experimental sections.

a) In Chapter 3 three visbreaking conditions were investigated (417 °C/30 min, 424.6 °C/20 min and 438 °C/10 min) and their corresponding heat up reaction (0 min). The selection of temperature and residence time was based on the equivalent residence time theory [5]. Based on the ERT theory, similar conversions and asphaltenes content were expected after the visbreaking at these conditions.
b) In Chapter 4, based on the results from Chapter 3 it has been found that the iso-conversion conditions as predicted by the ERT theory were not achieved. Therefore, the use of ERT concept before bitumen reach the set temperature (heating period) was evaluated. In addition, other factors that could result in different conversions were also evaluated and discussed.
c) In chapter 5, to investigate the storage stability of visbroken product, bitumen was reacted under 420 °C for 10 min. After the visbreaking reaction, the product was stored

for 12 weeks. Free radical content and other properties were determined shortly after the reaction, and then after 2 weeks, 4 weeks, 8 weeks and 12 weeks of storage.

At the end, all the investigations and results were concluded and presented in Chapter 6. More work that could be done in the future was discussed in section 6.3.

Reference cited

[1] Gray, M. R. (2015). *Upgrading oilsands bitumen and heavy oil*. Edmonton, Alberta: Pica Pica Press.

[2] Speight, J. G. (2007). *The chemistry and technology of petroleum*. Boca Raton: CRC Press/Taylor & Francis.

[3] Speight, J. (2012). Visbreaking: A technology of the past and the future. *Scientia Iranica*, *19*(3), 569–573.

[4] Gary, J. H., Handwerk, G. E., & Kaiser, M. J. (2007). *Petroleum refining: technology and economics*, 5ed. Boca Raton: CRC Press.

[5] Yan, T. (1990). Characterization of visbreaker feeds. *Fuel*, *69*(8), 1062–1064.

[6] Zhang, N., Zhao, S., Sun, X., Xu, Z., & Xu, C. (2010). Storage Stability of the Visbreaking Product from Venezuela Heavy Oil. *Energy & Fuels*, *24*(7), 3970–3976.

2. Literature Review

2.1 Introduction

The literature review chapter is divided into four main topics. In the first topic, the characteristics and composition of oilsands bitumen are presented. Then, the chemistry related to thermal conversion of heavy oil in general are introduced and discussed. In the third part, visbreaking thermal conversion process is reviewed and in the last topic some analytical methods used for bitumen characterization are explained.

2.2 Canadian oil sands bitumen

Oil sands are complex multiphase systems that are composed of bitumen, fines, sand, colloids, clay, organics, salts, water, trace of gas and chemisorbed carboxylic acids [1]. The bitumen present in oilsands is a type of heavy oil. Bitumen is separated from oilsands by using hot water, since most of the oil sands readily break up when placed in hot water [1]. The easy separability of the bitumen from the sand can be attributed to the presence of a water film surrounding each sand grain and separating it from the bitumen [1]. In (Figure 2-1) it shows the schematic diagram of a hypothetical microstructure of Athabasca oil sands.

The conversion of bitumen into liquid fuels is harder compared to lighter oil processing. This is because of the lack of lower boiling material making it viscous and more heteroatom-rich in nature, which will be discussed in section 2.3.

However, as the world consumption of petroleum keeps on increasing, bitumen has become a valuable resource. Around 250 billion barrels of bitumen are estimated as reserve energy resource in the world. Canada is the world leader in bitumen production. Significant bitumen resources also occur in the United States, Angola, Nigeria, Kazakhstan, Madagascar and Indonesia [2]. In Canada, oil sands reserves can be found in the four westernmost provinces, including the northeastern corner of British Columbia, all of Alberta, southern Saskatchewan and southern Manitoba [1]. The Alberta Energy Resources Conservation Board (AERBC) estimates that the potential reserves of recoverable bitumen from the oilsands is 173 billion barrels based on current technology and prices [2]. Around 96 percent of bitumen deposits are located in Alberta [3]. In Alberta, bitumen is located in three different areas, including the Peace River, Cold Lake and Athabasca where Athabasca is

the largest one, covering around 46,800 km^2 [1].

The CNOOC Long Lake site is located at 40 km southeast of Fort McMurray in the Athabasca region [2]. This is pointed out specifically, because the raw material used in this investigation originated from that facility.

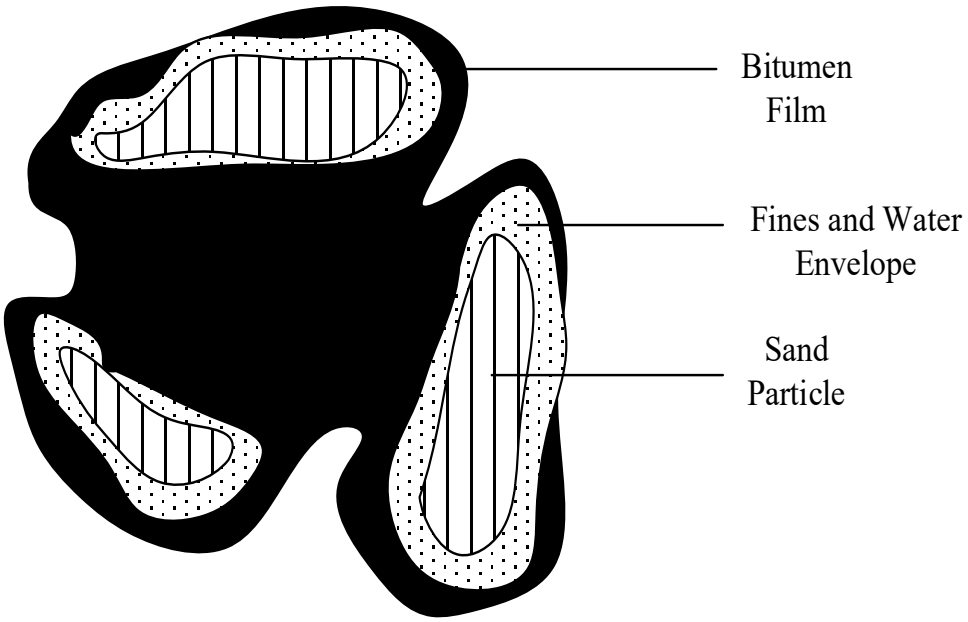

Figure 2-1. Hypothetical microstructure of Athabasca oil sands [1]

2.2.1 Bitumen Characterization

Bitumen is a very heavy petroleum material, it has a density of around 990 $kg \cdot m^{-3}$ and viscosity larger than 10^5 mPa·s at 25 °C (Table 2-1) [2]. It contains around 83 wt% of carbon, 10 wt% of hydrogen, 4.6 wt% of sulfur, and 0.4 wt% of nitrogen [2]. Most of the sulfur and nitrogen are present in bitumen in the form of different organic compounds such as thiophene and pyridine respectively [4, 5]. Bitumen also contains some trace metals like vanadium, nickel and iron. Nickel and vanadium are mainly present as porphyrins while other trace metals are present as inorganic mineral matter [2]. As an example, the main properties of Suncor coker feed bitumen are shown in in Table 2-1.

Density is one of the simplest properties to characterize bitumen and its conversion products. It is defined as mass per unit of volume of a substance [1, 2]. In SI units, density is measured in $kg \cdot m^{-3}$ and for bitumen, the numerical value of density depends on many different factors. In

general, increase in aromaticity, molecular weight, content of asphaltenes, sulfur, nitrogen, oxygen, vanadium and nickel, correlate with an increase in density of the bitumen and visbreaking product [1, 2]. As hydrogen content in bitumen increases the density of the material will decrease. Bitumen density is also temperature dependent, at constant pressure, its density decreased linearly with increasing temperature [6].

Table 2-1. General characterization data for Suncor coker feed bitumen [1].

Property	Historical data	
	Max	Min
Density ($g \cdot cm^{-3}$)	1.010	0.991
Viscosity (mPa·s)		
15 °C	371000	18000
25 °C	113000	6090
60 °C	1240	459
100 °C	119	72
Ramsbottom carbon residue (wt%)	12.7	10.1
Ash (wt%)	0.65	0.44
Carbon (wt%)	83.86	82.38
Hydrogen (wt %)	10.84	10
Nitrogen (wt%)	0.68	0.33
Sulfur (wt%)	4.98	4.43
Oxygen (wt%)	1.42	0.84
Vanadium (ppm wt)	200	151.1
Nickel (ppm wt)	87.2	49
Asphaltenes (wt%)	16.2	13.9

Density of bitumen is usually reported as specific gravity and/or American Petroleum Institute (API) gravity and they are calculated by equations 1 and 2 respectively [2].

$$SG = \frac{\rho_{oil}}{\rho_{water}} \quad (1)$$

$$API = \frac{141.5}{SG \text{ of oil at } 15.6°C} - 131.5 \quad (2)$$

Viscosity is defined as the frictional resistance of a fluid to flow under a constant shearing force. The dynamic viscosity (μ) is measured in SI units of mPa·s or in engineering units of centipoise (cP), where mPa·s = 1 cP [2]. Kinematic viscosity is defined as the ratio of dynamic viscosity and

density (μ/ρ) and it is measured in SI units of $mm^2 \cdot s^{-1}$ or in engineering units of centistokes (cSt), where 1 $mm^2 \cdot s^{-1}$ =1 cSt [2]. Viscosity is a very important property of bitumen. Since bitumen has very high viscosity, it first needs to be converted into a material of sufficiently low viscosity that can be pumped in a pipeline. Therefore, viscosity is widely used in estimation of transportation properties and other design calculations [1]. The value of bitumen viscosity is affected by the temperature, as temperature increases, its viscosity decreases [1]. Some examples are listed in Table 2-2 for different kinds of bitumen.

Table 2-2. Viscosities at atmospheric pressure for Athabasca and Cold Lake bitumens [2]

Athabasca		**Cold Lake**	
Temperature, °C	Viscosity, Pa·s	Temperature, °C	Viscosity, Pa·s
42.7	14.31	37.1	9.10
58.0	3.25	46.1	3.80
80.3	0.58	58.5	1.39
103.5	0.16	89.0	0.19
119.8	0.08	114.8	0.06

It was found that the viscosity of oil is affected by the amount of lighter material present (Figure 2-2) and the high viscosity of bitumen is at least partly due to the absence of lighter boiling material in raw bitumen. The bitumen from Athabasca and Cold Lake bitumen deposits has almost no material boiling below 250 °C, and only about 10 % boiling below 350 °C [1].

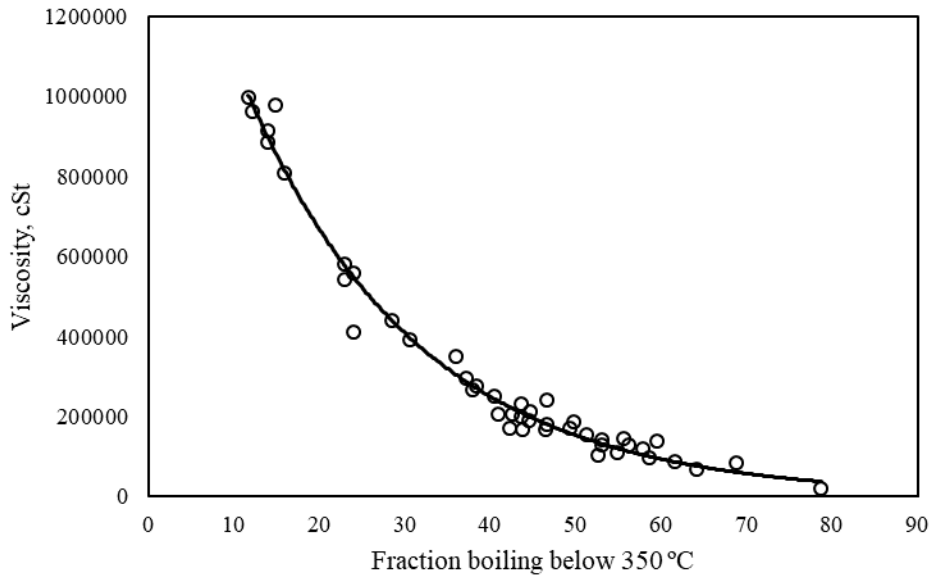

Figure 2-2. Dependence of viscosity on the wt% of the distillate boiling below 350 °C for asphaltic bitumen, heavy oils and crude oils from Canada, Venezuela, Russia, Africa and the Middle East [2]

Since bitumen is a very complex mixture, it contains thousands of different organic compounds, so it is very difficult to do the classification based on molecular level. Many classification procedures have been described in the literature. Here only solubility and boiling point classifications will be described, because both relate to this study.

One of the classifications often employed is SARA fraction, where bitumen is classified into four solubility fractions: saturates, aromatics, resins and asphaltenes [1]. These fractions do not represent chemical classes, for example, it would be incorrect to equate aromatics in SARA with the organic compound class aromatics. In Table 2-3 it shows the composition of each fraction of Alberta oil sand bitumen.

Table 2-3. Compositions of Alberta oilsands bitumen [1]

Name	Composition
Saturates	15-21%
Aromatics	18-19%
Resins	44-48%
C_5-Asphaltenes [a]	14-20%

[a] C_5-Asphaltenes is shorthand for asphaltenes obtained based on n-pentane insolubility.

Another way to classify bitumen is based on its boiling fractions. Commonly used terms for distillation fractions in refinery processing of crude oil are listed in Table 2-4 [2]. A crude oil is considered heavy when it contains a high content of vacuum residue.

As the content of light fractions increases, it becomes lighter and less viscous, as illustrated in Figure 2-2.

Table 2-4. Boiling ranges in refining and bitumen upgrading [2].

Name	Boiling Range, °C
Naphtha	26-193
Kerosene	165-271
Light gas oil (LGO)	215-321
Heavy gas oil (HGO)	321-426
Vacuum gas oil (VGO)	426-565
Vacuum residue (resid or residuum)	>524-565

2.2.2 Asphaltenes

Asphaltenes separated from bitumen is an amorphous, thermolabile, dark brown solid material. It does not have a sharp melting point and it can be separated from the bitumen by solvent precipitation, and therefore it is defined as a solubility class, i.e., it is species insoluble in paraffinic solvents and soluble in aromatic solvents [1]. Strictly speaking the classification also relies on liquid–solid separation, making the asphaltenes fraction dependent on its separation by filtration.

Asphaltenes have the least favorable composition of bitumen, since it has the highest metal, nitrogen, oxygen, sulfur, and ash contents, the highest molecular weight, and the lowest H/C ratios [1]. Some general characterizations for Athabasca asphaltene can be found in Table 2-5.

Table 2-5. General characterization data for Athabasca asphaltenes [1].

Property	Athabasca asphaltenes
Molecular weight [a]	3600
Elemental analysis (wt%)	
C	79.9
H	8.3
N	1.2
S	7.6
O	3.2
(H/C) molar ratio	1.24
Metal content ($\mu g \cdot g^{-1}$)	
Vanadium	630
Nickel	192

[a] Measured by vapor pressure osmometry (VPO)

The yield and composition of asphaltenes is dependent on the precipitant and precipitation conditions employed. It increases as the carbon number of the *n*-alkane solvent decrease from C_{10} to C_3 [1]. There are several different analytical procedures described in the literature that can determine the asphaltenes content of bitumen, such as UOP 614-68 [7], ASTM D4124 [8], and IP 143 [9].

Asphaltenes content in bitumen is commonly reported using insolubility in *n*-pentane. In Figure 2-3 the relationship between the volume of *n*-pentane: feedstock ratio and the asphaltenes yield is presented.

The amount of asphaltenes precipitated also depends on the contact time between the addition of the alkane solvent to the bitumen and the separation of the asphaltenes [10]. In Figure 2-4, as the contact time increases, the asphaltenes yield decreases rapidly and after 8 hours the yield of asphaltenes remain almost the same.

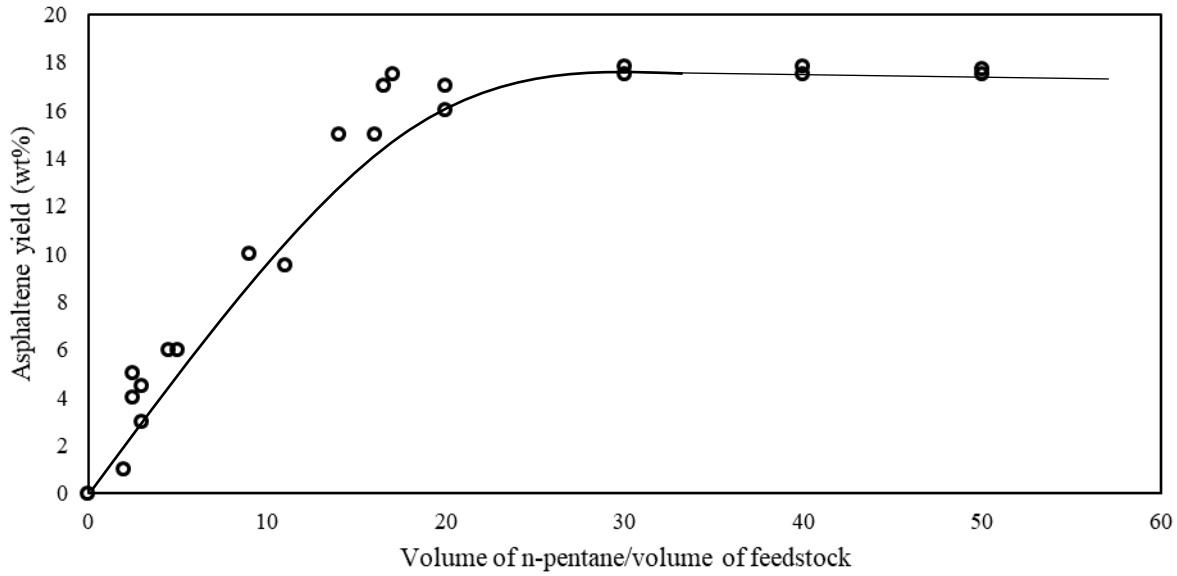

Figure 2-3. Relationship of asphaltenes yield to *n*-pentane/feedstock ratio. Time, 16 h, at 25 °C [10].

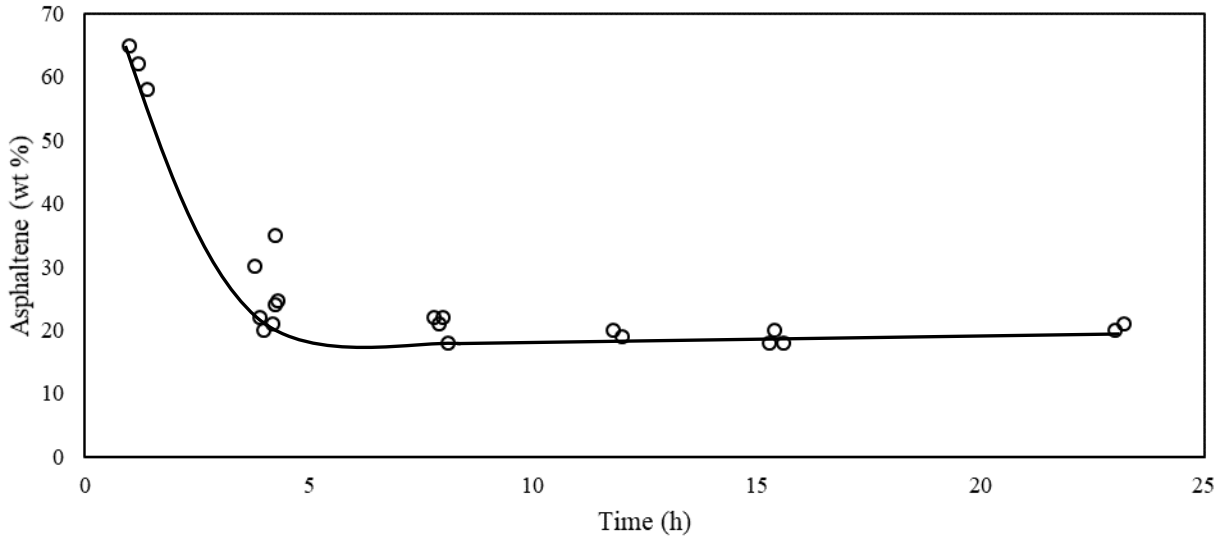

Figure 2-4. Relationship of asphaltenes yield to feedstock/paraffin contact time. T= 25 °C; 30-mL *n*-pentane·g^{-1} bitumen [10].

Oxygen in air can react with asphaltenes [1]. The rate of reaction is very slow but increases rapidly with increasing temperature. Some species in bitumen can also react with oxygen and be converted to asphaltenes, which causes an increase in asphaltenes content [1]. Oxidation is photo-sensitive

and both temperature and light will accelerate the oxidation reaction and conversion leading to an increase in the amount of asphaltenes [1]. This is pointed out, because the work presented in later chapters investigate the formation of new asphaltenes.

2.3 Thermal conversion chemistry

2.3.1 Free radicals

Species with unpaired electrons are referred to as free radicals. Based on their reactivity, free radicals can be classified as persistent radicals and transient radicals. Persistent free radicals appear to be unable to react with each other under the diffusion-controlled rate; however, they might be able to react over long period of time [11]. Transient radicals can react with each other under the controlled diffusion rate (usually under 1 μs) and termination reactions of free radicals can be by the combination of two radicals (equation 3) or by hydrogen disproportionation between two radicals (equation 4) [11].

$$R^{\bullet} + R^{\bullet} \rightarrow R - R \quad (3)$$

$$R^{\bullet} + H_2C^{\bullet} - CH_3 \rightarrow H_2C = CH_2 + RH \quad (4)$$

Based on previous sample report, Athabasca and Cold Lake bitumen contains more than 1×10^{17} spins·g^{-1} of persistent organic free radicals [12]. The concentration of the persistent organic free radicals in the asphaltenes fraction are relatively higher than in bitumen, the range is between 0.8-20×10^{18} spins·g^{-1} asphaltenes [2].

2.3.2 Free radical and hydrogen transfer reactions

Free radicals play an important role in thermal chemistry, because the first objective of any upgrading process is to break chemical bonds and giving lighter products. In this process, the thermal cracking follows free radical chemistry.

The elementary reaction steps and chain reactions can be illustrated by cracking of the *n*-alkanes [2]:

Initiation:

$$A \longrightarrow 2R\bullet$$

Example: $CH_3 - CH_2 - CH_3 \rightarrow CH_3 - CH_2^{\bullet} + CH_3^{\bullet}$

Propagation:

- Hydrogen abstraction:

$$R\bullet + A \longrightarrow RH + A\bullet$$

Example: $CH_3^{\bullet} + CH_3 - CH_2 - CH_3 \rightarrow CH_4 + CH_3 - CH_2 - CH_2^{\bullet}$

- β-Scission:

$$A\bullet \longrightarrow R\bullet + O$$

Example: $CH_3 - CH_2 - CH_2 - CH_3^{\bullet} \rightarrow CH_3 - CH_2^{\bullet} + CH_2 = CH_2$

Termination:

$$\text{Radical} + \text{Radical} \longrightarrow \text{Products}$$

Example: $CH_3 - CH_2^{\bullet} + CH_3 - CH_2^{\bullet} \rightarrow CH_3 - CH_2 - CH_2 - CH_3$

A and A• represent the parent alkane and the corresponding parent radicals, respectively. R• and RH are lower alkyl radicals and their corresponding alkanes and O represents the olefins [2]. Three possible termination reactions can be expected [2]:

$$R\bullet + R\bullet \longrightarrow \text{Product}$$

$$R\bullet + A\bullet \longrightarrow \text{Product}$$

$$A\bullet + A\bullet \longrightarrow \text{Product}$$

During the initial step, free radicals are formed by breaking the thermodynamically favorable bonds, such as carbon-carbon, carbon-hydrogen, and carbon-sulfur bonds. The bond energy indicates the difficulty level of the breakage [2]. However, as was noted before, bitumen already contains some free radicals and initiation is not a prerequisite for free radical reaction in bitumen to proceed.

In Table 2-6 it provides some information is provided about homolytic bond-dissociation energies.

Table 2-6. Homolytic bond-dissociation energies [2]

Chemical Bond	Energy, $kJ \cdot mol^{-1}$
C-C (aliphatic)	344±4
C-H (primary)	411±4
C-H (secondary)	398±4
C-H (aromatic)	464±8
C-S	307±8
C-N	342±8
C-O	344±4

Without catalyst, to break the C-C bonds of *n*-alkanes requires a temperature on the order of 420 °C to achieve the useful reaction rates. Carbon-carbon bonds (C-C) in aromatic compounds are much stronger and difficult to break due to the resonance stabilization energy. For example, it provides an extra 25 $kJ \cdot mol^{-1}$ to the C-C bonds in benzene. The aromatic C-C bond is unbreakable at the normal process conditions (T< 600 °C) unless it is first destroyed by hydrogenation [2].

Usually the most crucial step in a free radical reaction is the initial step, i.e. free radicals' formation [2]. In hydrogen abstraction step, once the free radical has been formed, hydrogen transfer reactions will take place in their surroundings to form the most stable radical species which for alkyl free radicals for example are in the following order: tertiary > secondary > primary [2].

In general, the hydrogen abstract reaction will form a more stable radical than the reacting radical species [13]. Under β-scission, when there are unsaturated species such as olefin, radical species can also expand by addition to the unsaturated bonds [13]. The addition reaction can produce species with higher molecular weight, so it is an undesired step during upgrading [13]. This is of relevance to this study, because it is possible that the formation of species with higher molecular weight will become paraffin insoluble.

The addition of hydrogen donor solvent is one of a special case of hydrogen transfer reaction. Hydrogen donor solvents are molecules that can donate more than one hydrogen during reactions and after donation it will turn into another molecule instead of becoming a free radical or olefin

[14]. In thermal cracking, a hydrogen donor can react with the free radicals formed during initiation and propagation steps and terminate the chain reaction by donating hydrogen through hydrogen transfer. For example, solvents such as tetralin can donate four hydrogens and after the donation it will be converted to naphthalene (Figure 2-5) [15]. On the other hand, hydrogen acceptor such as olefin or free radicals can abstract hydrogen from the hydrogen donor solvent.

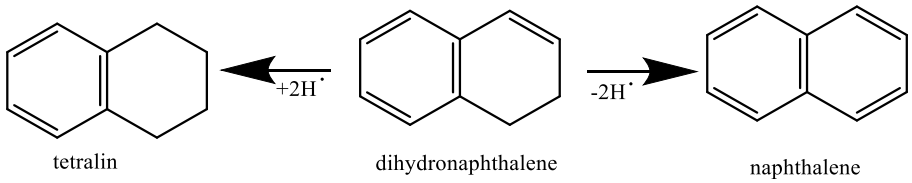

Figure 2-5. Dihydronaphthalene as hydrogen acceptor (left side reaction) and hydrogen donor (right side reaction) [14]

One thing that should be noted is that the above reactions are the simplified scheme of reactions. For bitumen and heavy oil, the overall reaction network is more complicated and there might be more reactions happening at the same time. On the other hand, different phases can also affect the overall reactions during thermal cracking [2]. In the liquid phase, the density of the reacting species is higher compared to the gas phase, so bimolecular reactions such as hydrogen transfer and radical addition reactions are favored over monomolecular reactions. However, in gas phase monomolecular reactions such as β-scission is favored during thermal cracking [2].

2.3.3 Coking

Coke is a carbonaceous solid material that can be formed during thermal conversion. This carbon-rich solid is toluene insoluble and it can be formed under certain conditions depending on temperature-time reaction combination. For process equipment such as heat exchangers, reactors, and columns, coke can accumulate and cause fouling of equipment [2]. In addition, as more coke is formed, the yield of desired liquid product decreases. Therefore, coke formation is undesirable in thermal conversion processes of bitumen.

Asphaltenes, based on solubility considerations, are coke precursors during thermal processes.

The coke formation mechanism is described by Wiehe [16]. Wiehe proposed a useful diagram (Figure 2-6) that describes coke formation based on the relationship between hydrogen content and molecular mass [16].

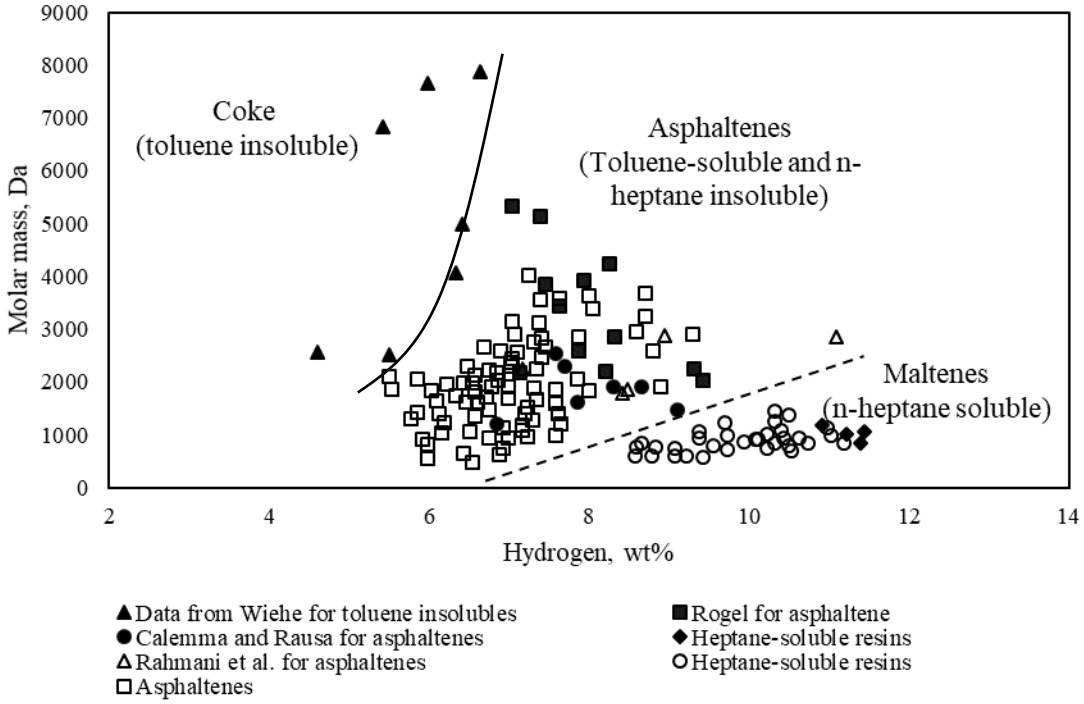

Figure 2-6. Phase diagram for residue fractions based on hydrogen content and molar mass measured by vapor pressure osmometry [16, 17, 18, 19, 20].

In this diagram, coke (toluene insoluble) has the lowest hydrogen content with highest molecular mass, i.e, the formation of coke is driven by molecules depleted of hydrogen and/or compounds of high molecular mass. High molecular mass compounds are formed during thermal conversion due to different kind of reactions, including free radical combination. These high molecular mass compounds are then phase separated from the bulk oil resulting in undesirable coke.

2.4 Visbreaking

Thermal conversion of bitumen can be achieved by using different processes, which may or may not form coke. Delayed coking is an example of thermal process that is designed to form coke, while visbreaking is an example of thermal process that is designed to operate without forming

coke. In practice, the formation of some coke during visbreaking cannot be prevented and from time to time visbreaking units must be decoked.

The process of interest in this study is visbreaking and visbreaking will be the focus of this section.

2.4.1. Visbreaking processes

Visbreaking is a mild thermal creaking process, which the main purpose is to decrease the viscosity of bitumen and therefore produce a material that can be pumped in a pipeline in order to be transported to refineries [2]. Even though this process improves the viscosity of the feed without attempting significant conversion of the vacuum residue into light fractions, it is desirable to achieve the highest conversion as possible.

There are two types of visbreaking processes that are available in industries, one is coil visbreaking and the other is soaker visbreaking. The operating condition for coil type (Figure 2-7) is high temperature with low residence time. In coil visbreaking, decoking is performed by using steam-air decoking [21].

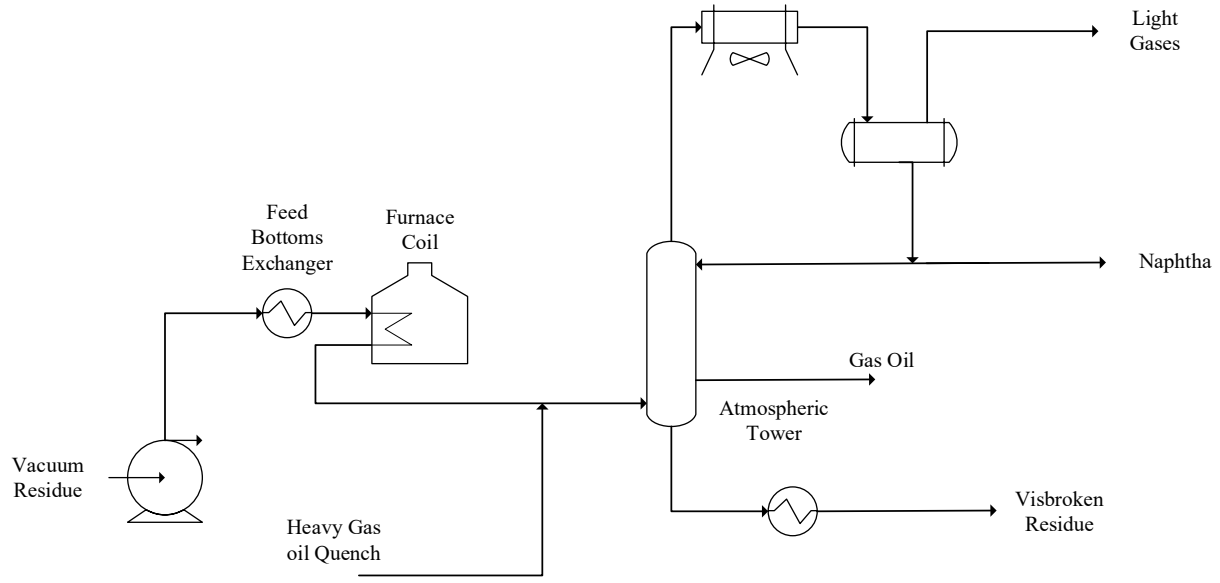

Figure 2-7. Coil type visbreaker [22].

Soaker visbreaking (Figure 2-8), is performed at low temperature with longer residence time. Most of the conversion happens in the reaction vessel or the soaker. Only some of the conversion

happens in the heater. The soaker type visbreaking allows the heater to operate at a lower outlet temperature, which requires less fuel to operate. However, decoking is more involved, since both coil and soaker must be decoked [21].

In theory, the product quality and yield should be the same regardless the type of visbreaking that has been used [21].

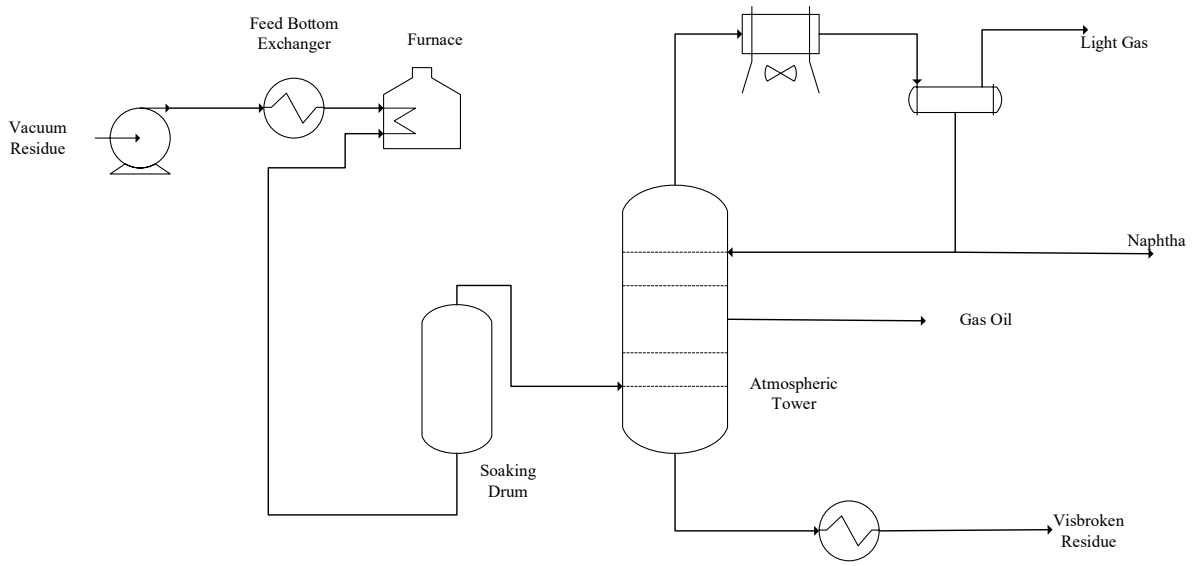

Figure 2-8. Soaker type visbreaker [22].

Visbreaking is used by CNOOC International as part of the oil upgrading technology in their BituMax^{TM} partial upgrading process (Figure 2-9).

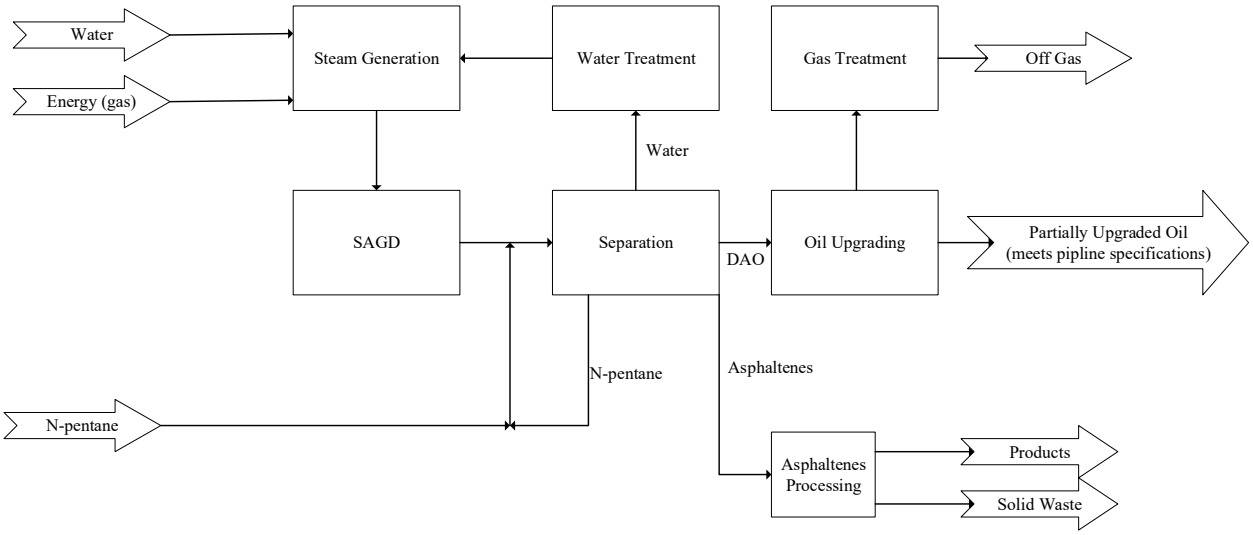

Figure 2-9. Block flow diagram of the BituMax^{TM} partial upgrading process.

In this process solvent deasphalting of the bitumen feed is performed before thermal cracking of the vacuum residue fraction by visbreaking. By removing asphaltenes prior to visbreaking, higher conversion is possible. The stability of the liquid products from visbreaking process is the main limitation for cracking bitumen and heavy oil. This stability refers to stability of the mixture to phase separation during visbreaking. On the other hand, during the storage of visbreaking product, stability refers to their resistance to changes in properties upon long time period storage [2].

Generally, as the amount of asphaltenes in the feed increases the maximum conversion before onset of coking will decrease, so the ability to maintain the asphaltenes in suspension is used to test the visbreaking product to make sure the feed is not overly cracked [2].

In the BituMax^{TM} process, solvent deasphalting is performed before visbreaking. The feed to the visbreaking process is vacuum residue deasphalted oil, which would produce a more stable product at the same conversion as a visbreaking process operated without prior deasphalting.

However, it was observed that there was an increase in asphaltenes content during visbreaking [23]. The formation of new asphaltenes is detrimental, because it deteriorates product stability and thereby reduces the maximum conversion that can be achieved by visbreaking before onset of coking.

2.4.2. Kinetics of thermal conversion by visbreaking

The description of thermal conversion during visbreaking usually makes use of the equivalent residence time (ERT) concept, which describes conversion in terms of a first order reaction [23]. The first order reaction can be represented as equation 5.

$$(-\mathrm{r_A}) = k_A C_A \tag{5}$$

In equation 5, C_A, ($mol \cdot m^{-3}$) is the concentration of reactant and k_A, (h^{-1}) is the reaction rate constant of the reactant. The reaction rate constant k_A can be expressed in the form of the Arrhenius equation (equation 6) [24].

$$k_A = Ae^{\frac{-E_a}{RT}} \tag{6}$$

In equation 6, A represents the pre-exponential factor, R, ($J \cdot \mathrm{mol}^{-1} \cdot \mathrm{K}^{-1}$) is the ideal gas constant, and E_a, ($J \cdot \mathrm{mol}^{-1}$) is the activation energy, and T, (K) is the reaction temperature.

The implication of the equivalent residence time is that various reaction temperature and residence time combinations can be selected that result in the same conversion [25] where equivalent residence time can be calculated by equation 7 [25].

$$t_{ERT} = residence\ \ time \times \exp\left(-\frac{E_a}{R}\right) \times \left(\frac{1}{T} - \frac{1}{T_{temperature\ at\ ERT}}\right) \tag{7}$$

This approach has been used to describe conversion and product formation during visbreaking in models of varying complexity. In this study the ERT description was employed in the description and comparison of visbreaking experiments at different conditions.

2.5 Analytical methods used for bitumen characterization

This section will introduce and explain some analytical methods or equipment that was used in this research study.

2.5.1. Electron Spin Resonance (ESR)

One of the techniques to quantify the presence of free radicals in a material is the electron spin resonance (ESR) [26]. In this technique, electrons and nuclei are charged particles under magnetic moments and they produce its own magnetic field [27].

For a paired electron, the net magnetic moment produced by two electrons will be cancelled out. For a single unpaired electron, there are only two allowed energy states, one is ms=+1/2 and the other is ms=-1/2 [26]. Since electrons and nuclei are charged particles with their own magnetic moments, they also produce their own magnetic field [27].

In an ESR spectrometer, samples are exposed to a magnetic and microwave field. In samples that might contain free radicals, the unpaired electrons will line up with the magnetic field and absorb energy, thus it will elevate free radicals to higher energy level [27]. The energy difference between the ms=+1/2 and ms=-1/2 spin states is determined by the nature of the free radical species and the magnetic field that is applied. If the energy of the microwave ($\Delta E = h\nu$) corresponds to the energy difference in spin states, it can be absorbed to change the spin state. The absorption of microwave energy can be measured, and it is proportional to the free radical concentration in the sample.

The ESR signal is usually represented as the first derivative of the absorption of microwave energy with change in magnetic field at constant microwave frequency. The amount of energy absorbed is the area under the curve of absorption plotted versus change in magnetic field. The area can be found by performing the double integration of the first derivative spectrum within a defined magnetic field scan range. For quantitative analysis, the signal intensity will be used to determine the number of spins in the sample [26].

2.5.2 Proton nuclear magnetic resonance (^{1}H-NMR)

Proton Nuclear Magnetic Resonance (^{1}H-NMR) spectroscopy is a very useful technique for identifying and analyzing organic compounds. Like the ESR, ^{1}H-NMR relates the atomic response to the magnetic fields and generated magnetic signal [28]. It provides information about the number of protons (^{1}H) in the molecule and it can also be used to determine the amount of protons in different chemical environments. The spectrum can therefore be used to determine the relative

amounts of aliphatic, olefinic and aromatic protons. Therefore, this technique has been used frequently on petroleum product to measure the distribution of hydrogen that attach to the aliphatic and aromatic carbon [28].

Some general regions can be found in ^{1}H NMR spectra. The region between 0.4 to 4 ppm corresponds to the aliphatic hydrogen region while the region between 6 and 9 ppm is associated with aromatic hydrogen [28]. In the aliphatic region, the peak between 0.4 to 1.1 ppm corresponds to the methyl hydrogens from alkanes [28]. Secondary hydrocarbons can be found around 1.3 ppm and peak for tertiary hydrocarbons is between 1.5 to 1.6 ppm [28]. Chemical shifts of some characteristic functional groups can be found in Table 2-7.

Table 2-7. ^{1}H-NMR chemical shifts of some characteristic functional groups [28]

Functional Group	Abbreviations	Chemical Shift
Cyclopropane		0.2
Primary hydrocarbons	R-CH3	0.9
Secondary hydrocarbons	R2Ch2	1.3
Tertiary hydrocarbons	R3CH	1.5-1.6
Allylic	-C=C-CH3	1.7
Amine	R-NH2	1.0-5.0
Alcohol	R-OH	1.0-5.5
Carbonyl	-CO-CH-	2.0-2.7
Acetylene	-C≡CH-	2.0-3.0
Benzylic	Ar-CH-	2.2-3.0
I	-CH2-I	2.0-4.0
Br	-CH2-Br	2.5-4.0
Cl	-CH2-Cl	3.0-4.0
F	-CH2-F	4.0-4.5
Alcohol	-CH-OH	3.4-4.0
Ether	RO-CH-	3.3-4.0
Ester	RCOOCH-	3.7-4.1
Olefine	-C=CH-	4.5-6.5
Aromatic	Ar-H	6.0-8.5
Aldehyde	R-CHO	9.0-10.0
Acid	R-COOH	10.0-14.0

2.5.3 Elemental composition (CHNS)

Elemental composition is usually presented as the molar ratio of different elements to carbon such as: H/C, N/C, S/C and O/C [29]. Molar ratio between hydrogen and carbon content of the bitumen

is an important parameter that can provide information on the reactions happening during visbreaking [30].

For Canadian bitumen the H/C molar ratio is around 1.55±0.03 (Table 2-1) [2]. Deasphalted oil (DAO) has a H/C molar ratio around 1.4. The value of the crude oil usually increases as its hydrogen to carbon molar ratio, increases [2]. This value can also be an indication of the aromaticity of a sample, i.e., the lower the hydrogen to carbon ratio, the higher the aromaticity [31].

2.5.4 Refractive Index

Refractive index (RI) is the ratio of the velocity of the light in vacuum compared to the given medium. In general, paraffinic compounds have low RI while aromatic compounds have high RI values [32]. With the similar molecular weight, RI value increases in the following order: paraffin, naphthenic and aromatic. Based on this order the RI value can be used to determine the aromaticity of the bitumen before and after visbreaking [33].

2.5.5 Coke forming tendency

The coke-forming tendency of a process stream is an important parameter for upgrading. This analysis is performed by pyrolyzing the sample under controlled conditions without the presence of oxygen [2]. The amount of solid residue is calculated by dividing the final weight of the pyrolyzed sample by the initial sample weight. This value indicates the tendency of coke formation during thermal conversion.

Conradson carbon residue (CCR), Ramsbottom carbon residue (RCR) and micro carbon residue (MCR) are three commonly used methods to determine the coke forming tendency [2]. These methods employ a similar concept but are different in the detail of equipment and heating conditions. The MCR determination (ASTM D4530) [34], which is the method employed in this study, has become an often employed standard method since it uses a semi-automatic analyzer and only requires small amount of sample [2].

For whole Athabasca bitumen in the absence of any diluent, the MCR value is around 13.6 wt%

[33]. Most of the species responsible for the MCR content is in the vacuum residue fraction (>524 °C), which has around 27.8 wt% MCR [35]. Therefore, the MCR value is usually proportional to the vacuum residue fraction.

The MCR does not correlate well with the *n*-pentane insoluble asphaltenes content, although the *n*-pentane insoluble fraction usually has higher MCR value than the other fractions [36].

Literature cited

[1] Strausz, O. P. (2003). *The chemistry of Alberta oil sands, bitumens and heavy oils*. Calgary: Alberta Energy Research Institute

[2] Gray, M. R. (2015). *Upgrading oilsands bitumen and heavy oil*. Edmonton, Alberta: Pica Pica Press.

[3] Oil sands facts and statistics. (2019). Retrieved October 28, 2019, from https://www.alberta.ca/oil-sands-facts-and-statistics.aspx#targetText=Reserves and production&targetText=Alberta's oil sands' proven reserves, 98, ST39, and ST53 reports.

[4] Hua, R., Wang, J., Kong, H., Liu, J., Lu, X., & Xu, G. (2004). Analysis of sulfur-containing compounds in crude oils by comprehensive two-dimensional gas chromatography with sulfur chemiluminescence detection. *Journal of Separation Science*, *27*(9), 691–698.

[5] Mirshamsi, S., Yan, Y., Kamal, S., Yasemi, A.-A., Gupta, R., De Klerk, A., & Prado, G. H. C. (2019). Thermal behaviour of nitrogen oxides relevant to oxidative denitrogenation. *The Journal of Chemical Thermodynamics*, *136*, 28–43.

[6] Kariznovi, M., Nourozieh, H., & Abedi, J. (2014). Measurement and correlation of viscosity and density for compressed Athabasca bitumen at temperatures up to 200ºC. *Journal of Canadian Petroleum Technology*, *53(06)*, 330–338.

[7] ASTM UOP614-68. (2003). *Heptane-insoluble matter in petroleum oils using a membrane filter.* West Conshohocken, PA: ASTM International.

[8] ASTM D4124. (2009). *Standard test method for separation of asphalt into four fractions.* West Conshohocken, PA: ASTM International.

[9] IP 143. (2016). *Determination of asphaltenes (heptane insoluble) in crude petroleum and petroleum products*. London, UK: Institute of Petroleum.

[10] Speight, J. G., Long, R. B., & Trowbridge, T. D. (1984). Factors influencing the separation of

asphaltenes from heavy petroleum feedstocks. *Fuel*, *63*(5), 616–620.

[11] Subramanian, H., Landais,Y., Sibi, M. P. (2014). *Radical addition reactions.* Comprehensive *organic synthesis*. Amsterdam: Elsevier.

[12] Schultz, K. F.; Selucky, M. L. (1981). ESR measurements on asphaltene and resin fractions from various separation methods. *Fuel, 60(10)*, 951-956.

[13] Kaiser, M. J., De Klerk, A., Gary, J. H., & Handwerk, G. E. (2020). *Petroleum refining: technology, economics, and markets*. Boca Raton: CRC Press,Taylor & Francis Group.

[14] Payan, F., & De Klerk, A. (2018). Hydrogen transfer in asphaltenes and bitumen at 250 °C. *Energy & Fuels*, *32*(9), 9340–9348.

[15] Choudhury, R., Bhaktavatsalam, A., & Singh, R. (1993). Desulfurization of various Indian coals by hydrogen donor solvent extraction. *Fuel*, *72*(5), 707–708.

[16] Wiehe, I. A. (1992). A solvent-resid phase diagram for tracking resid conversion. *Industrial & Engineering Chemistry Research*, *31*(2), 530–536.

[17] Rahmani, S., Mccaffrey, W. C., Dettman, H. D., & Gray, M. R. (2003). Coking kinetics of asphaltenes as a function of chemical structure. *Energy & Fuels*, *17*(4), 1048–1056.

[18] Gray, M. R. (2003). Consistency of asphaltene chemical structures with pyrolysis and coking behavior. *Energy & Fuels*, *17*(6), 1566–1569.

[19] Rogel, E. (1997). Theoretical estimation of the solubility parameter distributions of asphaltenes, resins, and oils from crude oils and related materials. *Energy & Fuels*, *11*(4), 920–925.

[20] Calemma, V., & Rausa, R. (1997). Thermal decomposition behaviour and structural characteristics of asphaltenes. *Journal of Analytical and Applied Pyrolysis*, *40-41*, 569–584.

[21] Speight, J. G., & Özüm, B. (2002). *Petroleum refining processes*. New York: Marcel Dekker.

[22] Gary, J. H., Handwerk, G. E., & Kaiser, M. J. (2014). *Petroleum refining: technology and economics*. Boca Raton: CRC Press.

[23] Cabrales-Navarro, F. A., & Pereira-Almao, P. (2017). Reactivity and comprehensive kinetic modeling of deasphalted vacuum residue thermal cracking. *Energy & Fuels*, *31*(4), 4318–4332.

[24] Hayes, R. E., & Mmbaga, J. P. (2013). *Introduction to chemical reactor analysis*. Boca Raton: CRC Press.

[25] Yan, T. (1990). Characterization of visbreaker feeds. *Fuel*, *69*(8), 1062–1064.

[26] Maurer, C. A. (1983). *Electron spin resonance spectroscopy: a potential technique for dating*

ancient ceramics. Ann Arbor, MI: Univ. Microfilms Intern.

[27] Gerson, F., & Huber, W. (2003). *Electron spin resonance spectroscopy of organic radicals*. Weinheim: Wiley-VCH.

[28] Balc, M. (2005). *Basic ^{1}H- and ^{13}C-NMN spectroscopy*. Amsterdam: Elsevier.

[29] Speight, J. G. (2015). *Handbook of Petroleum Product Analysis* (2nd ed.). Laramie, Wyoming: Wiley.

[30] Kapoor, M. P.; Kothiyal, V.; Singh, I. D. (1993). Compositional and structural studies of visbroken residues. *Fuel Sci. Technol. Int.Fuels, 11 (7)*, 975-989.

[31] Stratiev, D., Shishkova, I., Tsaneva, T., Mitkova, M., & Yordanov, D. (2016). Investigation of relations between properties of vacuum residual oils from different origin, and of their deasphalted and asphaltene fractions. *Fuel*, *170*, 115–129.

[32] Ramakrishna, S. A., & Grzegorczyk, T. M. (2009). *Physics and applications of negative refractive index materials*. Bellingham: SPIE Press.

[33] Speight, J. G. (2014). *The chemistry and technology of petroleum*; CRC press: Boca Raton.

[34] ASTM D4530-15. (2015). *Standard test method for determination of carbon residue (micro method)*. West Conshohocken, PA: ASTM International

[35] Rahmani, S., McCaffrey, W., & Gray, M. R. (2002). Kinetics of solvent interactions with asphaltenes during coke formation. *Energy & Fuels*, *16*(1), 148–154.

[36] Siskin, M., Kelemen, S. R., Eppig, C. P., Brown, L. D., & Afeworki, M. (2006). Asphaltene molecular structure and chemical influences on the morphology of coke produced in delayed coking. *Energy & Fuels*, *20*(3), 1227–1234.

3. Visbreaking of vacuum residue deasphalted oil: new asphaltenes formation

3.1. Introduction

Mild thermal cracking by visbreaking emerged as an important partial upgrading technology for reducing the viscosity of Canadian oilsands bitumen to enable pipeline transport. The viscosity of bitumen recovered from oilsands deposits is typically higher than 10^3 Pa·s at 20 °C [1]. The extent to which viscosity can be reduced by visbreaking is determined by the level of conversion. The maximum conversion that can be achieved in a visbreaker, is limited by the onset of coking. The maximum vacuum residue (>524 °C boiling fraction) conversion for oilsands bitumen before onset of coking is around 34 wt% [2].

Coking follows after the development of a second phase during the thermal conversion [3], and for this reason the limitation on conversion during visbreaking has been linked to the asphaltenes content of the feed material [4]. In practice the relationship between maximum conversion, onset of coking, and asphaltenes content is more complex [5, 6, 7]. Nevertheless, the benefit of performing solvent deasphalting before visbreaking is well established [8].

Higher conversion can be achieved when visbreaking deasphalted oil compared to visbreaking oil that was not deasphalted. However, during visbreaking new asphaltenes are formed, irrespective of whether the feed material is deasphalted or not [7, 9, 10, 11]. The formation of new asphaltenes erodes the conversion advantage gained by solvent deasphalting before visbreaking and is therefore a detrimental side-reaction.

The description of conversion during visbreaking usually makes use of the equivalent residence time (ERT) concept [12], which describes conversion in terms of a first order reaction. The implication of this description is that various reaction temperature and residence time combinations can be selected that result in the same conversion. This approach has been used to describe conversion and product formation during visbreaking in models of varying complexity, e.g. [11, 12, 13, 14, 15], some of which consider new asphaltenes formation explicitly.
Considering the impact of new asphaltenes formation the following question was posed: Would process conditions that in principle lead to the same conversion, also lead to the same type and concentration of asphaltenes in the final product?

The objective of this work was to investigate if different process conditions representative of coil-and-soaker visbreaking, and that would result in the same conversion, would also lead to the same type and concentration of asphaltenes in the final product. As a secondary objective, visbreaking products and their associated asphaltenes sub-fraction were characterized with the hope that it may help elucidate the pathway of new asphaltenes formation during visbreaking.

3.2. Experimental

3.2.1. Materials

The feed employed for this study is industrially produced vacuum residue deasphalted oil (VR DAO) that was obtained from the Nexen (now CNOOC International) Long Lake upgrading facility in Alberta, Canada. A description of the process can be found in literature [16]. For this work the VR DAO was sub-sampled in the laboratory and kept in a freezer at -20 °C.

Characterization of VR DAO feed and its sub-fractions (*n*-pentane insoluble and *n*-pentane soluble) are presented in Table 3-1. Standard uncertainties reported correspond to repeatability of the measurements. It is important to highlight that the *n*-pentane insoluble material includes not only asphaltenes, but also solid materials, such as mineral matter and carbonaceous deposits.

Table 3-1. Characterization of the vacuum residue deasphalted oil (VR DAO) feed material and its *n*-pentane insoluble and *n*-pentane soluble sub-fractions[a]

Property	VR DAO		VR DAO subfractions			
			n-pentane insoluble[b]		*n*-pentane soluble[b]	
	x	***u***	**x**	***u***	**x**	***u***
boiling point distribution (wt%)[c]			-[d]	-[d]		
naphtha (28 – 190 °C)	0.0	0.0	-[d]	-[d]	0.0	0.0
kerosene (190 – 260 °C)	0.0	0.0	-[d]	-[d]	0.0	0.0
diesel (260 – 343 °C)	0.0	0.0	-[d]	-[d]	0.0	0.0
light gas oil (343 – 454 °C)	1.9	0.2	-[d]	-[d]	1.4	0.0
heavy gas oil (454 – 560 °C)	9.8	1.0	-[d]	-[d]	12.3	0.1
vacuum residue (> 560 °C)	88.2	1.2	-[d]	-[d]	85.6	0.9
n-pentane insoluble content (wt%)[e]	5.7	0.3	-[d]	-[d]	-[d]	-[d]
elemental analysis (wt%)[f]						
carbon	83.2		81.5		83.0	
hydrogen	9.8		7.9		10.0	
sulfur	5.4		7.6		5.3	
nitrogen	0.6		1.1		0.5	
oxygen[g]	1.0		1.9		1.2	
H:C molar ratio	1.4		1.2		1.4	
density (kg/m^3)						
20 °C	1075	53	-[d]	-[d]	-[d]	-[d]
40 °C	977	22	-[d]	-[d]	-[d]	-[d]
density (kg/m^3)[h]	1043		1157		1028	
viscosity (Pa·s)						
40 °C	3513	6	-[d]	-[d]	-[d]	-[d]
50 °C	545	3	-[d]	-[d]	-[d]	-[d]
60 °C	93	2	-[d]	-[d]	-[d]	-[d]
mineral matter content (wt%)	0.3	0.1	0.7	0.4	0.0	0.0
micro carbon residue (wt%)	5.4	0.4	30.1	2.1	5.1	0.3
micro carbon residue (wt%)[i]	5.1		29.4		3.3	
vanadium content (µg/g)	211	13	527	2	180	28
nickel content (µg/g)	127	6	271	2	103	12
Free radical content (spins/g)[j]	1.0×10^{18}	0.1×10^{18}	1.5×10^{18}	-[f]	-[k]	-[k]

[b] *n*-pentane insoluble material and *n*-pentane soluble material subfractions obtained from frozen VR DAO feed

[c] Determined by simulated distillation analysis in duplicate. Pentane free basis for *n*-pentane soluble.

[d] Analysis not performed for this sample

[e] See Table 4

[f] Analysis performed on single sample

[g] Oxygen content calculated by difference

[h] From elemental analysis: $\rho = 1033 - 13.69H + 13.85S + 115.7N$, where *H, S,* and *N* refer to the mass fraction of each element

[i] Calculated mineral matter free basis for VR DAO and *n*-pentane insoluble and pentane free basis for *n*-pentane soluble

[j] Based on ESR analysis calibrated with DPPH

[k] Free radical content could not be determined due to the presence of *n*-pentane

Cylinder gases, chemicals, and calibration materials used in this study are presented in Table 3-2.

Table 3-2. Chemicals and cylinder gases employed in this study.

Compound	Formula	CASRN[a]	Mass fraction purity[b]	Supplier
Chemicals				
toluene	C_7H_8	108-88-3	0.995	Fisher Scientific
n-pentane	C_5H_{12}	109-66-0	0.997	Fisher Scientific
carbon disulfide	CS_2	75-15-0	0.9999	Fisher-Scientific
Cylinder gases				
nitrogen	N_2	7727-37-9	0.99999[c]	Praxair
helium	H_2	7440-59-7	0.99999[c]	Praxair
Air	O_2/N_2 mix	132259-10-0	-	Praxair
Calibration materials				
2,2-diphenyl-1-picrylhydrazyl (DPPH)	$C_{18}H_{12}N_5O_6$	1898-66-4		
reference material 5010	-	-	-	Supelco
polywax 655	-	-	-	Agilent

[a] CASRN = Chemical Abstracts Services Registry Number
[b] This is the purity of the material guaranteed by the supplier; material was not further purified
[c] Mole fraction purity

3.2.2. Visbreaking reactions

Iso-conversion process conditions evaluated in this study (Table 3-3) were obtained by using the CNOOC proprietary kinetic model developed from the work of Cabrales-Navarro et al. [11], where the ERT concept defined by Yan [12] is used in the model.

Table 3-3. Visbreaking reaction conditions

Reaction conditions			Liquid product yield (wt%)		
			Physical recovery (with a spatula)[b]		Total yield (physical + cleaning)[c]
Description	Temperature (°C)	time (min)[a]	x	*u*	
Control	417	0	75	3	96
	425	0	74	9	102
	438	0	81	3	94
Regular reactions	417	30	79	5	95
	425	20	81	4	97
	438	10	80	4	97

[a] Reactions time exclude any heat-up and cool-down periods
[b] Average (x) and standard deviation (*u*) of samples in quadruplicate are reported
[c] Sample recovered during cleaning was obtained from a single run

These process conditions are of industrial interest and are representative of coil and soaker visbreaking. Vacuum residue conversion was calculated by using equation 1.

$$Conversion = 1 - \frac{mass\ of\ vacuum\ residue\ in\ product\ (g)}{mass\ of\ vacuum\ residue\ in\ feed\ (g)} \quad (1)$$

Visbreaking reactions were performed in a Swagelok 316 stainless steel micro-batch reactor (2.7 cm internal diameter and 14.6 cm long). In a typical experiment, approximately 15 g of the frozen VR DAO was loaded into a micro batch reactor and the exact mass was recorded. The reactor was leak tested before being flushed and then pressurized with nitrogen to an initial pressure of 2 MPa gauge. The weight of the pressurized reactor was recorded.

The pressurized reactor was then placed in a preheated fluidized sand bath heater (Omega fluidized bath FSB-3) to heat the reactors up to reaction temperature (Table3-3). The temperature inside the reactor was measured using a thermocouple. The total heat-up time for the reactor internal temperature to reach the set point was recorded. The time to reach the set point temperature was 8.3, 10.0, and 13.1 min for 417, 425, and 438 °C, respectively.

After reaching reaction temperature, the reactor remained in the sand bath as indicated in Table 3-3 for each of the temperatures evaluated. After reaction time, the reactor was removed from the sand bath heater and cooled down. The time to cool down from reaction temperature to around 100 °C, was 29–32 min.

The final pressure of the reactor after cooling varied and it was between 2.5 MPa and 3 MPa gauge. The reactor was depressurized by releasing the gases in the fumehood and it was weighed before and after depressurization for mass balance calculation. The liquid reaction product remaining in the reactor was manually removed by scraping out the reactor and was accomplished without using any solvent.

One of the challenges in performing batch reactor studies is that there are heat-up and cool-down periods. The use of micro-batch reactors reduces the time period to reach temperature, but past experience indicated that meaningful changes took place in this period [17]. The experimental

work therefore included control experiments that involved only heat-up to the reaction temperature, followed by cooling down. These experiments are indicated as “0 min reaction time”, since no time was spent at the set point temperature once the set point was reached. All reaction conditions were performed four times, where one of the repeat experiments was intended for mass balance calculation to account for losses during cleaning and it was not further analyzed. In this procedure, after product recovery with a spatula, the reactor was weighed before and after cleaning with toluene. The material that was accounted for, but that was not recovered during mechanical cleaning, was 0.1-0.3 g/g feed.

3.2.3. Analyses

n-Pentane insoluble material of feed and visbroken products was determined by mixing ~ 6 g of sample with *n*-pentane in a ratio equal to 1:40 (wt:vol) in an 500 mL amber flask. The mixture was stirred for 1 hour by using a magnetic stirrer. After stirring, the sample was left in contact with the solvent for 24 hours. After this period, the mixture was filtered under vacuum by using a 0.22 μm Millipore nitrocellulose membrane filter. The membrane filter was transferred to an aluminum cup and it was left in the fumehood for 24 h. The membrane filter and the aluminum cup were previously weighed in order to determine the *n*-pentane insoluble content of the feed and reaction products. The *n*-pentane soluble was separated from *n*-pentane solvent by using a rotary evaporator at 50 °C for 6 hours. After evaporation, the *n*-pentane soluble was transferred to a 50 mL glass vial and was left in the fumehood until constant weight. Residual *n*-pentane solvent in the *n*-pentane soluble fraction was estimated from thermal gravimetric analysis by combining *n*-pentane boiling point (36.1 °C) with the rate of mass loss. The *n*-pentane content in the *n*-pentane soluble of the VR DAO feed was estimated as 1.8 wt% with standard uncertainty u = 0.5 wt% while for the *n*-pentane soluble originated from the visbroken products, the residual *n*-pentane content could not be determined by thermal gravimetric analysis and was therefore assumed as negligible. *n*-Pentane insoluble and *n*-pentane soluble materials from VR DAO feed (Table 3-1) and visbroken products were characterized. As mentioned in section 3.2.1, *n*-pentane insoluble material of VR DAO feed contains asphaltenes, as well as mineral matter and carbonaceous deposits. *n*-Pentane insoluble material of visbroken products may also contain coke, even though minimal coke formation is expected for these reaction conditions.

Elemental analyses were performed by the Analytical Services of the Chemistry Department at University of Alberta using a Carlo Erba Elemental Analysis EA1108 Analyzer. Briefly, small amount of sample is oxidatively pyrolized at 1700−1800 °C in order to produce N_2, CO_2, H_2O, and SO_2. The product gases pass through a reactive column with helium as the carrier and they are separated on a chromatographic column at 70 °C where they are detected by a thermal conductivity detector. A calibration curve based on the concentration of known standards is used to quantify the gases.

An active spectrum micro-electron spin resonance (ESR) was used to measure the free radical content of the feed and the products. The analysis was performed by diluting 20 mg of sample in 600 µL of toluene and were measured at 1.2 Gauss coil amplitude, a digital gain of 12 dB, and a microwave power of 10 mW. The analyses were the average of 7 scans with a sweep delay of 30 seconds. Free radical content was quantified as the number of spins per sample by performing the double integration of the ESR peak using a calibration curve of toluene in 2,2-diphenyl-1-picrylhydrazyl (DPPH). The double integration was done by using the MicroESR software.

Refractive index of visbroken product were determined by an Anton Paar Abbemat were determined relative to that of air using the sodium D-line (589 nm). The measurements were performed at controlled temperatures of 20, 40, and 60 °C.

Thermogravimetric analysis (TGA) was used to determine the micro carbon residue (MCR) of the feed, visbroken products and their respective *n*-pentane insoluble fraction. TGA was also used to measure the mineral matter of the feed and its sub-fractions (Table 3-1). The instrument used was a Mettler Toledo TGA/DSC1 equipped with LF 1100 furnace, sample robot, and MX5 internal microbalance. For the mineral matter analysis, approximately 10 mg of sample was weighed in an aluminum oxide crucible. The sample was then heated from 25 to 900 °C at 10 °C/min in an oxidizing atmosphere to remove the organic matter by combustion. The air flow rate was 100 mL/min. For the MCR analysis, approximately 10 mg of sample was placed in an aluminum oxide crucible and heated from 25 to 500 °C at 10 °C/min followed by an isothermal period of 30 min at 500 °C in a nitrogen atmosphere. The nitrogen flow was 100 mL/min. Both nitrogen and air flow rate were controlled with a Mettler GC 10 gas controller.

The boiling point distribution of the feed and visbroken products was obtained by simulated distillation using an Agilent 7890B high temperature gas chromatograph equipped with flame ionization detector (FID). The procedure was obtained by ollowing the ASTM D7169 standard method. Approximately 0.1 g of sample was dissolved in 10 mL CS_2 (the exact mass was recorded). Polywax 655 was used as calibration material for the boiling point distribution while 5010 standard reference material was used for FID response calibration. Blank (pure CS_2) subtraction was made automatically at the end of the run where the blank was run at the beginning of the sequence as well as after each standard or sample injection.

Due to the viscous nature of the sample, density measurements of VR DAO feed were performed by following the principles described in the ASTM D70 [18] method. Gas chromatographic vials (5 mL) were used instead of glass pycnometers. VR DAO feed was heated to 120 °C and poured into the vial of predetermined volume to about three fourth of the vial capacity. The remainder of the volume was filled with deionized water. The exact mass of the sample was recorded by using a Mettler Toledo XS 105 balance (120g capacity with 0.0001 readability). Since the density of the water was known, the density of the sample could be calculated. Density measurements were performed at 20 and 40 °C by using a temperature-controlled water bath. The temperature water bath was controlled using a Julabo F25-EH circulating heater/chiller.

The viscosity of the VR DAO feed was measured by using the Anton Paar RheolabQC viscometer. Due to the viscos nature of the sample, the feed was heated to 90 °C and poured into a concentric cylinder CC17/QC-LTC measuring cup. The internal diameter of the measuring cup is 16.664 mm and 24.970 mm length. Around 4 g of sample was used for analysis. Viscosity was measured at 40 °C, 50 °C and 60 °C and remained constant within ± 0.006 °C. Temperature was controlled by the Julabo F25-EH circulating heater/chiller. At each temperature, around 10 min was waited to ensure the sample reached the desired temperature and sample was measured at two constant 10 s^{-1}. At each shear rate viscosity was measured for three times.

3.3 Results

3.3.1 Feed characterization

One interesting observation from Table 3-1 is the content of the n-pentane insoluble material of VR DAO feed. First, industrial deasphalting is not as rigorous as laboratory deasphalting and the VR DAO still contained n-pentane insoluble material. Second, it was observed that the phase of VR DAO feed prior to precipitation affected the content of n-pentane insoluble material that was measured. The results for each precipitation procedure are presented in Table 3-4.

Table 3-4. *n*-pentane insoluble material of VR DAO obtained from different precipitation procedures

Material	***n*-pentane insoluble (wt%)**		
	n	**x**	***u***
Frozen VR DAO	6	5.7	0.3
Melted VR DAO	3	8.6	0.6
Frozen VR DAO followed by melting	1	7.9	

[a] (n) number of experiments, (x) average, and (*u*) standard uncertainty

For example, asphaltenes precipitation starting with frozen VR DAO resulted in 5.7 wt% with standard uncertainty u=0.3% of n-pentane insoluble material, while melted VR DAO that was not previously frozen resulted in 8.6 wt% with standard uncertainty u=0.6 wt% of n-pentane insoluble material. Freezing VR DAO following by subsequent melting resulted in 7.9 wt% of *n*-pentane insoluble material. It can be concluded from these observations that melting VR DAO before mixing with n-pentane caused an increase in the amount of precipitated n-pentane insoluble material.

A material balance was performed on the n-pentane insoluble and n-pentane soluble materials obtained from the frozen VR DAO feed (Table 1). The material balance closure on carbon, hydrogen, sulfure, nitrogen, nickel, vanadium, and micro carbon residue (mineral matter and pentane free basis) was 100 %, 101 %, 100 %, 91 %, 89 %, 95 %, and 94 %, respectively.

3.3.2 Material balance for visbreaking reactions

To avoid analytical complications introduced using a solvent during recovery, the visbroken product after reaction was recovered by mechanical means. The amount of product that could be recovered with a spatula, on average for each reaction condition as described in section 3.2.2, ranged from 74-81 wt% of initial feed (Table 3-3). The remainder of the material was recovered using solvent to calculate material balance closure but was kept separate. When the material recovered by mechanical means and during solvent cleaning was considered, the liquid product yield was 95%-97 wt% for the regular reactions (Table 3-3). The liquid product yield for the corresponding control experiments ranged from 94-102 % (Table 3-3). The uncertainty in the product yield is caused by its viscous nature (specially the products from the control experiments) where some material loss occurred during liquid transfer and cleaning.

The reactors were pressurized with nitrogen at 2 MPa gauge initially and it was observed that there was an increase in pressure during reaction to 5-7 MPa gauge. However, after cooling, the final internal pressure ranged between 2.5 MPa and 3 MPa gauge. This indicates that the pressure increase during reaction was due to temperature and limited gas formation. Most of the gases responsible for the increase in pressure during the reaction were condensed or dissolved in the liquid during cooling. The gas yield was determined based on the mass difference between the pressurized reactor and depressurized reactor. The uncertainty with this procedure is related to the weight of the pressurized reactor. Despite the uncertainty, gas yield from the regular reactions at different reaction conditions (Table 3-3) was in the range of 0.02-0.04 g/g feed, which resulted in a mass balance closure of 97-99 wt%.

On the other hand, the amount of gas released during depressurization from the control reactions (0 min reaction time) was somewhat less than the amount of nitrogen gas added into the reactor. It is well recognized that nitrogen gas can dissolve in organic materials [19, 20] and it could explain the observed behavior during depressurization of control experiments. Therefore, it was decided to determine gas yield based on the difference between complete material balance closure and the measured liquid/solid product yields. When the procedure is employed, the gas yield from reaction conditions in Table 3-3 and their corresponding control runs (0 min reaction time) was calculated to be 5-6 wt%.

3.3.3 Cracking conversion

Cracking conversion of the vacuum residue fraction of DAO was determined by using eq. 1 and the boiling point distribution of the visbroken products (Table 3-5) and the feed (Table 3-1). The gas yield formed during reactions was considered negligible for conversion calculation (Section 3.3.1).

Table 3-5. Boiling point distribution of visbreaking products obtained at different reaction conditions[a]

Reaction conditions		Naphtha (25 - 190 °C)		Kerosene (190 - 260 °C)		ATM GO (260 - 343 °C)		LVGO (343 - 454 °C)		HVGO (454 - 524 °C)		Residue (+ 524 °C)	
Temperature (°C)	time (min)[b]	x	*u*	x	*u*	x	*u*	x	*u*	x	*u*	x	*u*
417	0	2.1	1.7	1.4	0.3	2.3	0.4	5.7	0.7	11.9	0.5	76.5	3.0
425	0	3.2	0.9	2.9	0.5	5.3	0.8	10.0	0.9	13.7	0.2	64.9	3.3
438	0	10.9	0.5	9.2	0.6	12.9	1.0	15.5	1.4	12.4	0.8	39.1	2.6
417	30	5.2	1.4	5.6	1.0	8.4	1.2	14.4	1.2	14.8	0.5	51.6	4.8
425	20	7.2	0.4	7.1	0.3	10.9	0.2	15.0	0.1	13.2	0.4	46.7	0.7
438	10	10.2	1.4	9.2	1.2	12.9	1.5	14.5	0.9	11.5	1.0	41.7	2.2

[a] Average (x) and standard uncertainty (*u*) of analyses in triplicate;
[b] Reactions time exclude any heat-up and cool-down periods

This assumption causes a near constant bias towards lower conversion, because the conversion to gas is not accounted for. The results are shown in Table 3-6 and the following conclusions can be made.

Table 3-6. Cracking conversion of the vacuum residue fraction of VR DAO at different reaction conditions[a]

Reaction conditions			Vacuum residue conversion[b]	
Description	**Temperature (°C)**	**time (min)**	**x**	***u***
Control	417	0	0.13	0.03
	425	0	0.27	0.04
	438	0	0.56	0.03
Regular reactions	417	30	0.41	0.05
	425	20	0.47	0.01
	438	10	0.53	0.03

[a] (x) average and (*u*) standard uncertainty of samples in triplicate are reported
[b] Cracking conversion calculated by using equation 1 and boiling point distribution from SimDist analysis (Table 3-5)

The first observation is that the conditions studied should provide iso-conversion for the regular reactions according to the ERT assumption [12], but this is not what was observed (Table 3-6). Vacuum residue conversion increased by increasing reaction temperature and decreasing reaction time. This may be due to the changes happening during heating and cooling down periods, which are not considered in the ERT assumption. This was confirmed with control experiments where the reactor was cooled down immediately after reaching reaction temperature. As shown in Table 3-6, conversion during heating and cooling periods (control experiments) increased as temperature increased, which is expected, since the time to reach the set-point increased as temperature increased (Section 3.2.2).

The second observation is that high standard deviations were obtained. This is commonly encountered for very viscous materials, e.g. VR DAO, since it is very difficult to work with it.

3.3.4 Relationship between conversion and bulk properties of visbroken products

The primary objective of this work was to verify if process conditions that in principle would lead to the same conversion would also lead to the same *n*-pentane insoluble content. Iso-conversion was not achieved at conditions that were predicted to have iso-conversion (Table 3-3), but the number of experiments was sufficient to evaluate the relationship between the product properties and the conversion by looking at the results collectively.

The *n*-pentane insoluble content of the products for each individual run as a function of vacuum residue conversion is shown in Figure 3-1. The average and standard deviation for each temperature condition is presented in Table A1 from Appendix A as the Supporting Information.

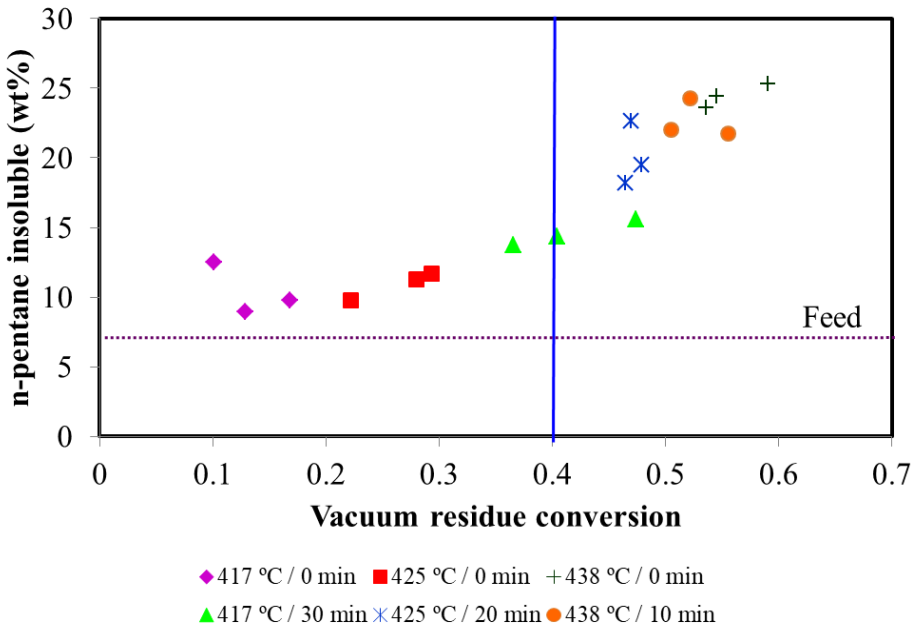

Figure 3-1. Relationship between *n*-pentane insoluble content of visbroken products and vacuum residue conversion

It can be noted from Figure 3-1 that the *n*-pentane insoluble content of all visbroken products, including those of the control experiments, was higher than the feed. This indicated that asphaltenes are also formed during the heat-up process.

Another observation is that *n*-pentane insoluble content of the products remained below 15 wt% up to 0.4 conversion, indicated by the vertical line in Figure 3-1.

Micro carbon residue (MCR) is a measure of the solid material remains after pyrolizing a material under controlled conditions. It gives an indication of the coke-forming tendency of the material, which is relevant to upgrading and refining processes. The MCR of all visbroken products on a mineral matter free basis are shown in Figure 3-2 and Table A2 in Appendix A.

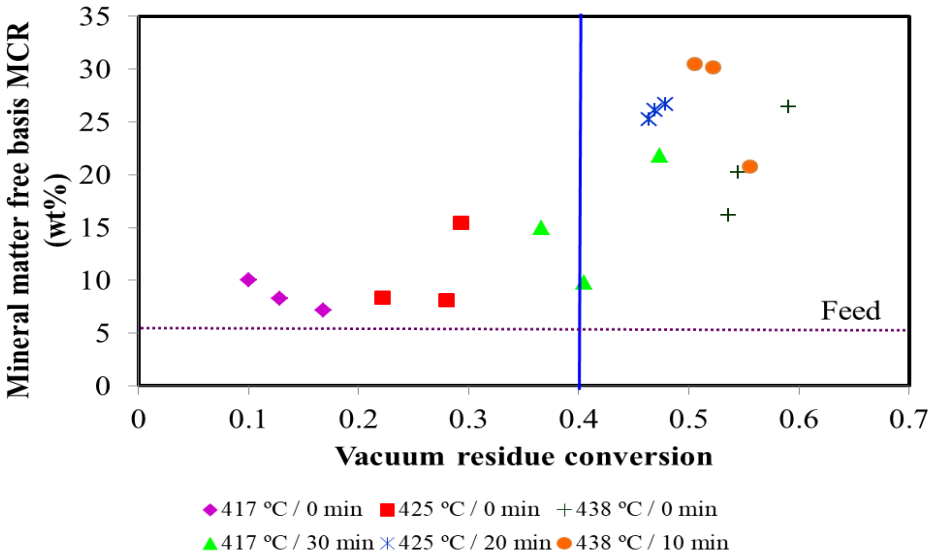

Figure 3-2. Relationship between mineral matter free basis MCR of visbroken products and vacuum residue conversion

Analogous observations can be made about the MCR (Figure 3-2) as those made about the *n*-pentane insoluble content (Figure 3-1). The MCR values of the products are all higher compared to the MCR of VR DAO feed. The MCR of the products remained below ~15 wt% up to 0.4 conversion.

The refractive index values measured at 20 °C (Figure 3-3) had the same trend as those measured at 40 and 60 °C, which are shown in Table A3 and Figure A1 from Appendix A. Similar to *n*-pentane insoluble and MCR content, the refractive index measured at 20 °C of the products remained in a narrow band up to 0.4 conversion and then increased for all but one product.

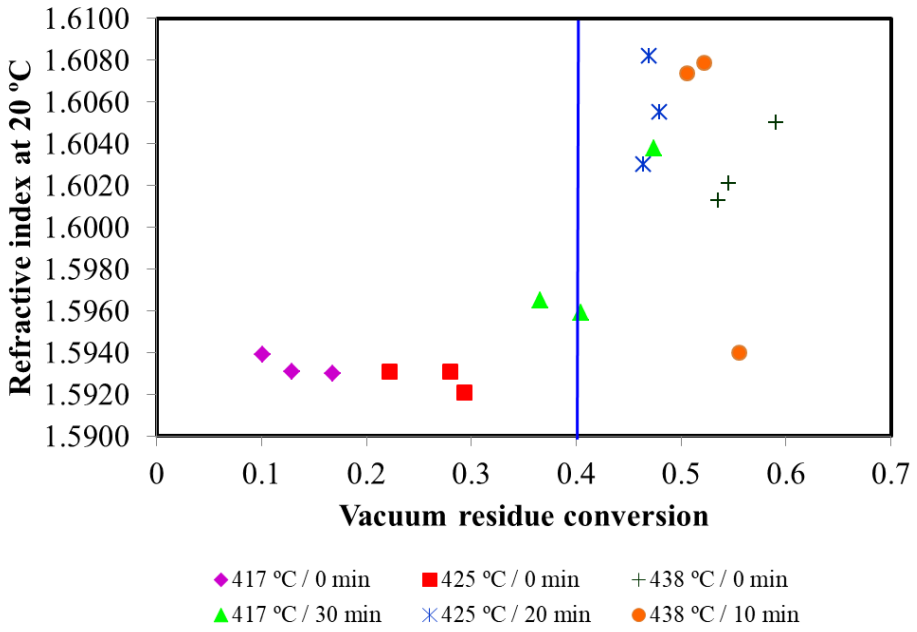

Figure 3-3. Relationship between refractive index of visbroken products and vacuum residue conversion

The free radical concentration in the products was determined using electron spin resonance spectroscopy and results are shown in Figure 3-4 and Table A4 in Appendix A.

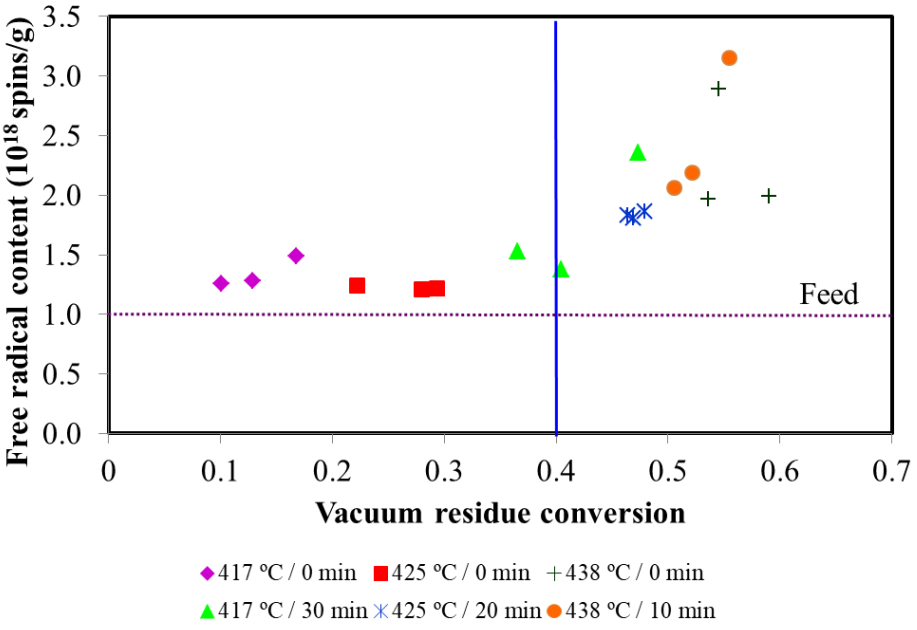

Figure 3-4. Relationship between free radical content of visbroken products and vacuum residue conversion

This was of interest, because conversion in a visbreaking process proceeds mainly by free radical chemistry and the persistence of free radical species in the product has some bearing on the conversion.

It can be observed from Figure 3-4 that the quantity of free-radical species present in the products from both regular reactions and control experiments are higher ($1.2 – 2.5 \times 10^{18}$ spins/g) than the feed (1.0×10^{18} spins/g). As for the previous properties, two different regions were observed for the free radical concentration. At 0.4 conversion and lower, the amount of free radicals formed is almost constant, regardless of the temperature/time combination, while at higher than 0.4 conversion, the quantity of free radicals formed increases as conversion is further increased.

3.3.5 Elemental composition of n-pentane insoluble material from the liquid product

Elemental analysis of the *n*-pentane insoluble material precipitated from the products obtained at different reaction conditions was determined. The results are shown in Table 3-7.

Table 3-7. Elemental analysis of *n*-pentane insoluble material precipitated from visbroken products obtained at different reaction conditions[a,b]

Reaction conditions		*n*-pentane insoluble											
		C (wt)%		H (wt%)		S (wt%)		N (wt%)		O (wt%)	H:C[d]	N:C[d]	S:C[d]
Temperature (°C)	time (min)[c]	x	*u*	x	*u*	x	*u*	x	*u*	x			
417	30	83.28	0.03	6.64	0.01	6.88	0.03	1.32	0.01	1.87	0.957	0.014	0.031
417	0	83.80	0.20	6.90	0.16	6.49	0.15	1.19	0.02	1.63	0.988	0.012	0.029
425	20	84.61	0.23	6.18	0.02	6.70	0.07	1.29	0.01	1.22	0.877	0.013	0.030
425	0	83.53	0.08	7.09	0.01	6.65	0.04	1.27	0.01	1.47	1.018	0.013	0.030
438	10	85.02	0.12	5.87	0.02	6.56	0.08	1.29	0.00	1.26	0.829	0.013	0.029
438	0	84.69	0.02	5.89	0.02	6.66	0.07	1.30	0.00	1.46	0.834	0.013	0.029

[a] (x) average, and (*u*) standard uncertainty due to repeatability
[b] Analysis performed in single sample in duplicate
c Reactions time exclude any heat-up and cool-down periods
[d] Molar ratio

There was not much difference on the N:C and S:C molar ratios of the *n*-pentane insoluble products obtained at different visbreaking conditions. Moreover, N:C and S:C molar ratios of the *n*-pentane insoluble material precipitated from the visbroken products are similar to the *n*-pentane insoluble material initially present in the feed (compare Tables 3-1 and 3-7).

All the *n*-pentane insoluble material precipitated from the products have H:C molar ratios of 1 or less, which is lower than the H:C molar ratio of 1.2 of the *n*-pentane insoluble material in the feed (Table 3-1). The H:C molar ratio of the *n*-pentane insoluble material precipitated from the visbroken products decreased as their content in the products increased (Figure 3-5).

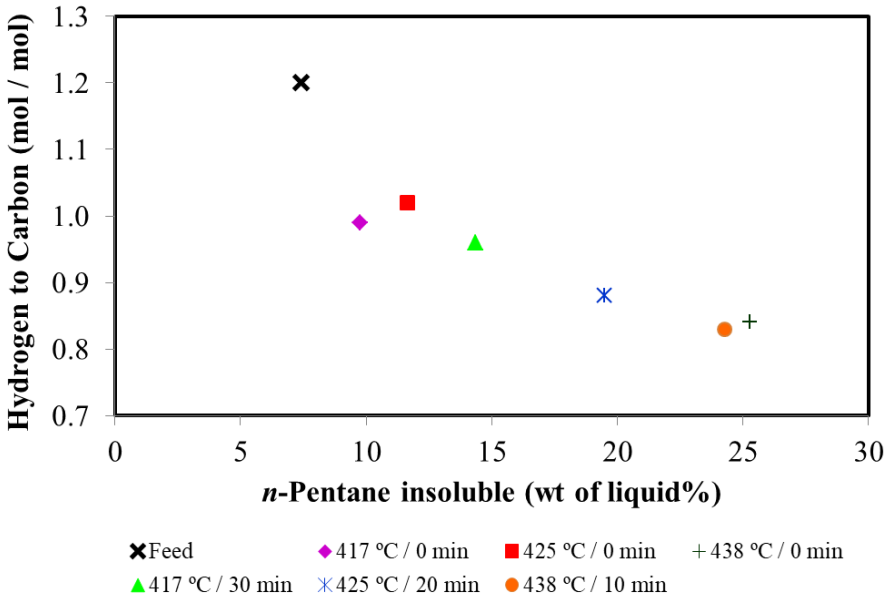

Figure 3-5. Relationship between the hydrogen-to-carbon molar ratio of the *n*-pentane insoluble material with the amount of the n-pentane insoluble in the feed and visbroken products

3.3.6 Micro carbon residue of n-pentane insoluble material from the visbroken product

The MCR on a mineral matter free basis of the *n*-pentane insoluble material precipitated from the visbroken products are shown in Figure 3-6 and Table A2 from Appendix A. All the n-pentane insoluble material formed during visbreaking at different conditions have a higher MCR (> 37 wt%) than the n-pentane insoluble initially present in the VR DAO feed (29 wt%). In addition, the MCR content of n-pentane insoluble material increased as the amount of n-pentane insoluble material in the visbroken product increased (Figure 3-6).

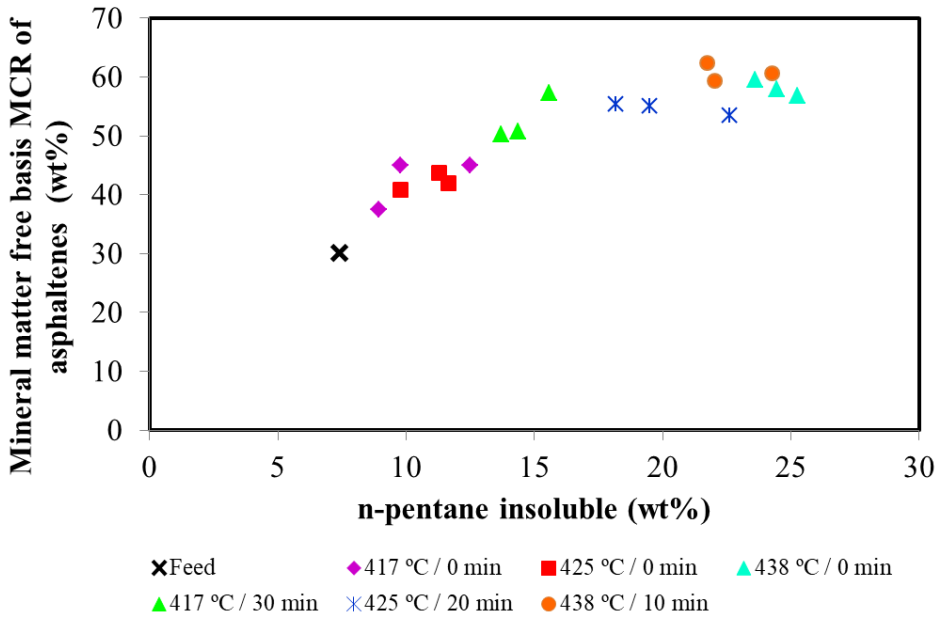

Figure 3-6. Relationship between the mineral matter free basis MCR of the *n*-pentane insoluble material with the amount of the n-pentane insoluble in the feed and visbroken products

3.3.7 Free radical content of n-pentane insoluble material from the visbroken products

Quantification of the free radical content of the *n*-pentane insoluble material precipitated from the visbroken products is shown in Figure 3-7 and Table A4 from Appendix A.

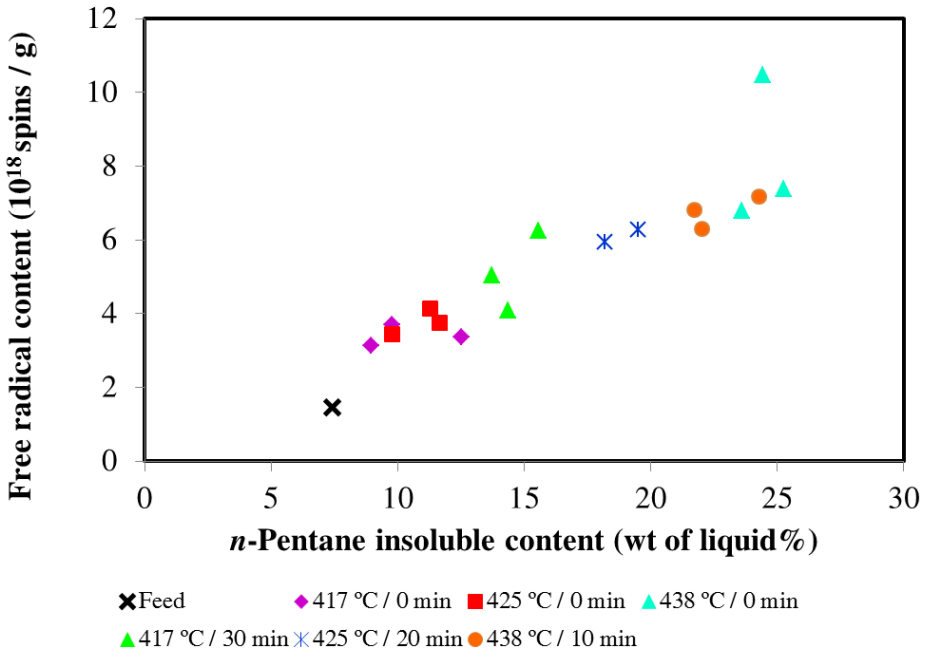

Figure 3-7. Relationship between free radical content of the *n*-pentane insoluble material with the amount of the n-pentane insoluble in the feed and visbroken products

The first observation is that all the *n*-pentane insoluble material present in the visbroken products has a higher free radical content ($3 – 11 \times 10^{18}$ spins/g) than present in the *n*-pentane insoluble fraction of the VR DAO feed (1.5×10^{18} spins/g).

The second observation is that the amount of free radicals in the *n*-pentane insoluble material of the product seems to correlate nearly linearly with the *n*-pentane insoluble content in the liquid products. This, as the *n*-pentane insoluble content in the visbroken product increased, the *n*-pentane insoluble material also had a higher concentration of free radicals.

3.3.8 Product characterization over time

The increase in free radical content of the products after conversion (Figure 3-7) prompted a question about the persistence of the formed radicals. To evaluate the free radical persistence over time, the reaction product from one of the experiments, thermal conversion at 417 °C for 30 min, was kept under nitrogen atmosphere to be re-analyzed later. The results of the analyses shortly after the thermal conversion experiment and the same product re-analyzed after 210 days is shown in Table 3-8.

Table 3-8. Comparison of product from visbreaking of vacuum residue DAO at 417 °C for 30 min shortly after reaction and after 210 days of storage under nitrogen atmosphere at ambient conditions[a]

Product property	Visbroken product characterization			
	shortly after reaction		after 210 days storage	
	x	*u*	x	*u*
n-Pentane insolubles (wt%)	14.9	1.5	23.8	3.1
Free radical content (10^{18} spins/g)	1.8	0.5	1.4	0.1
Refractive index, n_D:				
at 20 °C	1.5987	0.0044	1.6024	0.0022
at 40 °C	1.5904	0.0042	1.5941	0.0020
at 60 °C	1.5815	0.0032	1.5858	0.0019
dn_D/dT (K^{-1})	-0.00043		-0.00041	

[a] (x) average and (*u*) standard uncertainty of samples in triplicate are reported

There was a 9 wt% increase in the n-pentane insoluble content. The free radical content decreased and there was an increase in refractive index, although these changes were not as clear as the change in n-pentane insoluble content.

3.4 Discussion

3.4.1 Correlation between conversion and properties of visbroken products

When different product properties (*n*-pentane insoluble, MCR, refractive index, and free radicals content) were related with vacuum residue conversion (Figures 3-1 to 3-4), it was found that the product properties remained constant within a band of values until a conversion of 0.4 was reached. At higher than 0.4 conversion their values increased with increasing vacuum residue conversion. Differently put, up to a conversion of 0.4 thermal cracking caused a change in boiling point distribution, but it caused little change in the other properties of the liquid product. However, as conversion proceeded beyond 0.4, reactions that changed the properties of liquid product took place at a sufficient rate to cause observable changes in the properties of the liquid.

One possible explanation is that vacuum residue may have different groups of molecules ("easy" and "difficult" to convert molecules). After converting the "easy to convert" molecules we start to convert the "difficult" ones, and therefore the profile changes. Another explanation for the observations must be sought in one or more properties of the liquid product that reached a threshold. For example, this could be the formation of a reactive group of compounds that became significantly concentrated to change the nature of the reaction chemistry, such as olefins, or it could be the depletion of a moderating attribute, such as transferable hydrogen.

An additional clue to the origin of the change can be found in the properties that changed. The increase n-pentane insoluble content (Figure 3-1), increase in MCR (Figure 3-2), increase in refractive index (Figure 3-3), and increase in free radicals content (Figure 3-4) were all indicative of the formation of less soluble, more coke prone species.

3.4.2 Hydrogen transfer

Some interesting observations were made about the nature of the asphaltenes (which are part of the n-pentane insoluble material) in relation to the amount that was present in the visbroken product. The hydrogen to carbon ratio of the n-pentane insoluble decreased as their amount in the visbroken product increased (Figure 3-5), while the nitrogen to carbon and sulfur to carbon ratios remained constant (Table 3-7).

Although the n-pentane insoluble asphaltenes fraction has a higher nitrogen and sulfur content than the n-pentane soluble material (Table 3-1), the new asphaltenes that were formed during thermal conversion were not differentiated from asphaltenes in the feed based on their nitrogen or sulfur content. The main difference was that the new asphaltenes, and presumably the asphaltenes originally in the feed, became hydrogen depleted (Figure 3-5).

Interpreting these results in terms of the residue solubility diagram of Whiehe [21], insolubility is related to a combination of high molecular mass and low hydrogen content. Thus, if the hydrogen to carbon ratio decreases when the molecular mass remains the same, the material will be more likely to be insoluble in n-pentane. Although there is no direct evidence to indicate whether the average molecular mass was lower, higher or the same, only if the molecular mass became much lighter would the n-pentane insoluble material in the feed and product have comparable solubility characteristics. However, it should be kept in mind that the determination of n-pentane insoluble content is also influenced by other factors (see section 3.4.5).

The decrease in hydrogen-to-carbon ratio meant that a significant amount of hydrogen was transferred. If we assume that all the feed material that eventually became asphaltenes had the same composition as the asphaltenes in the feed, then the amount of hydrogen transferred can be calculated. The amount of hydrogen transferred during conversion at 438 °C were around 20 mg H/g asphaltenes in product (i.e. 79 - 59 mg H/g from Tables 3-1 and 3-7), which is equivalent to 5 mg H/g feed (i.e. 0.25 g asphaltenes/g feed × 20 mg H/g asphaltenes). The ability of asphaltenes to donate hydrogen was previously recognized [22, 23, 24]. Asphaltenes were capable of donating hydrogen at temperatures as low as 250 °C [22]. At 250 °C, 1.8 mg H/ g asphaltenes was transferred to α-methylstyrene, a hydrogen acceptor molecule. Using 2,3-dichloro-5,6-dicyano-p-benzoquinone as hydrogen acceptor, Gould et al [23] found that various asphaltenes and residue fractions were better hydrogen donors than tetralin and that hydrogen donor capacity generally decreased (but not always) as conversion time at 400 °C increased. In the work of Guo et al. [24] the hydrogen donating ability of residues and their SARA (saturates, aromatics, resins, and asphaltenes) fractions was evaluated during thermal process by using anthracene as hydrogen acceptor. It was found that the hydrogen donating ability of the residues and all SARA components increased when reaction temperature increased. Nevertheless, regardless of reaction temperature,

the hydrogen donor ability increased under thermal processing up to a maximum, and then started to decline. Typical values for the maximum amount of hydrogen transferred were in the range 0.7–0.8 mg H/g feed.

3.4.3 Asphaltenes and the formation of heavier material during visbreaking

The benefit of asphaltenes in donating hydrogen and keep the hydrogen in the oil is desirable. However, as pointed out by Gould et al.,[23] under thermal cracking conditions the formation of new asphaltenes by the combination of free radicals cannot be prevented, as can be observed from Figure 3-1. Figure 3-1 also indicated that amount of asphaltenes formed can be different at the same conversion, and that the same amount of asphaltenes can be formed at different conversion. The kinetics of asphaltenes formation was therefore different to the kinetics of vacuum residue conversion. It is recognized that some of the difference observed could also be attributed to changes in how the products respond to asphaltenes determination (see section 3.4.5).

Asphaltenes are generally considered coke precursors in thermal cracking processes. In the kinetic model for coke formation during thermal cracking of deasphalted oil suggested by Wiehe,[3] it is stated that the asphaltenes concentration increases up to a maximum and then decreases. The maximum concentration corresponds to the end of the induction period for coke formation. The asphaltenes formed remain in solution while the oil matrix can provide hydrogen by hydrogen transfer. Once the supply of transferable hydrogen from the oil is exhausted, asphaltenes will aggregate and phase separate to form coke. Within this context, the ability of asphaltenes to donate hydrogen under thermal cracking conditions was seen as a disadvantage.[23] This is because the formation of asphaltenic free radicals takes place due to the fast depletion of donor hydrogen in asphaltenes and therefore combination of asphaltenenic free radicals to form high molecular weight polyaromatic cores in a separate phase is unavoidable. If thermal cracking continues, insoluble coke will be formed.

3.4.4 Free radical content and storage stability

It is known that bitumen has persistent free radicals and that the persistent free radical content of the asphaltenes fraction in bitumen is higher than that of the maltenes fraction [25]. The n-pentane insoluble asphaltenes fraction in this study had a free radical content of 1.5×10^{18} spins/g (Table 3-

1). After thermal conversion, there was a two to sevenfold increase in the free radical content of the asphaltenes fraction (Figure 3-7).

It was speculated that at least some of the new persistent free radicals might be more reactive than the free radical species that were persistent and stable over geological time. This was of interest, because it would have implications for storage stability and pipeline transport. In fact, decreased storage stability was reported for visbroken products from Venezuelan heavy oil [26]. Since the quantity of persistent free radicals in the visbroken oil decreased over time, the authors concluded that free radical addition reactions may not terminate after thermal treatment. Although the reaction kinetics was likely slow, the time during storage can be of the order of weeks or months.

A similar observation was made in this work (Table 3-8). There was a meaningful change in the product during storage. The free radical content decreased over time, which was reflected by chemical changes in the product as indicated by the change in refractive index and the increase in the n-pentane insoluble asphaltenes content from 14.9 wt% with standard uncertainty = 1.5 wt% to 23.8 wt% with standard uncertainty = 3.1 wt%.

There was no direct evidence that the increase in persistent free radicals after thermal conversion was responsible for the changes noted in Table 3-8. Yet, the increase in asphaltenes with concomitant decrease in free radical concentration was suggestive of free radical termination reactions leading to the formation of heavier products (R• + 'R• $\rightarrow$ R–'R). Hypothetically, if it was the only type of reaction resulting in asphaltenes formation during storage, it would be possible to calculate the average molecular mass, M_n, of the free radical species from the change in mass of asphaltenes and free radical content:

$M_n = (0.238 - 0.149\ g/g) \div [(1.8\times10^{18} - 1.4\times10^{18}\ spins/g) \div (6.0\times10^{23}\ spins/mol) = 1.3\times10^{5}\ g/mol$

The calculated value for M_n is ridiculously large. The average molecular mass of asphaltenes is of the order 10^3 g/mol, not 10^5 g/mol. It is unlikely that free radical combination on its own could account for the increase in asphaltenes content. However, the calculation also made it clear that the mass of material converted to asphaltenes, expressed on a converted free radical content, is high, i.e. of the order 10^5 g/mol free radicals converted.

It is more likely that the free radicals that were converted participated in more than one chain transfer reaction, which would be consistent with arguments presented by Gray and McCaffrey [27]. Several chain transfer reactions before termination would lead to more than one product from addition reactions, each with a lower molecular mass than was calculated.

3.4.5 Determination of n-pentane insoluble material

Even though it was not the objective of this work to evaluate the effect of different asphaltenes precipitation procedures on asphaltenes content, the differences in the content of n-pentane insoluble material that was measured when VR DAO was frozen or melted (section 3.3.1) deserves an explanation.

Asphaltenes is defined as a solubility class. It was a convenient method of classification when it was developed, because it had bearing on practical technologies, such as solvent deasphalting used for lubricant base oil production. Asphaltenes as defined in 1935 and determined by the appropriate standard test method (ASTM D 91) made use of a petroleum naphtha fraction with narrow density, aniline point and boiling point range [28]. The composition suggested a mainly paraffinic solvent mixture, but although the mixture was clearly defined, it was not unique. The nature of the solvent affects what fraction of the material will become insoluble.

A further sub-classification of asphaltic substances required the material to be further treated to remove “carbenes” (not the organic species: CH2) and “carboids” by dissolving the asphaltenes in benzol (benzene) [29].

Present day practice defines asphaltenes as either n-pentane insoluble (ASTM D 2007) [30], or n-heptane insoluble (ASTM D 6560) [31] while soluble in toluene. The solvents used are pure compounds and, in this respect, asphaltenes are better defined. It should be noted that the two standard test methods used different solvents and different methods and different conditions for separation.

Although it is possible to write down a definition for the asphaltenes in terms of pure compound solubility, the separation of asphaltenes during experimental determination does not only depend

on solubility, but also on the morphology and size of the phase domains of the second phase. This is illustrated by Figure 3-8. In the three cases shown, the amount of the insoluble product may be the same but depending on the morphology and size of the second phase, it will either be efficiently retained by filtration, or not.

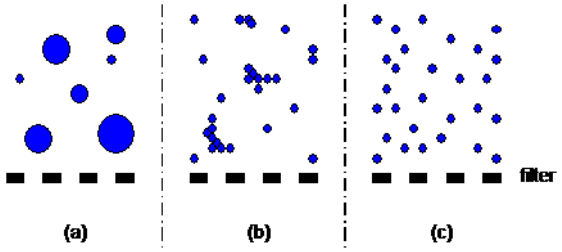

Figure 3-8. Impact of phase domain size and phase aggregation in separation of asphaltenes by filtration. (a) Large phase domains. (b) Aggregated small phase domains. (c) Small phase domains.

This description is supported by experimental observations. The amount of asphaltenes that were recovered from the same oil analysis depended on the filter size [32]. It was found that the size of different structures of asphaltenes that were separated by different sized filtration and without the aid of a solvent were similar and were not preferentially associated with any of the other solubility classes or mineral matter [33]. Thus, experiments looking at asphaltenes at sub-micrometer scale indicated that the ability to separate the second phase dependent on probability of aggregation and that there were no detectable differences in chemistry or solvating environment.

The role of aggregation kinetics in asphaltenes separation was documented [34,35], which depended on the solvent and the asphaltenes concentration. Time was also found to affect the observed onset of asphaltenes separation by spectroscopic means [36]. In essence, time plays a role in the formation of larger second phase domains and will therefore affect separation yield. After separation and solvent removal, the asphaltenes is a solid phase. This may leave the impression that the second phase formation is a form of precipitation, but this view is challenged by observations that indicate that the n-alkane rich phase is actually the second phase that forms from the bulk oil after addition of the n-alkane [37]. The depletion of the bulk oil leaves the asphaltenes enriched phase as the dispersed phase. The morphology of the asphaltenes enriched phase is spherical [32, 38], and the irregular shapes that are observed are aggregates of non-coalesced phase domains. The release of material from the asphaltenes enriched phase domains is limited by mass transport across the phase boundary, which also implies time dependence.

Note that the aggregation of phase domains is not the same as the aggregation of asphaltenes species on molecular scale. The aggregation of species in dilute solution are of the size order 3–6 nm [39], whereas individual phase domains can grow to be of the order of micrometers and the aggregates of phase domains can be correspondingly larger.

The observed differences in the measured n-pentane insoluble content in VR DAO (Table 3-4) that was initially frozen or melted reflects one or more on of the phenomena described. There was no difference in composition and the differences in Table 3-4 reflected the physical changes that were required for material to be separated as n-pentane insoluble material. In principle, the phenomena affecting n-pentane insoluble content measurements, may also have contributed to some of the other observed differences in n-pentane insoluble content caused by reaction or storage.

3.4 Conclusions

In this work it was investigated if asphaltenes formation kinetics was similar to vacuum conversion kinetics that would lead to the same selectivity at different iso-conversion conditions (calculated by using an industrial proprietary kinetic model developed from the ERT concept). As a secondary objective, visbreaking products and their associated asphaltenes sub-fraction were also characterized. The following observations were made from the experimental investigation:

(a) The kinetics of asphaltenes formation was different to the kinetics of vacuum residue conversion since the amount of asphaltenes formed were different at the same conversion and vice-versa.

(b) Iso-conversion conditions as predicted by the industrial kinetic model were not achieved and the differences were attributed to the assumption of ERT concept that may not be representative of the actual process (heat up and cool-down periods are not included in the ERT definition).

(c) Irrespective of reaction conditions, when conversion was lower than 0.4 there was no change in other properties (MCR, refractive index, n-pentane insoluble and free radical content) while for conversions higher than 0.4 the properties changed.

(d) Hydrogen transfer from asphaltenes took place during visbreaking, as indicated by the decrease in H:C molar ratio of asphaltenes precipitated from the visbroken products.

(e) The free radicals present in the products were reactive upon storage. After 210 days stored

under nitrogen, there was not only a decrease in free radical content, but also a 9 wt% increase in n-pentane insoluble material and an increase in refractive index (e.g from 1.5987 to 1.6024 at 20 ºC) of the product obtained at 417 ºC and 30 min. It is likely that the free radicals that were converted upon storage participated in more than one chain transfer reaction that resulted in the formation of different compounds [40].

Reference cited

[1] Strausz, O. P. (2003). *The chemistry of Alberta oil sands, bitumens and heavy oils*. Calgary: Alberta Energy Research Institute.

[2] Rahimi, P. M., Teclemariam, A., Taylor, E., Debruijn, T., & Wiehe, I. A. (2005). Thermal Processing Limits of Athabasca Bitumen during Visbreaking Using Solubility Parameters. *ACS Symposium Series Heavy Hydrocarbon Resources*, 183–196.

[3] Wiehe, I. A. (1993). A phase-separation kinetic model for coke formation. *Industrial & Engineering Chemistry Research*, *32*(11), 2447–2454.

[4] Thermal and Catalytic Processes in Petroleum Refining. (2003). *Thermal and Catalytic Processes in Petroleum Refining*.

[5] Brauch, R., Fainberg, V., Kalchouck, H., & Hetsroni, G. (1996). Correlations Between Properties Of Various Feedstocks And Products Of Visbreaktng. *Fuel Science and Technology International*, *14*(6), 753–765.

[6] Rahimi, P. M., & Gentzis, T. (2003). Thermal hydrocracking of Cold Lake vacuum bottoms asphaltenes and their subcomponents. *Fuel Processing Technology*, *80*(1), 69–79.

[7] Stratiev, D., Nedelchev, A., Shishkova, I., Ivanov, A., Sharafutdinov, I., Nikolova, R., … Atanassov, K. (2015). Dependence of visbroken residue viscosity and vacuum residue conversion in a commercial visbreaker unit on feedstock quality. *Fuel Processing Technology*, *138*, 595–604.

[8] SG, C., & M., D. (1992). *Resid and Heavy Oil Processing*. Paris, Editions Technip

[9] Singh, I., Kothiyal, V., Ramaswamy, V., & Krishna, R. (1990). Characteristic changes of asphaltenes during visbreaking of North Gujarat short residue. *Fuel*, *69*(3), 289–292.

[10] Casalini, A., Mascherpa, A., & Vecchi, C. (1990). Modifications Induced By Visbreaking On Composition And Structure Of Atmospheric Residues. *Fuel Science and Technology International*, *8*(4), 427–445

[11] Cabrales-Navarro, F. A., & Pereira-Almao, P. (2017). Reactivity and Comprehensive Kinetic

Modeling of Deasphalted Vacuum Residue Thermal Cracking. *Energy & Fuels*, *31*(4), 4318–4332.
[12] Yan, T. (1990). Characterization of visbreaker feeds. *Fuel*, *69*(8), 1062–1064.
[13] Aguilar, R. A., & Ancheyta, J. (2016). Modeling Coil and Soaker Reactors for Visbreaking. *Industrial & Engineering Chemistry Research*, *55*(4), 912–924
[14] Singh, J., Kumar, S., & Garg, M. O. (2012). Kinetic modelling of thermal cracking of petroleum residues: A critique. *Fuel Processing Technology*, *94*(1), 131–144.
[15] Kapadia, P. R., Kallos, M. S., & Gates, I. D. (2012). A new kinetic model for pyrolysis of Athabasca bitumen. *The Canadian Journal of Chemical Engineering*, *91*(5), 889–901.
[16] Castillo, J., & Klerk, A. D. (2018). Visbreaking of Deasphalted Oil from Bitumen at 280–400 °C. *Energy & Fuels*, *33*(1), 159–175.
[17] Wang, L., Zachariah, A., Yang, S., Prasad, V., & Klerk, A. D. (2014). Visbreaking Oilsands-Derived Bitumen in the Temperature Range of 340–400 °C. *Energy & Fuels*, *28*(8), 5014–5022.
[18] ASTM International. ASTM D70-09. (2009). Standard Test Method for Density of Semi-Solid Bituminous Materials (Pycnometer Method). West Conshohocken, PA: ASTM International.
[19] Battini, R., Rettich, T. H., Tominaga, T. (1984). The solubility of nitrogen and air in liquids. J. Phys. *Chem. Ref*, 13(2), 563-600.
[20] Zirrahi, M., Hassanzadeh, H., Abedi, J., Moshfeghian, M. (2014). Prediction of solubility of CH_4, C_2H_6, CO_2, N_2, and CO in bitumen. *The Canadian Journal of Chemical Engineering*, 92, 563-572.
[21] Wiehe, I. A. (1992). A solvent-resid phase diagram for tracking resid conversion. *Industrial & Engineering Chemistry Research*, *31*(2), 530–536.
[22] Naghizada, N., Prado, G. H. C., & Klerk, A. D. (2017). Uncatalyzed Hydrogen Transfer during 100–250 °C Conversion of Asphaltenes. *Energy & Fuels*, *31*(7), 6800–6811.
[23] Gould, K. A., & Wiehe, I. A. (2007). Natural Hydrogen Donors in Petroleum Resids†. *Energy & Fuels*, *21*(3), 1199–1204.
[24] Guo, A., Wang, Z., Zhang, H., Zhang, X., & Wang, Z. (2010). Hydrogen Transfer and Coking Propensity of Petroleum Residues under Thermal Processing. *Energy & Fuels*, *24*(5), 3093–3100.
[25] Tannous, J. H., & Klerk, A. D. (2019). Quantification of the Free Radical Content of Oilsands Bitumen Fractions. *Energy & Fuels*, *33*(8), 7083–7093.
[26] Zhang, N., Zhao, S., Sun, X., Xu, Z., & Xu, C. (2010). Storage Stability of the Visbreaking Product from Venezuela Heavy Oil. *Energy & Fuels*, *24*(7), 3970–3976.

[27] Gray, M. R., & Mccaffrey, W. C. (2002). Role of Chain Reactions and Olefin Formation in Cracking, Hydroconversion, and Coking of Petroleum and Bitumen Fractions. *Energy & Fuels*, *16*(3), 756–766.
[28] Sachanen, A. N. (1948). *Conversion of petroleum: production of motor fuels by thermal and catalytic processes*. New York: Reinhold.
[29] Kalichevsky, V. A., & Kobe, K. A. (1956). *Petroleum refining with chemicals*. Amsterdam: Elsevier Pub. Co, p.24.
[30] ASTM D 2007. (2016). Standard test method for characteristic groups in rubber extender and processing oils and other petroleum-derived oils by the clay-gel absorption chromatographic method. West Conshohocken, PA: ASTM.
[31] ASTM D 6560. (2012). Standard test method for determination of asphaltenes (heptane insolubles) in crude petroleum and petroleum products. West Conshohocken, PA: ASTM.
[32] Savvidis, T. G., Fenistein, D., Barré, L., & Béhar, E. (2001). Aggregated structure of flocculated asphaltenes. *AIChE Journal*, *47*(1), 206–211.
[33] Zhao, B., & Shaw, J. M. (2007). Composition and Size Distribution of Coherent Nanostructures in Athabasca Bitumen and Maya Crude Oil. *Energy & Fuels*, *21*(5), 2795–2804.
[34] Haji-Akbari, N., Teeraphapkul, P., & Fogler, H. S. (2014). Effect of Asphaltene Concentration on the Aggregation and Precipitation Tendency of Asphaltenes. *Energy & Fuels*, *28*(2), 909–919.
[35] Haji-Akbari, N., Teeraphapkul, P., Balgoa, A. T., & Fogler, H. S. (2015). Effect of n-Alkane Precipitants on Aggregation Kinetics of Asphaltenes. *Energy & Fuels*, *29*(4), 2190–2196.
[36] Tavakkoli, M., Grimes, M. R., Liu, X., Garcia, C. K., Correa, S. C., Cox, Q. J., & Vargas, F. M. (2015). Indirect Method: A Novel Technique for Experimental Determination of Asphaltene Precipitation. *Energy & Fuels*, *29*(5), 2890–2900.
[37] Mullins, O. C., & Sheu, E. Y. (1995). *Asphaltenes: fundamentals and applications*. New York: Plenum Press., p. 97-130.
[38] Sirota, E. B. (2005). Physical Structure of Asphaltenes†. *Energy & Fuels*, *19*(4), 1290–1296.
[39] Eyssautier, J., Espinat, D., Gummel, J., Levitz, P., Becerra, M., Shaw, J., & Barré, L. (2011). Mesoscale Organization in a Physically Separated Vacuum Residue: Comparison to Asphaltenes in a Simple Solvent. *Energy & Fuels*, *26*(5), 2680–2687.
[40] Yan, Y., De Klerk, A & Prado, G.H. (2019). Visbreaking of vacuum residue deasphalted oil: new asphaltenes formation. Energy & Fuels.

4. The potential factors that result in different conversion when equivalent residence time concept is applied

4.1 Introduction

In Chapter 3, visbreaking reactions were performed based on the equivalent residence time (ERT) concept. The implication of this description is that various reaction temperature and residence time combination can be selected that result in the same conversion. Based on the experimental results, it has been found that iso-conversion conditions as predicted by the industrial kinetic model were not achieved. Therefore, the objective of this work is to investigate factors that could result in different conversion when equivalent residence time concept is applied to visbreaking. The description of most of the experimental work is similar to that in Chapter 3.

4.2 Experimental

4.2.1 Materials

The feed employed for this study is industrially produced vacuum residue deasphalted oil (VR DAO) that was obtained from the Nexen (now CNOOC International) Long Lake upgrading facility in Alberta, Canada. A description of the process can be found in literature review. For this work the VR DAO was sub-sampled in the laboratory and kept in a freezer at -20 °C. The deasphalted oil that has been used in this experiment belong to the same barrel as the deasphalted oil that has been used in Chapter 3. The characterization of Nexen Long Lake deasphalted vacuum residue is shown in Table 3-1. Cylinder gases and chemicals used in this study are presented in Table 3-2.

4.2.2 Equipment and Procedure

The visbreaking reaction was conducted as described in Chapter 3 for Vacuum Residue based on the reaction condition in Table 3-3.

The temperature of Vacuum Residue was recorded every minute before it reached the designed conditions (temperature profile). In this experiment, 417 ºC/30min, 417 ºC/0min, 425 ºC/20min, and 425 ºC/0min were only performed one times to get the temperature profile. Visbreaking at 438 ºC/10min and 438 ºC/0min were performed four times to get the temperature profile and test the

heating rate of fluidized sand bath heater.

4.2.3 Analysis

Experimental products were analyzed to determine their boiling point distribution by simulated distillation, and it has been explained in Chapter 3. Full product characterization was not performed as it was for the previous runs in Chapter 3.

4.3 Results

4.3.1 Material Balance

Similar to section 3.3.2, the visbroken product after reaction was recovered by mechanical means and the material recovered by solvent cleaning was also considered. The amount of liquid product for that can be recovered by spatula on average for each regular reaction (Table 3-3) ranged from 93 %-95 %. The liquid product yield for the corresponding control experiments (Table 3-3) ranged from 91 %-100 %. The uncertainty in the product yield is caused by its viscous nature, specially the products from the control experiment where some material loss occurred during liquid transfer and cleaning. The gas yield was determined based on the mass difference between the pressurized reactor and depressurized reactor. For 417 ºC/30min, and 425 ºC/20min reactions, gas yield was 0.02 g/g feed and 0.015 g/g respectively. For all the control experiment (Table 3-3) and 438 ºC/10min reactions gas yield was less than the amount of nitrogen gas added into the reactor. As it explained in section 3.3.2 some nitrogen gas can dissolve in organic materials [1, 2] which could explain the observed behavior of these experiments.

4.3.2 Cracking conversion

Conversion of the vacuum residue fraction of DAO was determined by using equation 1 from section 3.2.2. And the boiling point distribution of the visbroken products (Table 4-1) and the feed (Table 3-1). During the reactions, the gas yield was considered negligible for conversion calculation (Section 3.3.1).

Table 4-1. Boiling point distribution of visbreaking products obtained at different reaction conditions[a]

Reaction temperature (ºC)	Time at reaction temperature (min)	Naphtha (25 - 190 °C)		Kerosene (190 - 260 °C)		ATM GO (260 - 343 °C)		LVGO (343 - 454 °C)		HVGO (454 - 524 °C)		Residue (+ 524 °C)	
		x	*u*	x	*u*	x	*u*	x	*u*	x	*u*	x	*u*
417[b]	0	1.62	_d	2.13	_d	5.67	_d	7.3	_d	13.21	_d	70.07	_d
425[b]	0	0	_d	2.75	_d	5.00	_d	6.62	_d	12.47	_d	73.16	_d
438[c]	0	5.14	0.86	4.23	1.22	8.68	2.73	12.37	1.11	14.10	0.67	55.48	3.73
417[b]	30	3.47	_d	7.45	_d	10.50	_d	16.99	_d	14.86	_d	46.73	_d
425[b]	20	9.35	_d	8.25	_d	15.30	_d	11.53	_d	11.31	_d	44.26	_d
438[c]	10	10.34	1.32	7.97	0.06	12.81	1.81	14.73	1.94	12.52	0.56	41.64	1.99

[a] (x) average and (*u*) standard uncertainty of samples in triplicate are reported
[b]Analysis only performed once.
[c]Analysis performed four times.

Table 4-2. Cracking conversion of vacuum residue fraction of VR DAO at different reaction conditions[a]

Reaction conditions			Vacuum residue conversion[b]	
Description	**Temperature (°C)**	**time (min)**	**x**	***u***
Control	417[b]	0	20.99	_d
	425[b]	0	17.50	_d
	438[c]	0	37.34	4.26
Regular reactions	417[b]	30	47.30	_d
	425[b]	20	50.09	_d
	438[c]	10	52.98	2.20

[a] (x) average and (*u*) standard uncertainty of samples in triplicate are reported
[b]Analysis only performed once.
[c]Analysis performed four times.

In Table 4-2, the conversion of vacuum residue fraction of VR DAO increase as the reaction temperature increase and residence time decrease. However, in one of the control experiments, product at 417 ºC has higher conversion compare to product at 425 ºC. This phenomenon could be due to the different heating rate experienced by each of the experiment which will be explained in section 4.3.3.

4.3.3 The impact of heating rate to the visbreaking reactions

Based on previous observations, the heating rate provided by sand bath was not stable. In this study 438 ºC/10min were performed three more times to evaluate the impact of heating rate to the visbreaking reactions. Figure 4-1 is the heating rate diagram of 438 ºC/10min in three runs. In this diagram each run has different heating rate. 438 ºC/10min run1 has the fastest heating rate, run 2 has the lowest heating rate and run 3 has the medium heating rate.

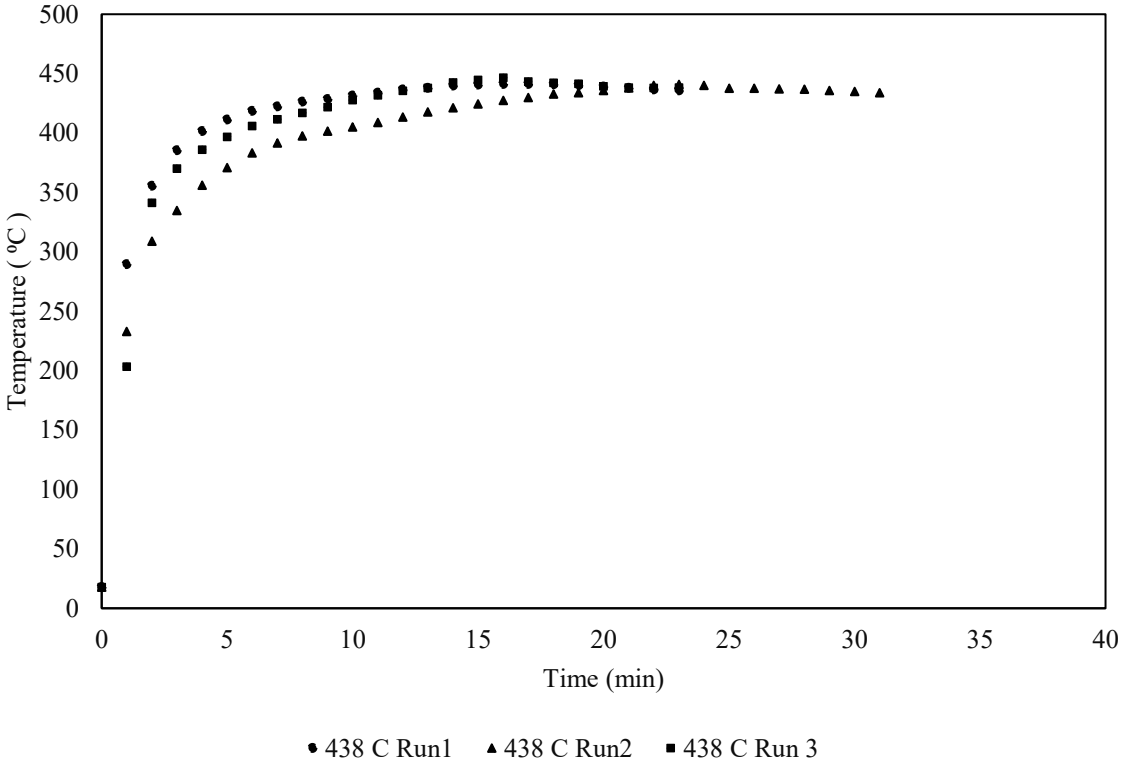

Figure 4-1. Temperature profile of 438 ºC/10min run 1 run 2 and run 3.

Due to the different heating rate and heating time, the amount of asphaltenes and residue conversion of the liquid product also changed (Figure 4-2). Regular product from 438 ºC/10min Run 1 reacted under highest heating rate and shorter heating time has the highest asphaltenes content. Regular product 438 ºC/10min from reacted under medium heating rate and time has the lowest asphaltenes content. On the other hand, regular products under 438 ºC/10min have similar residue conversions (Figure 4-3). However liquid product at 438 ºC/0min has different residue conversion under different heating rate.

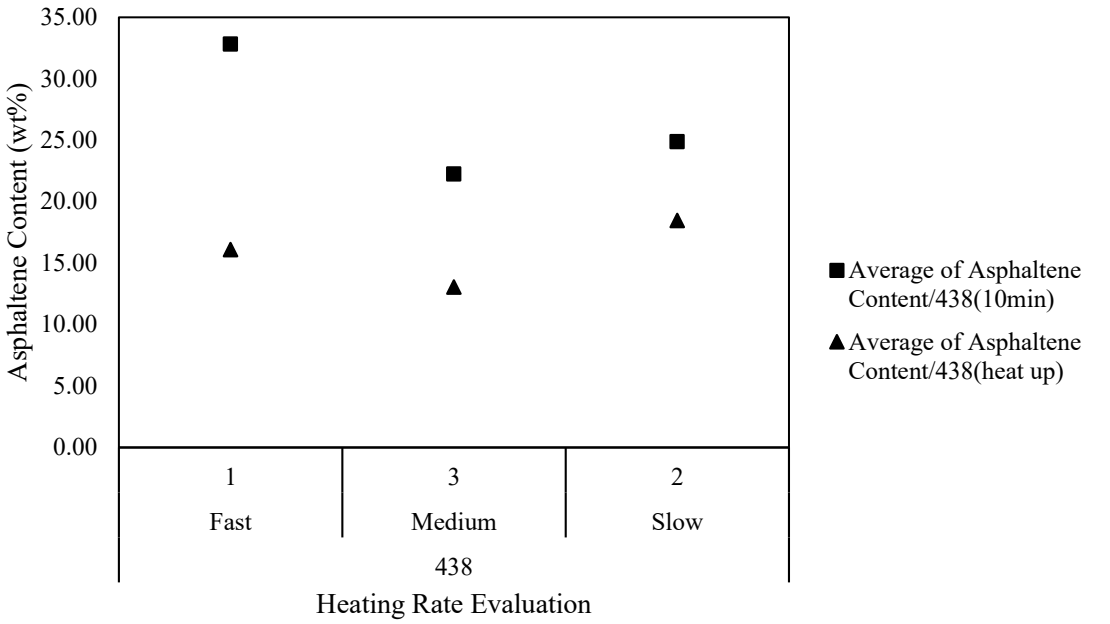

Figure 4-2. Asphaltenes content of 438 ºC regular and heat up reactions at different heating rate.

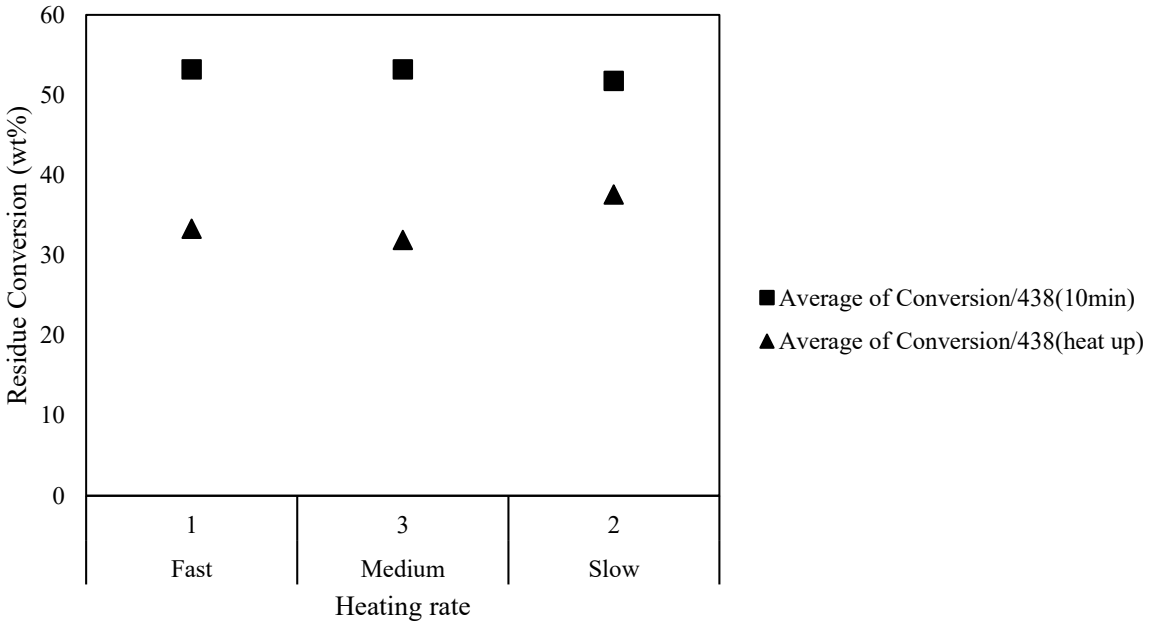

Figure 4-3. Residue conversion of 438 ºC regular and heat up reactions at different heating rate.

4.4 Discussion

4.4.1 Equivalent residence time (ERT) concept

With measured temperature versus time profiles, it was possible to calculate the ERT for visbreaking reactions that performed in this study and reactions in Chapter 3 (Table 3-3). The ERT during heating, cooling, and isothermal periods were calculated by using equation 1 as defined by Yan [3], where T_{ref} = 711 K (438 °C), E_a = 209.5 kJ·mol^{-1}, and R = 8.314 kJ·mol^{-1}·K^{-1}, and the results are presented in Table 4-3.

$$ERT\ at\ T_{ref} = \sum_{i=1}^{n} \Delta t_i . \exp \frac{-E_a}{R} \left(\frac{1}{T_i} - \frac{1}{T_{ref}} \right) \quad (1)$$

Table 4-3. Equivalent residence time (ERT) of visbreaking of VR DAO for different process conditions

Reaction temperature (ºC)	Time at reaction temperature (min)	Heating time (min)	Cooling time (min)	ERT heating (s)	Actual ERT isothermal (s)	ERT cooling (s)	Total ERT (s)	Temperature during isothermal period (°C)	
								x	*u*
417	0	13	94	117	0	15	132		
425	0	17	93	115	0	35	150		
438	0	16	110	399	0	92	491		
438	0	12	92	322	0	14	336		
438	0	20	79	397	0	23	420		
438	0	12	77	246	0	34	280		
417	30	8	108	61	536	7	604	414	4
425	20	16	102	128	549	12	689	421	8
438	10	9	97	110	772	71	953	441	5
438	10	12	92	322	703	14	1039	439	2
438	10	20	79	397	645	23	1066	438	2
438	10	12	77	246	780	34	1060	442	3

[a] (x) average and (*u*) standard uncertainty of recorded during the isothermal period

As can be seen from the equation 1, it represents the numerical integration of the ERT over time that was divided into *n* segments, where the ERT for each time segment (Δt_i, s) and temperature at that time segment (T_i, K) was calculated. The measured temperature values were used for heat-up, isothermal, and cool-down periods. A slight variation in measured temperature was noted during the isothermal period.

The relationship between vacuum residue conversion and calculated ERT is shown in Figure 4-4. Several observations can be made:

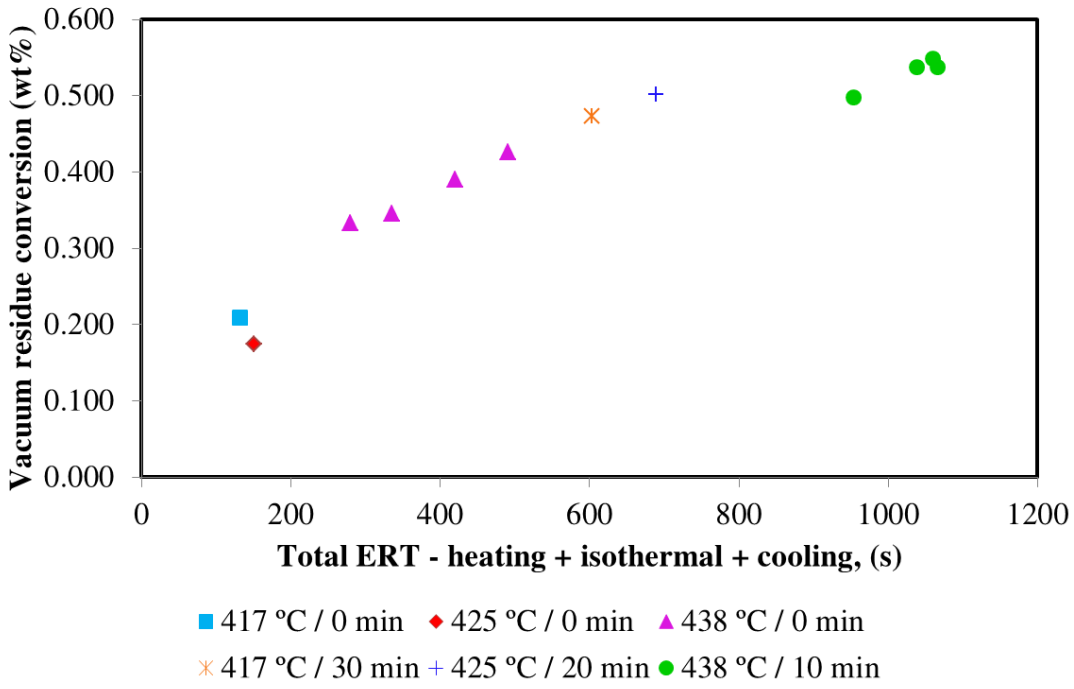

Figure 4-4. Relationship between vacuum residue conversion and ERT

(a) At equivalent residence times of 600 to 1100 s, near similar conversions (~ 0.50) were achieved, despite the differences in ERT.

(b) Conversion increased nearly linearly with increasing ERT between 100 and 600 s, which is not consistent with first order kinetics (section 3.1). (In a different study [4], zero-order kinetics was observed for thermal conversion of vacuum residue deasphalted oil at 360 °C).

(c) The rate of conversion within the first 100 s of the ERT accounted for about 30–40 % of the maximum conversion that was achieved.

(d) When the results in Figure 4-1 are compared to the results in Table 3-6 from section 3.3.3, the anomalous high conversion obtained the control experiments obtained at 438 °C were not observed, but the results highlighted the variation due to differences in heat-up and cool-down temperature profiles in repeat runs.

Similar ERT should provide similar conversion of vacuum residue, but this is not what was found, as was evident from the near similar conversion at ERT > 600 s. The work highlighted the importance of taking the temperature history into account. As the calculations in Table 4-3 showed, the heat-up and cool-down periods should not be discounted. As stated by Sachanen [5], "cracking begins as soon as temperature is sufficiently high", which started during the first stages of the heating process.

4.4.2 Assumptions in ERT theory

The ERT (equation 1) is a useful method for presenting thermal conversion data obtained at different conditions on a comparable basis. However, when employing the ERT concept for the modelling of visbreaking, additional assumptions are made, namely, single average activation energy, first order reaction, and ideal plug-flow reactor behavior.

During the experiment, a constant volume batch reactor was used, in this calculation, an isothermal reaction at steady state was considered. The mathematical expression for constant volume batch reactor is given by equation 2

$$(-r_A) = -\frac{1}{V}\frac{dN_{Ao}(1-x)}{dt} \tag{2}$$

Where r is the reaction rate, V is the volume of the reactor, N_{Ao} is the weight of the feed, x is the conversion of the feed and t is the residence time of the reaction condition. The first order rate law is given by

$$(-r_A) = k_A C_{Ao}(1-x) \tag{3}$$

Where k_A is the kinetic constant for reaction and C_{Ao} is the concentration of the feed. Combining equation 2 and 3 the kinetic constant for each reaction could be calculated by

$$k_A = \frac{-\ln(1-x) + \ln(1-x_o)}{t} \tag{4}$$

Where x_o represent the average conversion that happed during the heat up process. The kinetic constants could also be expressed by the Arrhenius equation [6]

$$k_A = Ae^{\frac{-E_a}{RT}} \quad (5)$$

Where T is the reaction temperature, R is the ideal gas constant and A is the pre-exponential factor. In this work A was assumed as lnA equal to 42.27 h^{-1}[6]. Finally, the activation energy can be calculated by

$$E_a = -\ln(\frac{k_A}{A})RT \quad (6)$$

Figure 4-5. shows the calculated activation energy at each reaction conditions.

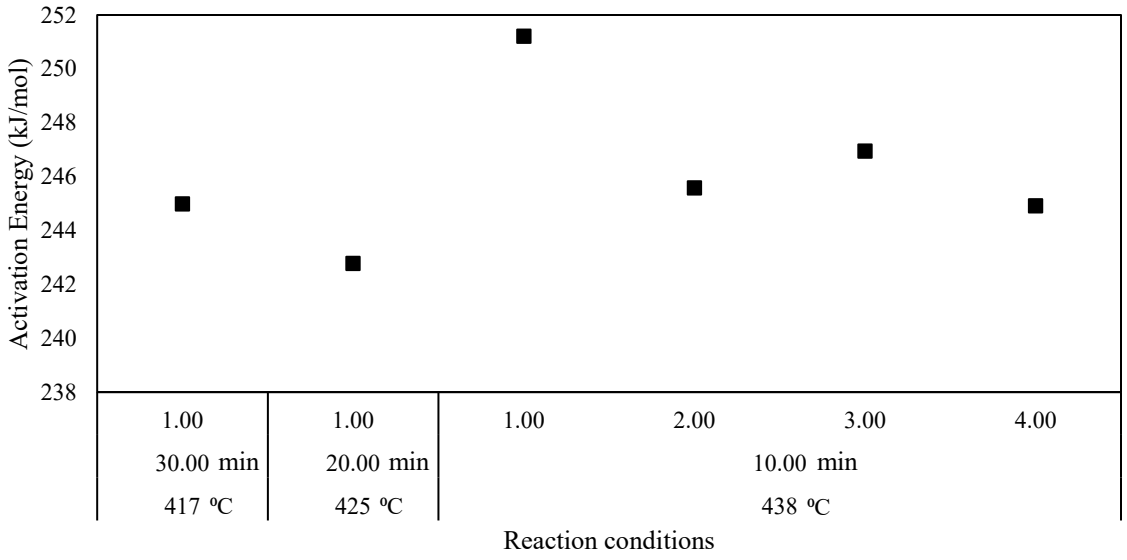

Figure 4-5. Estimated activation energy at each reaction conditions.

Based on Figure 4-5, it is unlikely that the activation energy remains constant, or that there is a single activation energy value. The activation energy is the average activation energy of thermal cracking that is employed to represent a distribution of different activation energies. As conversion progresses, the distribution of activation energies changes, causing a change in the average activation energy. This conversion dependent change in activation energy is approximated in some kinetic models for pyrolysis [7, 8].

4.5. Conclusion

The iso-conversion conditions as predicted by the industrial kinetic model were not achieved and the difference were attributed to the assumptions of ERT concept that may not be representative of the actual process (constant activation energy, plug-flow reactor vs batch reactor, first-order reaction, and the fact that heat up and cool-down periods are not included in the ERT definition).

When heat-up and cool-down periods were considered to calculate the total ERT for each of the reaction conditions, it was observed that iso-conversion is achieved when ERT was in the range of 600-1100 s.

For ERT lower than 600s, conversion increased nearly linearly with increase of ERT, which indicated that it was not a simple first order reaction and first order reaction kinetics is one of the assumptions of the ERT concept. In addition, before reach the designed visbreaking temperature, different heating rate will also affect the amount of asphaltenes that will be formed in the visbroken product.

Reference cited

[1] Battino, R., Rettich, T. R., & Tominaga, T. (1984). *The solubility of nitrogen and air in liquids*. New York: American Chemical Society and the American Institute of Physics for the National Bureau of Standards.

[2] Zirrahi, M., Hassanzadeh, H., Abedi, J., Moshfeghian, M. (2014). Prediction of solubility of CH4, C2H6, CO2, N2, and CO in bitumen. *The Canadian Journal of Chemical Engineering,* 92, 563-572.

[3] Yan, T. (1990). Characterization of visbreaker feeds. *Fuel*, *69*(8), 1062–1064.

[4] Castillo, J., & Klerk, A. D. (2018). Visbreaking of Deasphalted Oil from Bitumen at 280–400 °C. *Energy & Fuels*, *33*(1), 159–175.

[5] Sachanen, A. N. (1948). *Conversion of Petroleum; Production of Motor Fuels by Thermal and Catalytic Processes*. New York, Reinhold Pub. Corp.

[6] Hayes, R. E., & Mmbaga, J. P. (2013). *Introduction to chemical reactor analysis*. Boca Raton: CRC Press.

[7] Foltin, J. P., Lisboa, A. C. L., & Klerk, A. D. (2017). Oil Shale Pyrolysis: Conversion Dependence of Kinetic Parameters. *Energy & Fuels*, *31*(7), 6766–6776.

[8] Wang, S., Chung, K., Masliyah, J. H., & Gray, M. R. (1998). Toluene-insoluble fraction from thermal cracking of Athabasca gas oil: formation of a liquid-in-oil emulsion that wets hydrophobic dispersed solids. *Fuel*, *77*(14), 1647–1653.

5. Storage stability of visbroken products

5.1. Introduction

Visbreaking is one of the strategies commonly used to reduce bitumen viscosity of Canadian oilsands bitumen to enable pipeline transport. It is a mild thermal cracking process where vacuum residue conversion is limited by the onset of coke formation. The visbroken product with low viscosity is favorable for transportation but the instability can make the transportation and storage difficult [1]. The stability of visbroken product usually refers to their resistance to change in properties in long-term storage due to chemical reactions. Generally, unsaturated components and free radicals produced by cracking reactions tend to make oils more prone to instability during storage [2].

In chapter 3, visbreaking reactions were performed under the following reaction conditions: 417 °C/30 min, 424.6 °C/20 min and 438 °C/10 min. The reaction product from one of the experiments (thermal conversion at 417 °C/30 min) was kept under nitrogen atmosphere for 210 days and re-analyzed. There was a 9 wt % increase in the *n*-pentane insoluble content. The free radical content decreased and there was an increase in refractive index. However, free radicals could have reacted immediately after reaction, i.e, changes in product properties could have happened before 210 days storage.

Therefore, the objective of this work was to investigate whether free radicals formed during visbreaking were stable and persistent or would some of these species continue to react even at ambient conditions. The investigation was performed by analyzing visbroken products immediately after reaction and after 2, 4, 8, and 12 weeks storage under nitrogen. Moreover, it was speculated in Chapter 3 that asphaltenes participate in hydrogen transfer reactions. Therefore, as a secondary objective, the nature of hydrogen transfer during storage was also evaluated by spiking visbroken product with model compounds and conversion of the model compounds was determined after 2, 4, 8, and 12 weeks storage.

5.2. Experimental

5.2.1. Materials

The feed used in this study is the bitumen obtained from the Athabasca region of Alberta, Canada. Characterization of bitumen feed and its *n*-pentane insoluble material are presented in Table 5-1.

Standard uncertainties reported correspond to the repeatability of the measurement.

Table 5-1. Characterization of the Athabasca bitumen feed material and its *n*-pentane insoluble material

Property	Athabasca bitumen		Athabasca bitumen sub fractions	
			n-pentane insoluble[b]	
	x	u	x	u
Boiling point distribution[c] (wt%)				
naphta (28-190 °C)	2.0	0.0	_d	_d
kerosene (190 - 260 °C)	2.7	0.6	_d	_d
atmospheric gas oil (260 - 343 °C)	10.0	0.0	_d	_d
light vacuum gas oil (343 - 454 °C)	22.7	2.3	_d	_d
heavy vacuum gas oil (454 - 524 °C)	12.3	0.6	_d	_d
vacuum residue (> 524 °C)	50.3	2.3	_d	_d
n-pentane insoluble content[e] (wt%)	22.3	0.8	_d	_d
elemental analysis (wt%)				
carbon	83.4	0.1	81.1	0.1
hydrogen	10.4	0.1	8.1	0.06
sulfur	4.9	0.1	8.4	0.2
nitrogen	0.5	0.0	1.2	0.02
H:C molar ratio	1.5		1.2	
density (kg/m^3)				
20 °C	1008.3	1.8	_d	_d
40 °C	995.8	1.7	_d	_d
60 °C	983.3	1.9	_d	_d
viscosity at 20 °C[f]				
10 s^{-1}	665.5	0.8	_d	_d
1 s^{-1}	611.6	0.7	_d	_d
mineral matter content (wt%)	2.1	0.4	_d	_d
micro carbon residue (wt %)	10.4	0.4	_d	_d
free-radical content (spins/g) [g]	1.5×10^{18}	0.01	6.9×10^{18}	0.08

[a] Average (x) and standard uncertainty (*u*) of analyses in triplicate
[b] *n*-pentane insoluble material subfraction obtained from Athabasca bitumen
[c] Determined by simulated distillation analysis in triplicate.
[d] Analysis not performed for this sample
[e] See Table B3
[f] Average viscosity for 10 measured points at each shear rate
[g] Based on ESR analysis calibrated with DPPH

Cylinder gases, chemicals, and calibration materials used in this study are presented in Table 5-2. In this study, α-metylstyrene, dihydronaphthalene and 9,10-dihydroanthracene were commercially obtained to measure the hydrogen transfer rate during storage of the product obtained at 420 ºC and 10 min. These compounds were used directly without further purification.

Table 5-2. Chemicals and cylinder gases employed in this study.

Compound	Formula	CASRN[a]	Mass fraction purity[b]	Supplier
chemicals				
toluene	C_7H_8	108-88-3	0.995	Fisher Scientific
n-pentane	C_5H_{12}	109-66-0	0.997	Fisher Scientific
carbon disulfide	CS_2	75-15-0	0.9999	Fisher Scientific
methanol	CH_4O	67-56-1	0.999	Fisher
α-metylstyrene	C_9H_{10}	98-83-9	0.99	Sigma Aldrich
dihydronaphthalene	$C_{10}H_{10}$	447-53-0	0.98	Sigma Aldrich
9,10-dihydroanthracene	$C_{14}H_{12}$	613-31-0	0.97	Sigma Aldrich
Ccylinder gases	N_2	7727-37-9	0.99999[c]	Praxair
nitrogen	H_2	7740-59-7	0.99999[c]	Praxair
helium	O_2/N_2 mix	132259-10-0	-	Praxair
air				
Calibration materials				
2,2-diphenyl-1-picrylhydrazyl (DPPH)	$C_{18}H_{12}N_5O_6$	1898-66-4	-	Sigma Aldrich
reference material 5010	-	-	-	Supelco
polywax 655	-	-	-	Agilent

[a] CASRN = Chemical Abstracts Services Registry Number
[b] This is the purity of the material guaranteed by the supplier; material was not further purified
[c] Mole fraction purity

5.2.2. Equipment and Procedure

The visbreaking reaction was conducted as described in Chapter 3 for Vacuum Residue. In this

study, Athabasca bitumen from Suncor was used as the feed material and it was reacted at 420 °C for 10 minutes.

The reaction was performed for 12 runs in one day and the products were mixed for analysis. For each run, around 25 g of bitumen was added and after the reaction about 180 g of visbroken product was obtained in total. The product was also collected only by mechanical means. The combined visbroken product from 12 runs produced at 420 °C for 10 min is called Product A.

In this study, to understand if bitumen behaves as hydrogen donor or hydrogen acceptor during thermal cracking or storage of the visbreaking product, α-methylstyrene, 9, 10-dihydroanthracene and dihydronaphthalene were used to evaluate hydrogen transfer on a species-level. If bitumen is spiked with hydrogen acceptor molecules such as α-methylstyrene, the hydrogen donor ability of bitumen is indicated by the conversion of α-methylstyrene into cumene as shown in Figure 5-1.

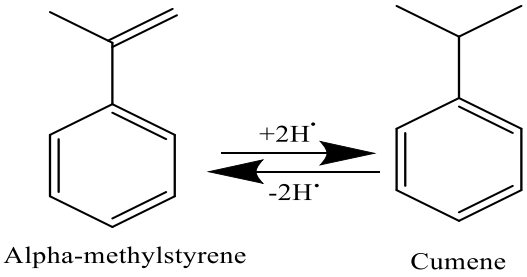

Figure 5-1. Hydrogen transfer between α-methylstyrene and cumene [3]

On the other hand, if bitumen is spiked with a hydrogen donor molecule such as 9,10-dihydroanthracene (Figure 5-2), the hydrogen accept ability of the bitumen is indicated by the conversion of 9,10-dihydroanthracene into anthracene [3].

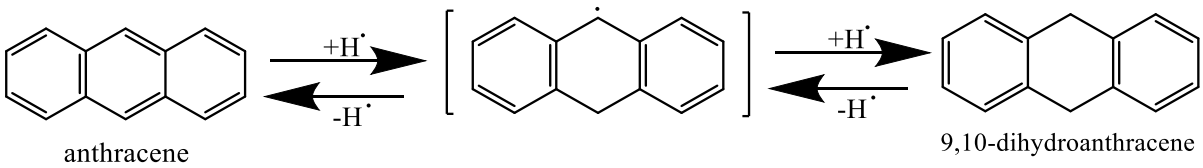

Figure 5-2. Hydrogen transfer between anthracene and 9,10-dihydroanthracene [3]

In addition, chemicals such as dihydronaphthalene has both hydrogen acceptor and hydrogen

donor properties (Figure 5-3) [4]. It can accept two hydrogen atoms to become tetralin, or it can donate two hydrogen atoms to become naphthalene [4]. This chemical can then be used to measure the capacity of hydrogen donor and hydrogen acceptor of a species related to the conversion of dihydronaphthalene [4].

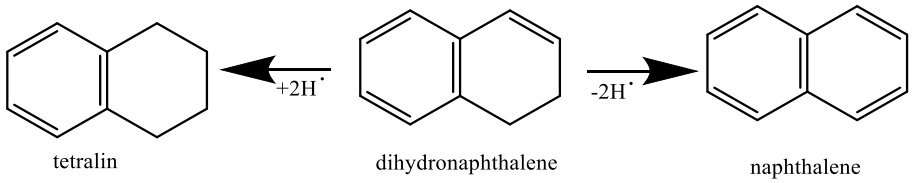

Figure 5-3. Dihydronaphthalene as hydrogen acceptor (left side reaction) and hydrogen donor (right side reaction) [4]

Around 9 g of Product A was mixed with 10 wt% of α-mthylstyrene (Product A-α), the exact mass of liquid product and α-mthylstyrene were recorded. Around 7 g of liquid product was mixed with 10 wt% of dihydronaphthalene (Product A- β), the exact mass of liquid product and dihydronaphthalene were recorded. Around 7 g of liquid product was mixed with 10 wt% of 9, 10-dihydroanthracene (Product A-γ), the exact mass of liquid product and 9, 10-dihydroanthracene were recorded.

The following analysis were performed for Product A within 3 days after the reaction: electron spin resonance (ESR), proton nuclear magnetic resonance (^{1}H-NMR), density, refractive index, viscosity, microcarbon residue (MCR), mineral matter and *n*-pentane insoluble content. For the *n*-pentane insoluble material from product A, elemental analysis, ESR, and ^{1}H-NMR analysis were performed.

Product A-α, product A-β and product A-γ were characterized by using the methanol extraction procedure explained in section 5.2.3 and then methanol extract was analyzed by the gas chromatography with flame ionization detector (GC-FID). The identity of the species was analyzed by using the chromatography with mass spectrometry (GC-MS).

After the analysis, product A, product A-α, product A-β and product A-γ were stored under the

nitrogen atmosphere. Same analysis was performed after 2, 4, 8, and 12 weeks of storage.

5.2.3. Analysis

Most of the analyses were already described in section 3.2.3. In this study the following new analyses were also performed.

Density of the feed and liquid product were measured by the Anton Paar DMA 4500M at 20 ºC, 40 ºC and 60 ºC. Results were accurate to 0.00002 g/cm^3 and the temperature accuracy was 0.01 ºC. A calibration was carried out with a standard (ultra-pure water) provided by Anton Paar at 20 ºC.

About 0.1 g of each product A-α, product A-β and product A-γ (as described in section 5.2.2) were extracted with 10 mL of methanol to recover the model compounds. The methanol extraction was performed under constant stirring at room temperature over a period of 30 min. The methanol extract was filtered, and about 0.1 g of biphenyl was added as an internal standard to a known amount to the methanol extract. Conversion calculation of product A-α, product A-β and product A-γ is included in Appendix B.

The methanol extracts were quantitatively analyzed by using a gas chromatograph with a flame ionization detector (GC-FID). Quantification of reaction products was performed using a 7890A Agilent GC. An Agilent J&W VF-200ms capillary column (30 m × 0.25 mm × 0.25 μm) with trifluoropropyl-type stationary phase was employed for separation. The split/splitless injector was kept at 300 °C and a split ratio 100:1 was employed. Nitrogen was used as the carrier gas with flow rate of 1.5 ml/min. The temperature program was: 100 °C for 0 min; increased from 100 °C to 220 °C at 10 °C/min; increased from 220 °C to 300 °C at 5 °C/min and hold for 5 min at 300 °C.

Methanol extracts from liquid product with model compounds were also analyzed by gas chromatography mass spectrometry (GC-MS). The instrument used was an Agilent 7820 with 5977E mass spectrometer. Separation was performed on an HP-5 column, 30 m×0.25mm×0.25 µm, using helium as a carrier gas. The temperature started at 100 ºC and was increased by 10 ºC/min to 220 ºC. After temperature reached to 220 ºC, it was increased by 5 ºC/min to 300 ºC and

hold for 5 min.

Thermogravimetric analysis was used to determine the micro carbon residue (MCR) of the feed and liquid products as well as the mineral matter of the feed and asphaltenes formed during visbreaking. The instrument used was a Mettler Toledo TGA/DSC1 equipped with LF 1100 furnace, sample robot, and MX5 internal microbalance. For the mineral matter analysis, approximately 15 mg of sample was weighed in an aluminum oxide crucible. The sample was then heated from 25 to 900 °C at 10 °C/min in an oxidizing atmosphere to remove the organic matter by combustion. The air flow rate was 100 mL/min. For the MCR analysis, approximately 15 mg of sample was placed in an aluminum oxide crucible and heated from 25 to 500 °C at 10 °C/min followed by an isothermal period of 30 min at 500 °C in a nitrogen atmosphere. The nitrogen flow was 100 mL/min. Both nitrogen and air flow rate were controlled with a Mettler GC 10 gas controller.

Proton nuclear magnetic resonance (^{1}H-NMR) analysis was used to determine the percentage of saturated, olefinic and aromatic hydrogen of feed, products, n-pentane insoluble material of the feed and products. About 100 mg of samples were dissolved in 700 μL of chloroform-D. The analysis was performed using a 60 MHz NMReady-60 spectrometer from Nanalysis Corporation. Analyses were the average of 32 scans with a scan delay of 20 seconds. The percentage of saturated, olefinic and aromatic hydrogen was determined based on their shift values on the ppm-scale by using MestReNova software. The sample diagram can be found in figure B1 from Appendix B.

5.3. Results

5.3.1. Material balance for visbreaking reactions

Similar to section 3.3.2, the visbroken product after reaction was recovered by mechanical means. The amount of product that could be recovered with a spatula from 12 reactors as described in section 5.2.2, was about 96 wt% of initial feed (Table 5-1). The remainder of the material was recovered using solvent to calculate material balance closure but was kept separate.

Table 5-3. Mass balance (wt %) for visbreaking reactions at 420 °C for 10 min and initial pressure of 2 MPa for 12 runs.

Run number	Balance Material for each run (wt %)	x	u
1	103.0	95.5	7.5
2	89.9		
3	102.0		
4	88.7		
5	99.1		
6	98.1		
7	103.0		
8	102.5		
9	100.2		
10	92.3		
11	80.9		
12	86.6		

Like section 3.3.2 each reactor was pressurized with nitrogen to 2 MPa gauge initially and it was observed that there was an increase in pressure during reaction which ranged from 5 MPa to 7.5 MPa gauge. After cooling, the final internal pressure ranged between 2 MPa to 3 MPa gauge. This observation indicates that most of the gases responsible for the increase in pressure during the reaction were condensed or dissolved in the liquid product during cooling. The gas yield was determined by calculating the mass difference between the pressurized reactor and depressurized reactor. However, gas released during depressurization from 4 of the reactors was less than the amount of nitrogen gas added into the reactor. As it is explained in section 3.3.2, some of the nitrogen can dissolve in organic materials. Therefore, the gas yield was calculated based on the difference between complete material balance closure and the measured liquid/solid product yields. Based on this calculation, the total gas yield from 12 reactors was calculated to be 4 wt%.

5.3.2. Characterization of product A and its asphaltenes

In this study, product A was the mixture of visbroken product from 12 reactors. After the visbreaking reaction, density of liquid product A was measured immediately for three times after the reaction. This was referred as the “first measurement”. Product A was re-analyzed after 2 weeks, 4 weeks, 8 weeks, and 12 weeks. Standard deviation for this analysis was very small which was between 0 to 0.1. Figure 5-4 shows the density of liquid product at different storage time. For each measurement, density was measured at 20 ºC, 40 ºC, and 60 ºC, since density measured at 40 ºC

and 60 ºC shows the similar trend as density measured at 20 ºC, Figure 5-4 only shows the average results measured at 20 ºC. The average and standard deviation for density measured at each temperature is presented in Table B1 from Appendix B.

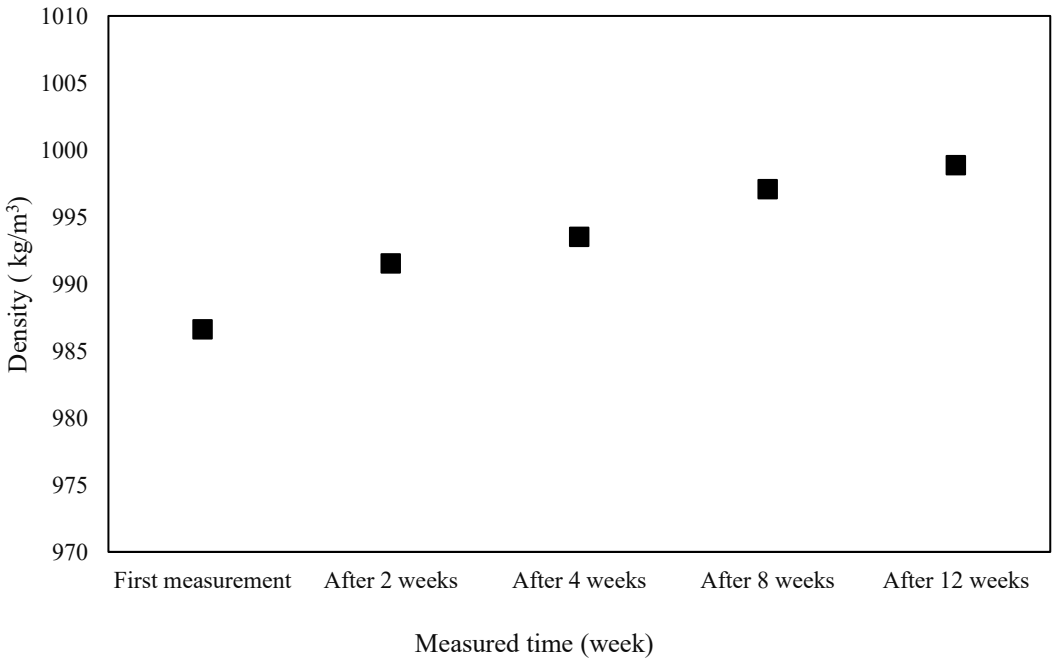

Figure 5-4. Density of visbroken product A measured at 20 °C at different storage time.

It can be noted from Figure 5-4 that the density of visbroken product increased during the first 8 weeks of storage and remained nearly constant between 8 and 12 weeks at 997 kg/m^{3}and 998 kg/m^3 respectively.

Like the measurement of density, viscosity of product A was measured at the same periods of time. For the first measurement, viscosity was measured at 20 ºC with 10 s^{-1} and 1 s^{-1} shear rate, however due to the practical reasons, after the first measurement, viscosity was measured at 20 ºC with 10 s^{-1} and 5 s^{-1} shear rates, respectively. At each shear rate, one analysis was performed with 10 measuring points. Standard deviation for each measurement was very small which was between 0.01 and 0.03. Figure 5-5 shows the average viscosity of product A measured at 20 ºC with 10 s^{-1} shear rates at different storage periods. The average and standard deviation of viscosity measured at different time and shear rate is presented in Table B2 from Appendix B.

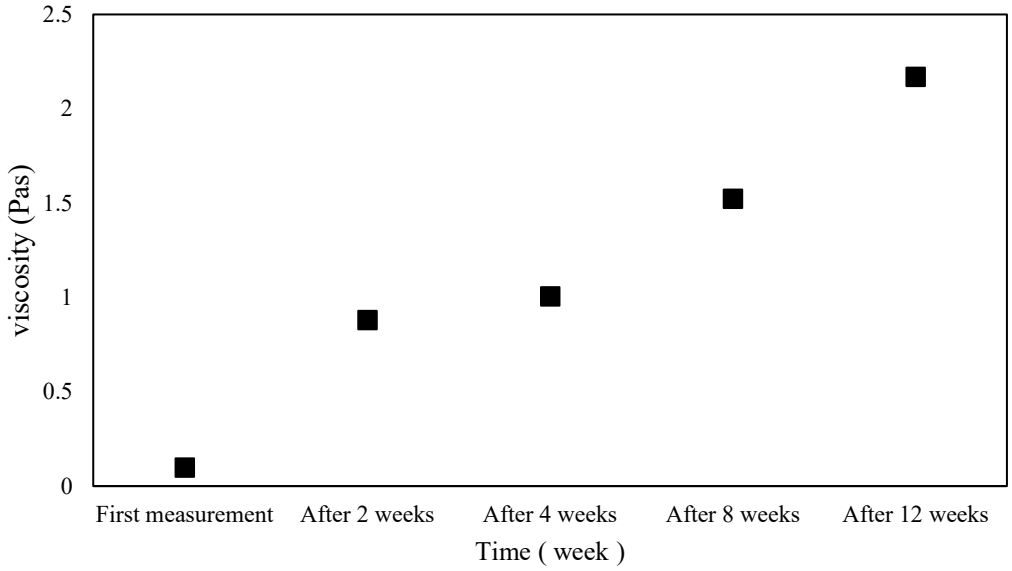

Figure 5-5. Viscosity of visbroken product A measured at 20 ºC and 10 s^{-1} shear rates, at different storage time.

The viscosity of product A measured at different time is shown in Figure 5-5. As the storage time increased, the viscosity of product A was also increased. However, compared to the density, viscosity was increased slowly in the first 4 weeks and after 4 weeks the viscosity of product A increased dramatically.

n-Pentane insoluble content of product A was determined at different storage periods (Figure 5-6). The average and standard deviation of asphaltenes content measured at different time is presented in Table B3 from Appendix B.

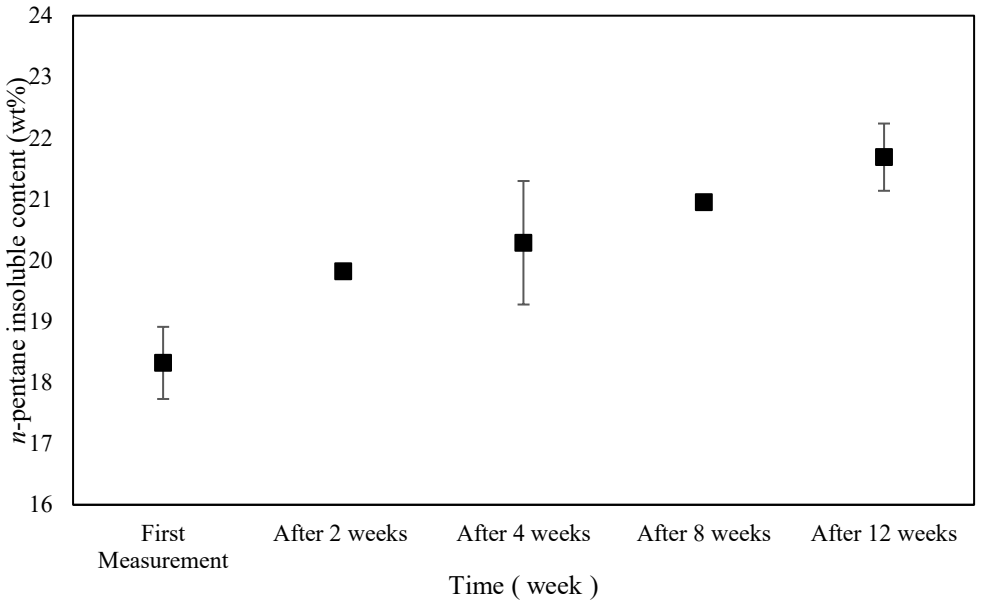

Figure 5-6. *n*-pentane insoluble content of product A measured at different storage time

From figure 5-6 it is obvious to see that as the storage time increased, the asphaltenes content of product A was also increased. After the first measurement, the asphaltenes content of product A measured at each time has been increased compare to the previous measurement and it is statistically significant at 95 % confidence except week 8.

Quantification of the free radical content of product A and its asphaltenes (*n*-pentane insoluble material) at different storage time are shown in Figures 5-7 and 5-8, respectively. Average and standard deviation of free radical contents for product A and of its asphaltenes is shown in Table B4 in Appendix B.

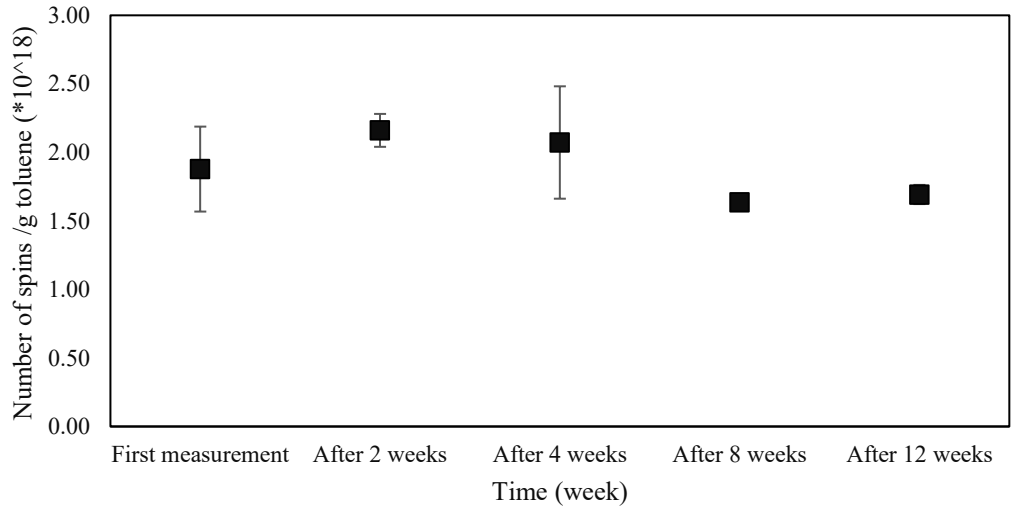

Figure 5-7. Free radical content of product A at different storage time

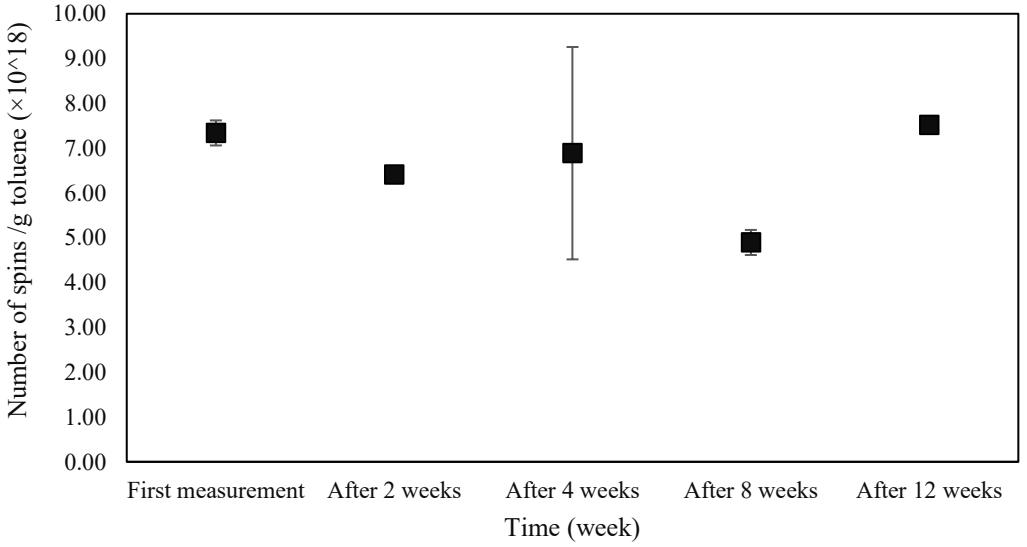

Figure 5-8. Free radical content of asphaltenes from product A at different storage time

It can be observed from Figures 5-7 and 5-8 that as the storage time increased, the free radicals in product A remained nearly at a constant value. On the other hand, free radical content in asphaltenes changed with the storage time. In the first 8 weeks, free radicals in asphaltenes tend to decrease as the storage time increased. However, after 8 weeks the free radicals in asphaltenes increases back to the first measurement value.

The refractive index values measured at 20 ºC has the same trend as those measured at 40 and 60 ºC, so Figure 5-9 only shows the refractive index of product A at different storage time at 20ºC. The sample from product A was measured for three times. Average and standard deviation of refractive index at 20, 40 and 60 ºC are very small, they are between 0 and 0.0018 which is shown in Table B5 from Appendix B as the supporting information.

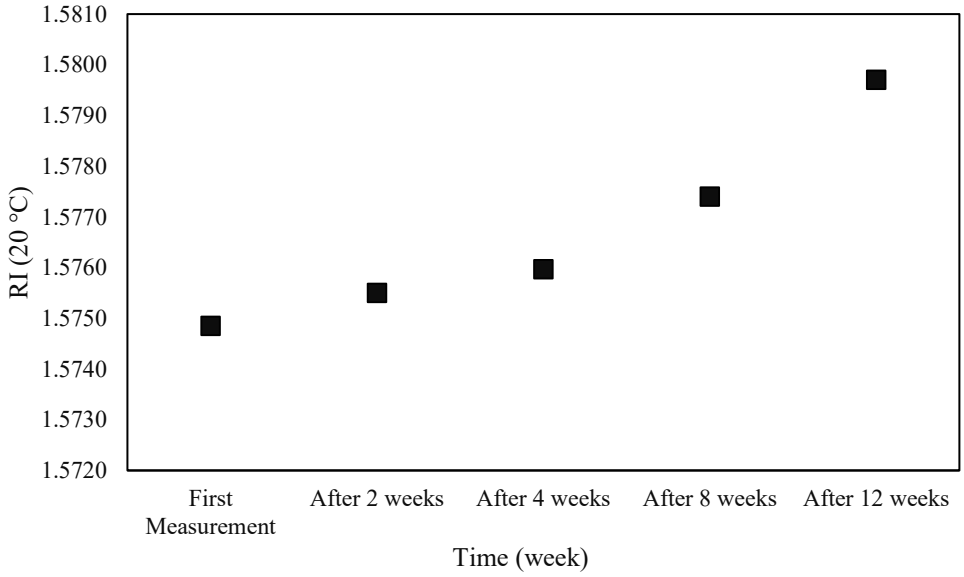

Figure 5-9. Refractive index (RI) of product A measured at 20 ºC

From Figure 5-9, it is observed that in the first 4 weeks, refractive index increased slowly from 1.5749 to 1.5760. After 4 weeks of storage refractive index of product A increased dramatically from 1.5760 to 1.5797. In general, paraffinic compounds have low RI while aromatic compounds have high RI values, so the results in Figure 5-9 may indicate that as the storage time increases, product A will become more aromatic than before. It is also possible that the increase RI reflects addition reactions, because the RI of higher molecular weight compounds in the same class is higher than that of the lower molecular weight compounds. Additional alternative interpretation will be discussed in section 5.4.1.

At each storage time, the content of carbon, hydrogen, sulfur, and nitrogen of the asphaltenes precipitated from product A was determined. Figures 5-10, 5-11, and 5-12 presents the H:C, N:C and S:C molar ratio of asphaltenes from product A at each storage time. Analysis were performed

three times. Table B6 in Appendix B shows the average and standard deviation of H:C, N:C and S:C in molar ratio of asphaltenes from product A as the supporting information.

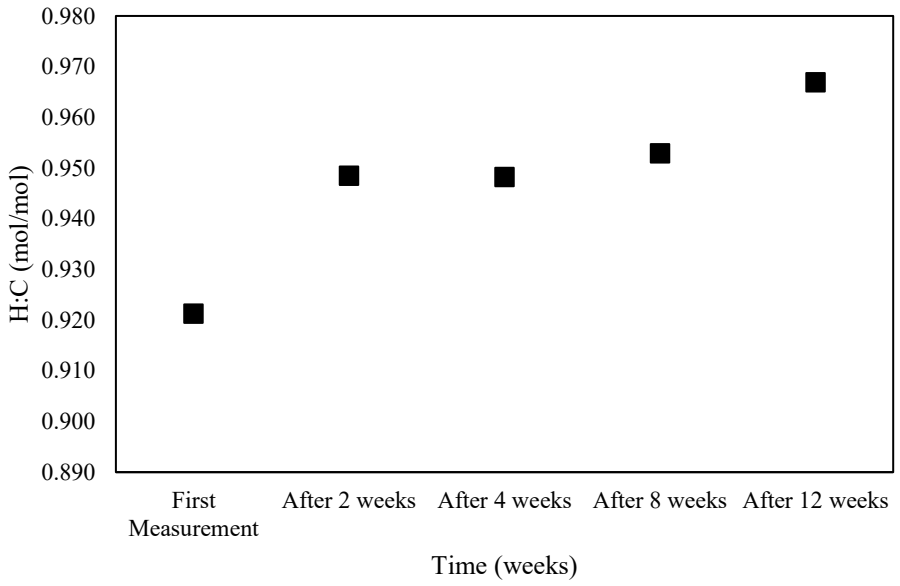

Figure 5-10. H:C ratio of asphaltenes from product A at different storage time

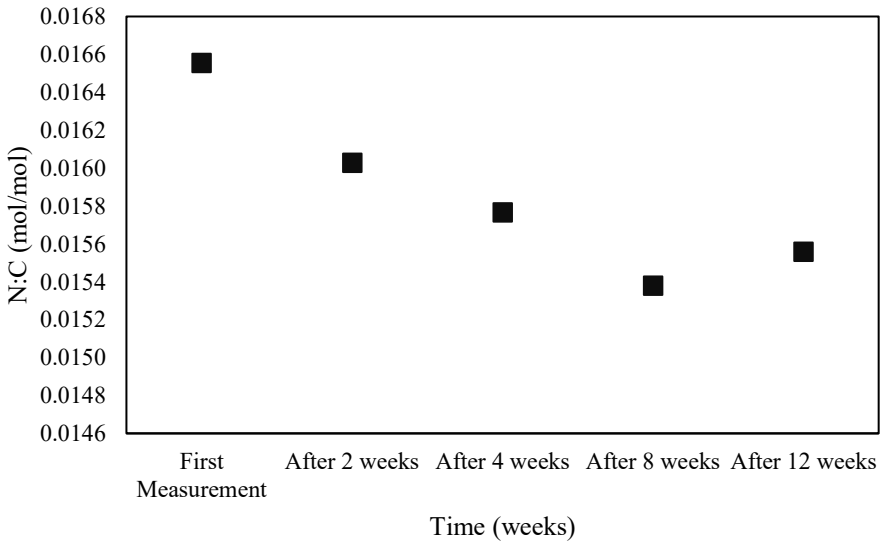

Figure 5-11. N:C ratio of asphaltenes from product A at different storage time

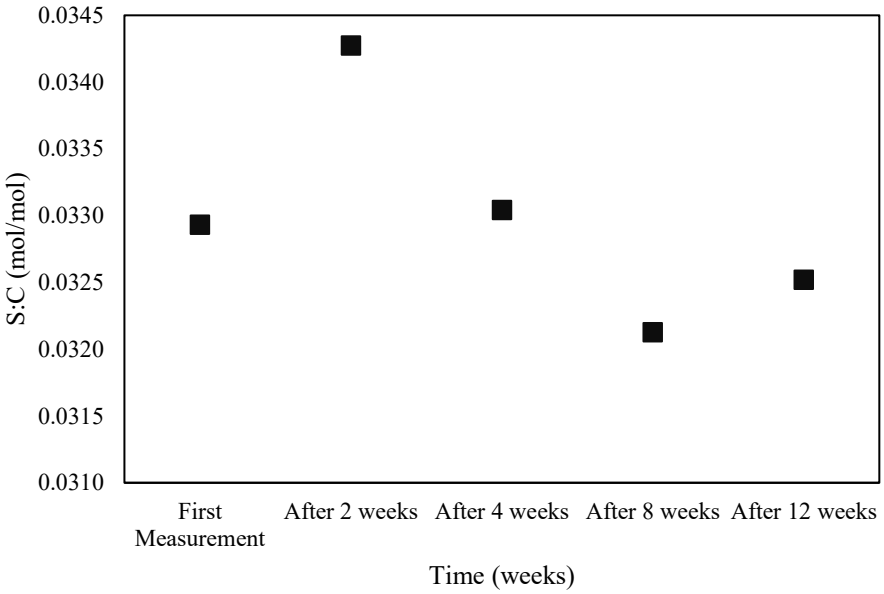

Figure 5-12. S:C ratio of asphaltenes from product A at different storage time

In Figures 5-10 and 5-11, as the storage time increases, H:C ratio will also be increased but N:C ratio will decrease. However, for N:C ratio, after 8 weeks of storage, N:C ratio start to increase. Unlike H:C and N:C ratio, during the storage S:C ratio was very unpredictable.

Micro carbon residue (MCR) is one of the most used methods to determine the coke forming tendency [2, 5] and Figures 5-13 and 5-14 shows the MCR and mineral matter of product A at different storage time, respectively. Two samples were taken from product A to perform the analysis. Table B7 from Appendix B presents the average and standard deviation of MCR and mineral matter measured at different storage time as the supporting information.

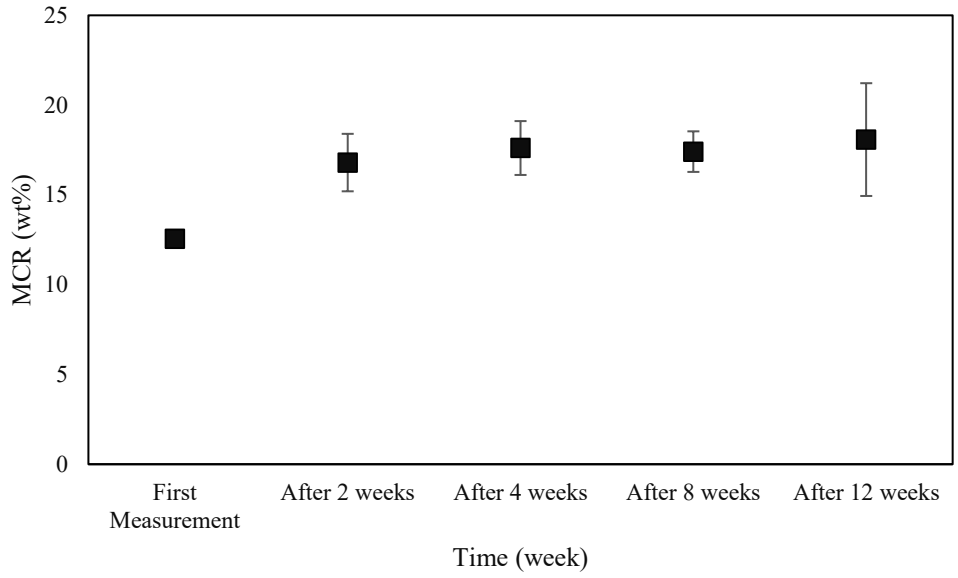

Figure 5-13. MCR of product A measured at different storage time

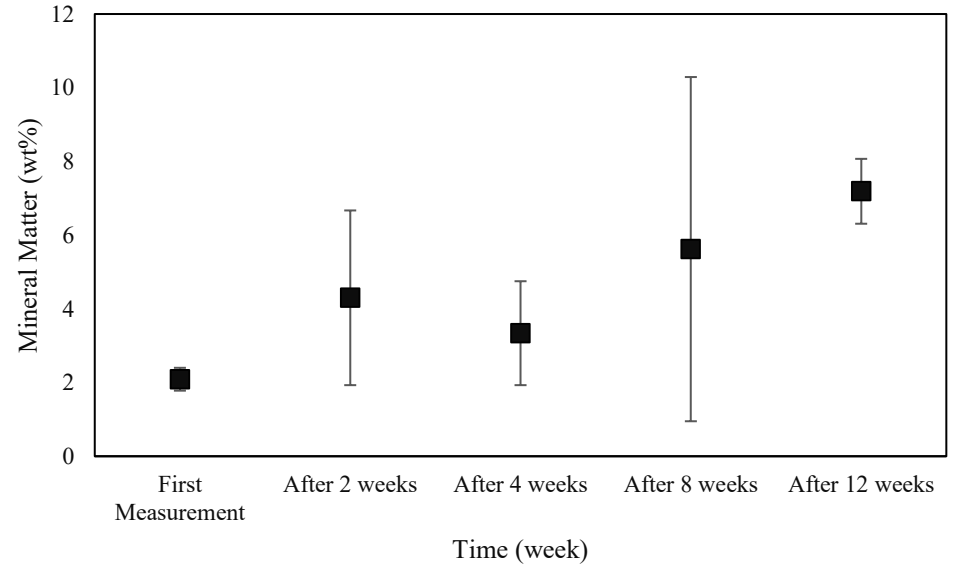

Figure 5-14. Mineral matter of product A measured at different storage time

In Figure 5-13, in the first 4 weeks as the storage time increases, the MCR of product A was also increased and after 4 weeks of storage the MCR in product remained nearly constant at 18 wt%. On the other hand, since the standard deviation of mineral matter of product A measured at certain time had large standard deviation. Therefore, ANOVA: single factor analysis was performed for

the mineral matter measured at different storage time. Based on the ANOVA analysis, the P value for mineral matter is 0.3 which is smaller than 0.5 so the mineral matter measured at different storage time are different from each other. During the storage, the measured mineral matter values were supposed to remain the same. However, these anomalous results for the present remains unknown. One possible explanation is, during the storage a small amount of material in product A has been converted to coke that can not be combusted. In addition, visbroken product is a very complex mixture which could also cause the difference in each measurement.

Since the MCR measure the coke forming tendency [2], the results indicate that in the first 4 weeks as the storage time of visbroken product increases, the coking forming tendency of the visbroken product will increase and after 4 weeks it will eventually maintain at the same level.

As mentioned in section 2.5.2, ^{1}H-NMR has been used frequently on petroleum product to measure the distribution of hydrogen that attach to the aliphatic and aromatic carbon. In this study, product A and asphaltenes from product were analyzed by ^{1}H-NMR at different storage time. Three samples were taken from product A and asphaltenes of product A to perform the analysis. Figures 5-15 and 5-16 present the aromatic hydrogen of product A and asphaltenes precipitated from product A, respectively. Average and standard deviation of aromatic and saturate for product A and asphaltenes from product A are presented in Table B8 and Table B9 respectively in Appendix B.

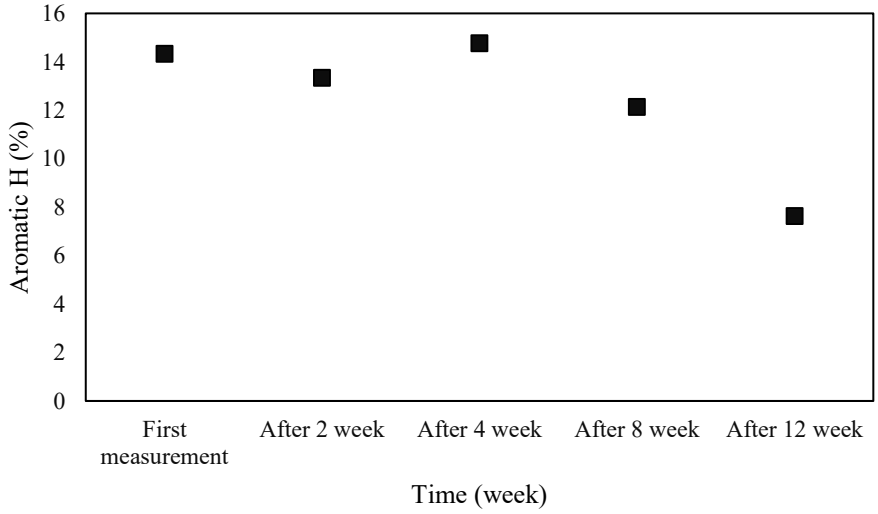

Figure 5-15. ^{1}H-NMR results of product A measured at different storage time

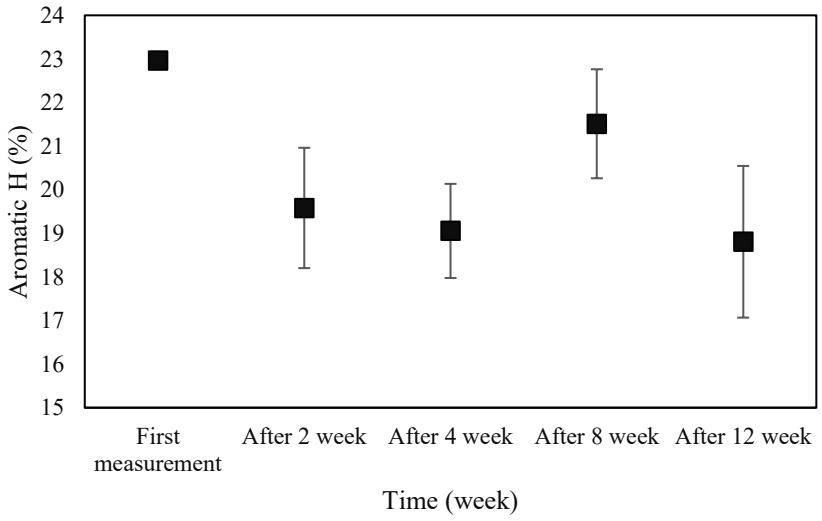

Figure 5-16. ^{1}H-NMR results of asphaltenes precipitated from product A measured at different storage time

Based on Figures 5-15, 5-16 and Table B8 after 12 weeks of storage, aromatic hydrogen in liquid product has been decreased from 14.3 % to 7.6% and saturated hydrogen in liquid product has been increased from 85.7% to 92.4%. On the other hand, from Figure 5-16 and Table B9, aromatic hydrogen in asphaltenes has been decreased from 23.0 % to 18.8 % and saturated hydrogen in asphaltenes has increased from 77.0 % to 81.2 %.

5.3.3. Characterization of product A-α, product A-β and product A-γ

As mentioned in section 5.2.2, α-methylstyrene, 9, 10-dihydroanthracene and dihydronaphthalene were stored separately with visbroken product and they were labeled as product A-α, product A-β and product A-γ. The conversion of these model compounds at different storage time is shown in Table 5-4. Sample conversion calculation of the model compounds can be found in Appendix B.

Table 5-4. Conversion of model compounds at different storage time (%) [a]

Measured time	α-metylstyrene	dihydronaphthalene	9,10-dihydroanthracene
First Measurement	0.002	0.002	0.004
After 2 weeks	-0.001	0.002	0.004
After 4 weeks	0.001	0.001	0.005
After 8 weeks	0.002	0.002	0.012
After 12 weeks	0.003	0.003	0.005

[a]Analysis performed once

In Table 5-4, as the storage time increases the conversion for each of the model compound is remained around 0. However, this result cannot not be used as evidence to prove that there was no hydrogen transfer reaction that happed during the storage. Since other hydrogen transfer reactions may have occurred within the visbroken product, such as hydrogen transfer between asphaltenes and liquid product.

5.4. Discussion

5.4.1. The change of refractive index

During the 12 weeks of storage, the refractive index of product A measured at 20 ºC increased from 1.5749 to 1.5797 and the density of product A has also increased from 987 kg/m^3 to 999 kg/m^3. In Figure 5-17 as the RI of product A measured at different storage time increased, the density of product A was also increased and eventually reached a plateau.

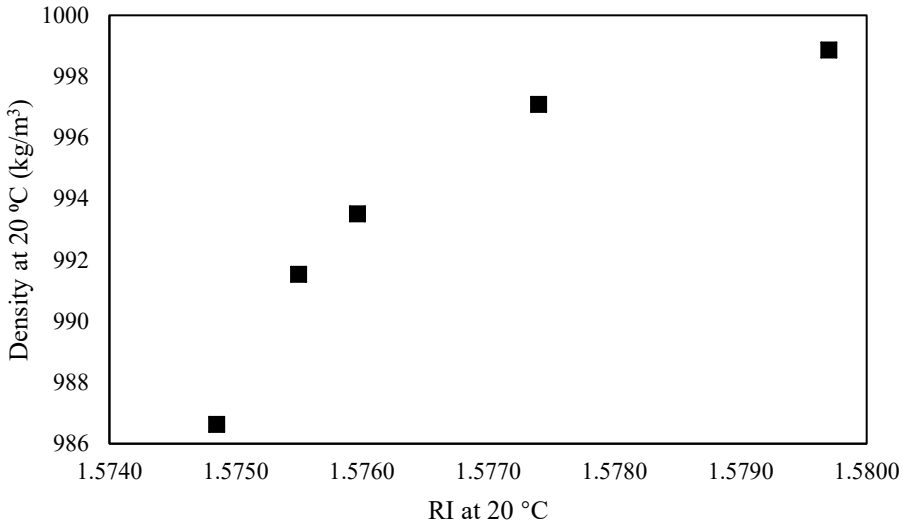

Figure 5-17. Relationship between density and refractive index of product A

There is a general tendency for the refractive index to increase as the molecular weight of the material increases [6]. Therefore, based on Figure 5-17, during the storage, it is possible that the molecular weight of product A increased. In addition, the chemical structure of the molecule can also influence the refractive index. Usually, the refractive index is constant for a particular liquid at a given temperature [7]. Therefore, the change of refractive index of material temperature (temperature coefficient) should also be a constant. In this study, refractive index has been measured at 20ºC, 40 ºC, and 60 ºC so the temperature coefficient (dn/dT) of refractive index measured at different storage time was calculated (Table 5-5).

Table 5-5. Temperature coefficient measured at different storage time

Measured time	Temperature coefficient
First measurement	-0.000370
After 2 weeks	-0.000394
After 4 weeks	-0.000385
After 8 weeks	-0.000410
After 12 weeks	-0.000433

After 12 weeks of storage, the temperature coefficient of refractive index measured at different

storage has been decreased from -0.000370 to -0.000433. This indicate that the structure or the nature of the visbroken product A has been changed during the storage.

5.4.2. Potential causes of density increment of visbroken product

During the 12 weeks of storage, density of the visbroken product A measured at 20 °C has increased from 987 kg/m^3 to 999 kg/m^3. Therefore, it is necessary to investigate the potential factors that may affect the density of the visbroken product during storage. It was reported in literature that after 90 days of storage of visbroken product from Venezuelan heavy oil, H:C ratio of the asphaltenes of product has been decreased from 0.85 to 0.80 [1]. In addition, asphaltenes content has been increased from 0.64 to 0.67 [1]. The change of H:C ratio indicate that hydrogen transfer has been taken place during the storage. In this study, H:C ratio of asphaltenes of Product A has been increased from 0.92 to 0.96 and asphaltenes content has been increased from 0.18 to 0.22. Based on these observations, it was speculated that during the storage in the first 8 weeks of storage due to the decrease of H:C ratio of the liquid visbroken. In other words, hydrogens may have been transfer from the maltene (*n*-pentane soluble fraction) to the asphaltenes of visbroken product. After the hydrogen transfer, part of the material in maltene may became *n*-pentane insoluble which cause the increase in density of visbroken product.

In this study, the H:C ratio of the asphaltenes from Product A were measured at different storage time. The relationship between H:C ratio of asphaltenes from Product A and density of Product A was also evaluated. (Figure 5-18).

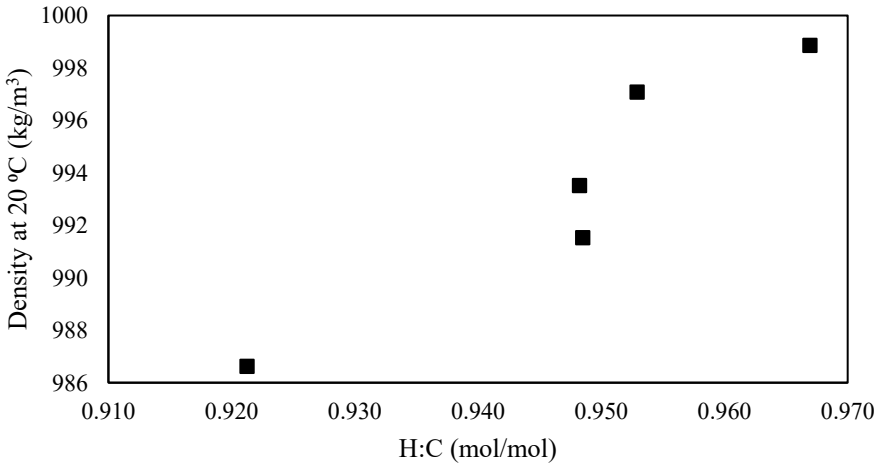

Figure 5-18. Relationship between density of product A and H:C ratio of asphaltenes from product A

To determine whether hydrogen has been transferred the maltenes to the asphaltenes, the elemental balances were performed. It was assumed that the hydrogen content remained the same during the storage. The amount of hydrogen in maltenes per grams of feed was calculated based on the difference between the hydrogen amount in 1 grams of the feed (Table 5-1) and the amount of hydrogen in asphaltenes per grams of feed (Table 5-1, Table B3 and Table B6 in Appendix B). Based on this calculation, the amount of hydrogen in maltenes per grams of feed at different storage time can be found in Figure 5-19.

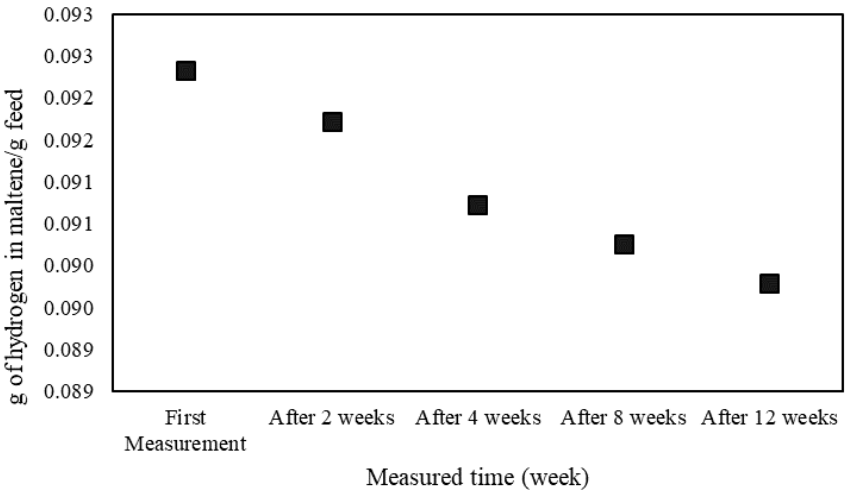

Figure 5-19. Amount of hydrogen in maltene per grams of feed at different storage time.

From Figure 5-19, it is obvious to see that as the storage time increases, the amount of hydrogen in maltene has been decreased which support the statement that hydrogens in maltene may have been transferred to the asphaltenes.

In Figure 5-18, it was found that as the H:C ratio of asphaltenes increases, the density of product A is also increased. However, in this analysis, the R-square value was found as 0.9, which means about 0.9 of the variation in the density was due to the variation of the H:C of asphaltenes from Product A. Another question would be what are some other factor that may cause the increase in the density of Product A. In section 5.3.3, it was found that as the storage time increased, the N:C ratio of the asphaltenes from Product A decreased except the last measurement. Therefore, the relationship between density and N:C ratio of asphaltenes from Product A was also evaluated (Figure 5-20).

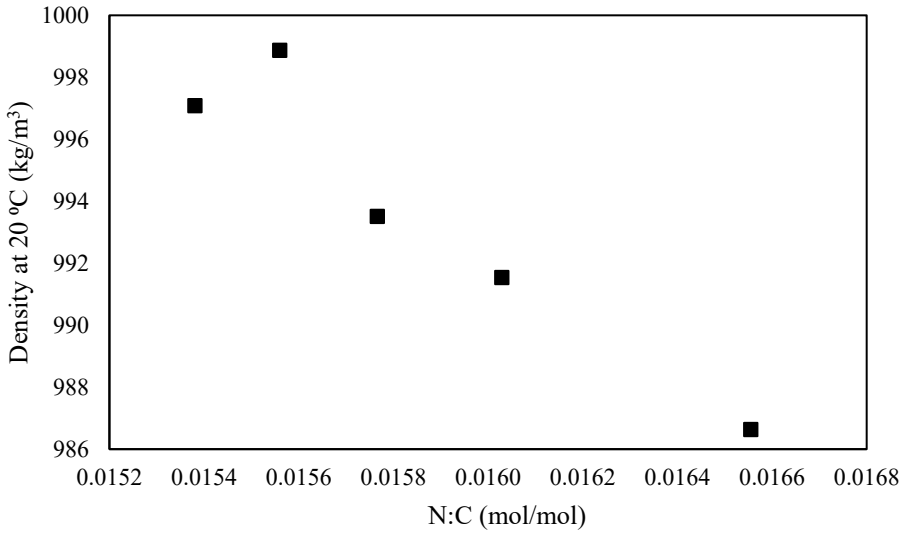

Figure 5-20. Relationship between density of product A and N:C ratio of asphaltenes from product A

In Figure 5-20 as the N:C ratio of asphaltenes decreases, density of product A is increased except one measurement. In addition, to understand the change of nitrogen in maltene and asphaltenes, by assuming the nitrogen amount remained the same during the storage, the amount of nitrogen in maltenes per 100 g of feed was calculated at different storage time. Like the amount of hydrogen in maltene per grams of feed, it was calculated based on the difference between the nitrogen amount in 100 grams of the feed (Table 5-1) and the amount of nitrogen in asphaltenes per 100 g of feed (Table 5-1, Table B3 and Table B6 in Appendix B). Based on this calculation, Figure 5-21 can be obtained.

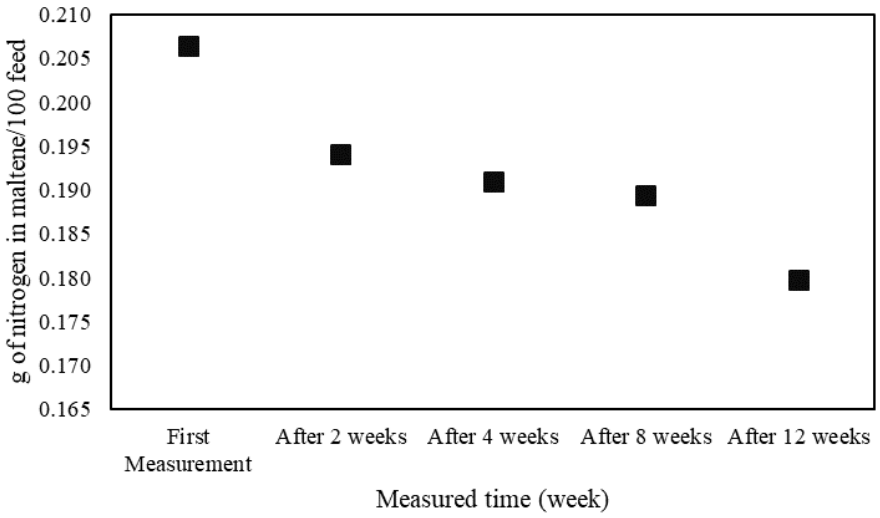

Figure 5-21. Amount of nitrogen in maltene per 100 g of feed at different storage time.

In Figure 5-21, as the storage time increases, the amount of nitrogen in maltene has been decreased which means the amount of nitrogen in asphaltenes should be increased. However, in Figure 5-11 as the storage time increases, the N:C ratio decreased. Therefore, it is necessary to check the amount of carbon in maltene or asphaltenes. Like the amount of hydrogen in maltene per grams of feed, it was calculated based on the difference between the carbon amount in 1 grams of the feed (Table 5-1) and the amount of carbon in asphaltenes per grams of feed (Table 5-1, Table B3 and Table B6 in Appendix B). Based on this calculation, Figure 5-22 could be obtained.

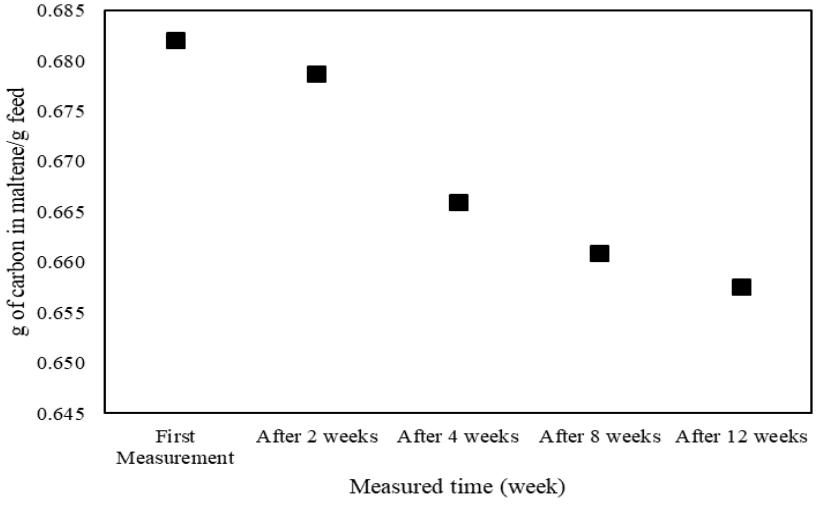

Figure 5-22. Amount of carbon in maltene per grams of feed.

In Figure 5-22, as the storage time increases, the amount of carbon in maltenes is decreased which

means the amount of carbon in asphaltenes has been increased. However, in asphaltenes the amount of carbon increased was larger than the amount of nitrogen increased which caused the decreasing in N:C ratio in asphaltenes.

In addition, the following explanation may explain the decrease in nitrogen and carbon from the maltenes. During the storage the nitrogen compound in maltene may start addition reaction with other free radicals or compounds in maltenes or asphaltenes to form more heavy compounds which cause the increase in density of the visbroken product. For example, quinolines is one of the typical nitrogen compounds that are present in crude oil [8]. It may undergo the electrophilic substitution reaction such as the reaction that has been shown in Figure 5-23 [9, 10].

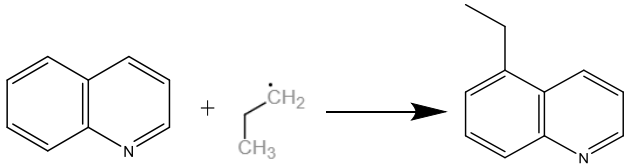

Figure 5-23. Reaction of quinolines with an example of electrophile [9]

One thing should be point out is, in Figure 5-8 in the first 8 weeks of storage, as the storage time increase, the free radical is decreased except week 4. In Figure 5-7, as the storage time increases, the free radicals in liquid product (maltene and asphaltenes) remained nearly the same. Therefore, the nitrogen compound in maltene and asphaltenes could mostly react with the free radical in asphaltenes which result in increase of density of Product A and decrease in free radical content in asphaltenes.

5.4.3. Free radical and hydrogen transfer during storage

In section 5.3.2, free radical in liquid product A remained nearly constant during 12 weeks of storage. However, the free radical in asphaltenes from product A initially had a decreasing trend during the first 8 weeks of storage and suddenly increased at week 12. On the other hand, as it is mentioned in 5.3.3, during the storage there was no conversion of any model compounds that has been added to the visbroken product. However, this result cannot not be used as evidence to prove that there was nearly no hydrogen transfer reaction that happed during the storage. From Figure 5-15, Figure 5-16, Table B8 and Table B9, it was observed that as the storage time increases the

aromatic hydrogen in product A and asphaltenes were decreased but saturated hydrogen was increased.

One possible explanation is that during the storage, propagation reaction by hydrogen abstraction played a very important role in liquid product (maltene and asphaltene) of Product A. In Product A, hydrogen abstraction may take place between the aromatic compounds and free radicals, where A and A• represent the parent aromatic and the corresponding aromatic radicals, respectively R• and RH are radicals and their corresponding alkanes which means the following reaction may take place.

$$R\bullet + A \longrightarrow RH + A\bullet$$

During this process, the nature of hydrogen has been changed from aromatic hydrogen to aliphatic hydrogen, but propagation reaction will not change the radical content.

For example, from Clar's sextet theory six π-electrons localized in a single benzene-like ring separated from adjacent rings by formal carbon-carbon single bonds [11]. Application of this rule to anthracene indicate that the following reactions (Figure 5-24) might have happened.

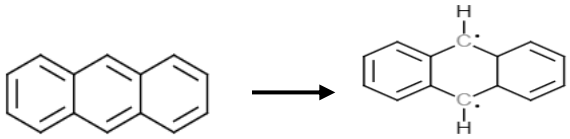

Figure 5-24. Anthracene ant its corresponding Clar aromatic π-sextets [11]

Therefore, compounds in visbroken product that has similar structure like anthracene may follow the similar process like what has been demonstrated in Figure 5-24.

In addition, the Clar aromatic π-sextets that was from the original compound may donate hydrogen to alkane radical (Figure 5-25).

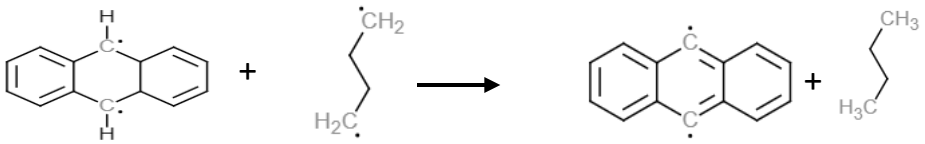

Figure 5-25. Hydrogen transfer from corresponding Clar aromatic π-sextets of anthracene to alkane radical.

It is important to point out that Figure 5-24 only shows one of the possible resonance structures, which is not the dominant resonance structure of anthracene. In addition, Figure 5-24 and Figure 5-25 it is just an illustrative example of how a compound that is not a free radical, but can react like a diradical that can participate in reactions that would cause a change in aromatic to aliphatic hydrogen content without affecting the measured free radical in liquid product of Product A.

One thing should be noticed is some hydrogens are not necessarily bond directly to aromatic carbon [4], however during the analysis they were still in the shift range of aromatic region of ^{1}H-NMR analysis (Figure 5-26). In this analysis they will be referred as "indirect aromatic hydrogen".

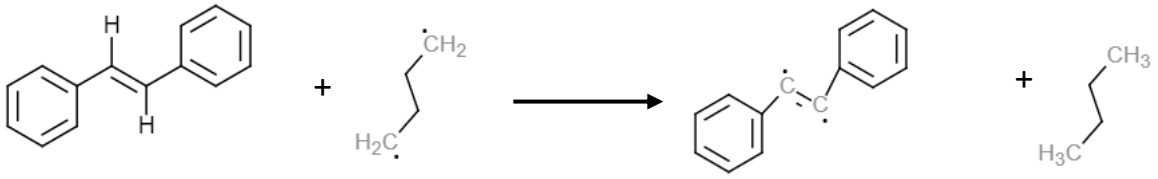

Figure 5-26. Example of hydrogen transfer between alkane and "indirect aromatic hydrogen" [12].

In Figure 5-26, hydrogen that is connect to alkene bond in the middle of the first compound has chemical shift of 7.03 which is in the aromatic region. In addition, it is important to know that Figure 5-26 is just an illustrative example of how a hydrogen in compound that is not directly bond to aromatic carbon but can participate in reactions that would cause a change in aromatic to aliphatic hydrogen content.

Similarly, in the asphaltenes of product A, hydrogen abstraction may also take place between aromatic compounds and alkane free radicals which cause the decrease in aromatic hydrogen and increase in saturated hydrogen. However, in asphaltenes, termination reaction may also play an important role, but it may only play a limited role in terms of entire Product A. Since the termination reactions will not change the nature of aliphatic or aromatic hydrogen which may explain about why in asphaltenes, free radicals have been decreased in the first 8 weeks of storage and aliphatic hydrogens have been increased during the 12 weeks of storage.

In addition, H:C ratio of asphaltenes precipitated at different storage time has been increased. The increase of H:C ratio of asphaltenes means that a significant amount of hydrogen was transferred, and it has been discussed in Section 5.4.2. Since aromatic hydrogen in both asphaltenes and liquid product have been decreased after storage where saturated hydrogen in asphaltenes and liquid product have been increased. Therefore, in general, the hydrogen transfer from aromatic hydrogen in asphaltenes and liquid product to unsaturated compound or free radicals should be higher. In addition, since more asphaltenes was precipitated as the storage time increased, it means more *n*-pentane soluble material has become insoluble during storage. This could be due to the hydrogen transfer from aromatic hydrogen in liquid product to unsaturated compounds or free radicals in asphaltenes or liquid product and after the hydrogen transfer some of the compounds may become *n*-pentane insoluble. However, in elemental analysis, H:C ratio of asphaltenes has increased during storage, therefore the compound that become insoluble should have structure such as C_nH_{n+2}.

5.4.4. Deasphalting before and after visbreaking

In section 3.4.2, it has been mentioned that during visbreaking asphaltenes were able to donate hydrogen during visbreaking. The ability of asphaltenes to donate hydrogen can also be found from previous study. In the work of Guo etal. [13], it was found that various residue fractions and asphaltenes were better hydrogen donors than tetralin. One thing should be noticed, in Chapter 3 vacuum residue deasphalted oil (VR DAO) was used to performed visbreaking. The amount of asphaltenes in VR DAO before visbreaking was 5.7 wt% and after visbreaking at 417 °C for 30 min, asphaltenes content was increased from 5.7 wt% to 14.6 wt%. On the other hand, in this study, Athabasca bitumen with 22.3 wt% asphaltenes was used to perform visbreaking at 420 °C for 10 min and after visbreaking asphaltenes content was decreased from 22.3 wt% to 18.3 wt%. In addition, the H:C ratio in asphaltenes from Athabasca bitumen before visbreaking was 1.198 and after visbreaking it was decreased from 1.198 to 0.921. The decrease in H:C ratio meant that a significant amount of hydrogen transfer was also happening during the visbreaking in this study. Based on the above analysis, it was suspected that bitumen with higher asphaltenes content could transfer more hydrogen compared to bitumen with less asphaltenes content and when some compound in asphaltenes got enough hydrogen, it might become *n*-pentane soluble which caused the decrease in asphaltenes content.

In the BituMax^{TM} partial upgrading process asphaltenes are rejected before visbreaking [14]. The purpose of forming solvent deasphalting before visbreaking is that it delays the onset of coke formation since the molecules that are more prone to form coke are previously removed. In this study, less asphaltenes was produced when bitumen with more asphaltenes were used. Since asphaltenes can donate hydrogen under visbreaking conditions, it seems advantageous to change the sequence of the process, i.e., perform solvent deasphalting after visbreaking. This strategy was previously evaluated for Cold Lake bitumen by Zachariah et al. [15], where visbreaking reactions were performed at 380 °C and 85 minutes. It was found that by changing solvent deasphalting and visbreaking sequence resulted in products with similar viscosity and density. On the other hand, the visbroken product from the process where visbreaking was performed before solvent deasphalting presented higher hydrogen to carbon ratio. Another advantage to perform solvent deasphalting after visbreaking is the increase in stability of the products. In this work, it was found that the nitrogen compound in maltene and asphaltenes could react with free radicals in asphaltenes of the visbroken product through addition reaction (section 5.4.2). In general, the concentration of free radical is higher in asphaltenes. Therefore, by performing solvent deasphalting after visbreaking, the free radical molecules, and nitrogen compounds that will most likely to react at room temperature to cause the increment in density and form more asphaltenes upon storage would be rejected during deasphalting leading to an increase in stability.

5.5. Conclusion

In this work it was investigated if the free radicals formed during visbreaking were stable and persistent or would some of these species continue to react even at ambient conditions. In addition, more properties such as viscosity and density were also analyzed to evaluate the changes of visbroken product during the long-term storage time under the nitrogen atmosphere. The following observations were made from the experimental investigation:

(a) As the storage time increased, density, viscosity, asphaltenes content, refractive index, H:C of asphaltenes and micro carbon residue also increased. However, for N:C ratio of asphaltenes, it was decreased with increased storage time.

(b) The increase of refractive index may indicate that the molecular weight of visbroken has been

increased. Different temperature coefficient of refractive index measured at different storage time shows that the nature of the visbroken product has been changed during the storage.

(c) The change of density in function of H:C, N:C in asphaltenes of Product A and refractive index of Product A were analyzed respectively. As the storage time increase, the amount of hydrogen, nitrogen, and carbon will decrease. The increase in density could be due to the increase of asphaltenes through hydrogen transfer from maltene to asphaltenes or the addition reaction between free radical in asphaltenes and nitrogen compound in maltene or asphaltenes.

(d) During the storage, propagation reaction by hydrogen abstraction may played a very important role in liquid product (maltene and asphaltene) of Product A. In this process, the nature of hydrogen has been changed from aromatic hydrogen to aliphatic hydrogen based on 1H NMR analysis, but propagation reaction will not change the radical content. In asphaltenes, termination reaction may also play an important role, but it may only play a limited role in terms of the entire visbroken product. Based on the elemental analysis a significant amount of hydrogen has been transferred, however the H:C ratio in asphaltenes has been increased during storage.

(e) It seems advantageous to perform solvent deasphalting after visbreaking, since asphaltenes in bitumen can donate hydrogen during visbreaking. In addition, by performing solvent deasphalting after visbreaking will most likely leading to an increase in stability of visbroken product.

Reference cited

[1] Zhang, N., Zhao, S., Sun, X., Xu, Z., & Xu, C. (2010). Storage Stability of the Visbreaking Product from Venezuela Heavy Oil. *Energy & Fuels*, *24*(7), 3970–3976.

[2] Gray, M. R. (2015). *Upgrading oilsands bitumen and heavy oil*. Edmonton, Alberta, Canada: Pica Pica Press, an imprint of The University of Alberta Press.

[3] Aghizada, N., Prado, G. H. C., & De Klerk, A. (2017). Uncatalyzed hydrogen transfer during 100–250 °C conversion of asphaltenes. *Energy & Fuels*, *31*(7), 6800–6811.

[4] Payan, F., & De Klerk, A. (2018). Hydrogen transfer in asphaltenes and bitumen at 250 °C. *Energy & Fuels*, *32*(9), 9340–9348.

[5] Bi, W., Mccaffrey, W. C., & Gray, M. R. (2007). Agglomeration and Deposition of Coke during Cracking of Petroleum Vacuum Residue†. *Energy & Fuels, 21*(3), 1205-1211.
Press
[6] Synapse Information Resources, Inc. (n.d.). *Handbook of Solvents (2nd Edition)*. S.l.
[7] Kenkel, J. (2014). *Analytical chemistry for technicians*. Boca Raton, FL: CRC.
[8] Manning, F. A., & Thompson, R. (1995). *Oilfield processing of petroleum. - 2: Crude oil*. Tulsa: PennWell.
[9] Ahluwalia, V. K. (2013). *Heterocyclic chemistry*. Oxford: Alpha Science Internat.
[10] Ryan, L. (2015). *Advanced chemistry for you*. Oxford, United Kingdom: Oxford University
[11] Clar, E. (1973). *The aromatic sextet*. London: Wiley.
[12] Balci, M. (2005). Basic ^{1}H and ^{13}C-NMR spectroscopy. Ankara, Turkey: Elsevier
[13] Guo, A., Wang, Z., Zhang, H., Zhang, X., & Wang, Z. (2010). Hydrogen Transfer and Coking Propensity of Petroleum Residues under Thermal Processing. *Energy & Fuels*, *24*(5), 3093–3100.
[14] Speight, J. (2012). Visbreaking: A technology of the past and the future. *Scientia Iranica*, *19*(3), 569–573.
[15] Zachariah, A., & De Klerk, A. (2017). Partial Upgrading of Bitumen: Impact of Solvent Deasphalting and Visbreaking Sequence. *Energy & Fuels*, *31*(9), 9374–9380.

6. Conclusions

6.1 Overview of accomplishments

This study formed part of a larger study in support of the development of the BituMax^{TM} partial upgrading of bitumen process.

Visbreaking is one of the commonly used strategies used to reduce bitumen viscosity. It is a mild thermal cracking process where the conversion of bitumen is limited by the onset of coke formation. The onset of coking is related to the *n*-pentane insoluble material in the feed. Since *n*-pentane insoluble materials (asphaltenes) in bitumen could limit the conversion of bitumen during visbreaking, therefore asphaltenes are rejected before visbreaking in from the BituMax^{TM} process. However, during visbreaking new asphaltenes are formed. Studying the formation of new *n*-pentane insoluble material during visbreaking (Chapters 3 and 4) [1] and its impact on the products from visbreaking (Chapter 5) were industrially relevant topics.

According to the equivalent residence time theory (ERT) discussed in Chapter 4, reaction temperature and residence time combination can be varied to achieve the same vacuum residue conversion, with the implication that product selectivity is related to conversion. It was found that formation of *n*-pentane insoluble material during visbreaking, which reflects reaction selectivity, was different at the same equivalent residence time. This is relevant to the design of visbreaking reactors, because current design practice is based on ERT. The conclusion that *n*-pentane insoluble formation was not the same at the same ERT, was a meaningful contribution to the BituMax^{TM} process development.

Observations indicated that the product from visbreaking at temperature in the range studied (417–438 °C) may continue to change during storage after visbreaking. It was found that during the storage, free radical content has been decreased and asphaltenes content has been increased. A systematic study to investigate the stability of visbroken product during storage under inert atmosphere was conducted. Changes during storage were monitored by periodic analysis over a period of 12 weeks. These observations came at the end of this study and will inform future development work on the BituMax^{TM} process.

6.2 Major specific conclusions

a) Iso-conversion was initially not achieved at conditions supposed to lead to the same conversion based on the ERT. The assumptions of ERT were first-order reaction, constant activation energy, and the fact that heat up and cool-down periods are not included in the ERT definition. Only when heat-up and cool-down periods were considered, was iso-conversion achieved for different equivalent residence times.

b) First order reaction is one of the assumptions of the ERT concept, however for ERT less than 600s at 438 °C, conversion increased nearly linearly with increase of ERT. This indicated that it was not a simple first order reaction. Near constant conversion was achieved between 600 and 1100 s at 438 °C.

c) Differences in heating rate affected the asphaltenes content of the product.

d) The amount of asphaltenes formed was different at the same conversion, which means the kinetics of asphaltenes formation was different to the kinetics of vacuum residue conversion.

e) At vacuum residue conversion of less than 0.4, i.e. 40% conversion, there was little or no change in some properties, such as refractive index, micro carbon residue (MCR) content, *n*-pentane insoluble content, and persistent free radical content. These properties were affected when conversion was higher than 0.4.

f) Based on the H:C molar ratio of asphaltenes precipitated from the visbroken products, hydrogen transfer from asphaltenes took place during the visbreaking.

g) After 210 days of storage under nitrogen, there was not only a decrease in free radical content, but also a 9 wt% increase in *n*-pentane insoluble material and an increase in refractive index of product obtained by visbreaking at 417 °C and 30 min. It was speculated that the free radicals present in the products were reactive and probably more than one chain transfer reaction occurred that resulted in the formation of different compounds during storage.

h) During the storage, some of the free radicals in liquid product may still react even at ambient conditions. One possible situation is, during the storage, hydrogen abstraction reaction might occur between free radicals and aromatics in the liquid product. Since a new free radical will also be generated during the reaction, the free radical content in the liquid visbroken product will remain nearly at constant. However, in asphaltenes, other than

hydrogen abstraction, addition reactions and termination reaction between different radicals may also take place.

i) As the storage time under inert atmosphere increased, density, viscosity, asphaltenes content, refractive index, H/C and micro carbon residue also increased.

j) The increase in density could be due to the increase of asphaltenes through hydrogen transfer from maltene to asphaltenes or the addition reaction between free radical in asphaltenes and nitrogen compound in maltene or asphaltenes.

6.3 Recommended future work

In this study, many interesting results were obtained. However, more things could be studied and discussed in the future following on the observations and conclusions from this study.

a) In this study, it was observed that asphaltenes in the bitumen could provide hydrogen during visbreaking. Therefore, it could be useful to investigate the relationship between asphaltenes content in the feed as potential hydrogen donors and the formation of new asphaltenes during visbreaking when the feed was not deasphalted.

b) From this study, it seems advantageous to perform solvent deasphalting after visbreaking. Therefore, it would be useful to investigate the storage stability of visbroken product after asphaltenes was removed.

Reference cited

[1] Yan, Y.; De Klerk, A.; Prado, G. H. C. (2020) Visbreaking of vacuum residue deasphalted oil: New asphaltenes formation. *Energy Fuels*, *34*, in press (9b03465).

Bibliography

ASTM UOP614-68. (2003). Heptane-insoluble matter in petroleum oils using a membrane filter.

West Conshohocken, PA: ASTM International.

ASTM D4124. (2009). Standard test method for separation of asphalt into four fractions. West Conshohocken, PA: ASTM International.

ASTM D4530-15. (2015). Standard test method for determination of carbon residue (micro method). West Conshohocken, PA: ASTM International

ASTM D 2007. (2016). Standard test method for characteristic groups in rubber extender and processing oils and other petroleum-derived oils by the clay-gel absorption chromatographic method. West Conshohocken, PA: ASTM.

ASTM D 6560. (2012). Standard test method for determination of asphaltenes (heptane insolubles) in crude petroleum and petroleum products. West Conshohocken, PA: ASTM.

Aguilar, R. A., & Ancheyta, J. (2016). Modeling Coil and Soaker Reactors for Visbreaking. Industrial & Engineering Chemistry Research, 55(4), 912–924

ASTM International. ASTM D70-09. (2009). Standard test method for density of semi-solid bituminous materials (Pycnometer Method). West Conshohocken, PA: ASTM International.

Aghizada, N., Prado, G. H. C., & De Klerk, A. (2017). Uncatalyzed hydrogen transfer during 100–250 °C conversion of asphaltenes. Energy & Fuels, 31(7), 6800–6811.

Ahluwalia, V. K. (2013). Heterocyclic chemistry. Oxford: Alpha Science Internat. Balci, M. (2005). Basic 1H and 13C-NMR spectroscopy. Ankara, Turkey: Elsevier

Battino, R., Rettich, T. R., & Tominaga, T. (1984). The solubility of nitrogen and air in liquids. New York: American Chemical Society and the American Institute of Physics for the National Bureau of Standards.

Brauch, R., Fainberg, V., Kalchouck, H., & Hetsroni, G. (1996). Correlations between properties of various feedstocks and products of visbreaktng. Fuel Science and Technology International, 14(6), 753–765.

Bi, W., Mccaffrey, W. C., & Gray, M. R. (2007). Agglomeration and deposition of coke during cracking of petroleum vacuum residue†. Energy & Fuels, 21(3), 1205-1211.

Choudhury, R., Bhaktavatsalam, A., & Singh, R. (1993). Desulfurization of various Indian coals by hydrogen donor solvent extraction. Fuel, 72(5), 707–708.

Calemma, V., & Rausa, R. (1997). Thermal decomposition behaviour and structural characteristics of asphaltenes. Journal of Analytical and Applied Pyrolysis, 40-41, 569–584.

Cabrales-Navarro, F. A., & Pereira-Almao, P. (2017). Reactivity and comprehensive kinetic modeling of deasphalted vacuum residue thermal cracking. Energy & Fuels, 31(4), 4318–4332.

Castillo, J., & Klerk, A. D. (2018). Visbreaking of Deasphalted oil from bitumen at 280– 400 °C. Energy & Fuels, 33(1), 159–175.

Casalini, A., Mascherpa, A., & Vecchi, C. (1990). Modifications induced by visbreaking on composition and structure of atmospheric residues. Fuel Science and Technology International, 8(4), 427–445

Cabrales-Navarro, F. A., & Pereira-Almao, P. (2017). Reactivity and comprehensive kinetic modeling of deasphalted vacuum residue thermal cracking. Energy & Fuels, 31(4), 4318– 4332.

Clar, E. (1973). The aromatic sextet. London: Wiley.

Eyssautier, J., Espinat, D., Gummel, J., Levitz, P., Becerra, M., Shaw, J., & Barré, L. (2011). Mesoscale organization in a physically separated vacuum residue: comparison to asphaltenes in a simple solvent. Energy & Fuels, 26(5), 2680–2687.

Foltin, J. P., Lisboa, A. C. L., & Klerk, A. D. (2017). Oil Shale Pyrolysis: Conversion dependence of kinetic parameters. Energy & Fuels, 31(7), 6766–6776.

Gray, M. R. (2015). Upgrading oilsands bitumen and heavy oil. Edmonton, Alberta: Pica Pica Press.

Gary, J. H., Handwerk, G. E., & Kaiser, M. J. (2007). Petroleum refining: technology and economics, 5ed. Boca Raton: CRC Press.

Gray, M. R. (2003). Consistency of asphaltene chemical structures with pyrolysis and coking behavior. Energy & Fuels, 17(6), 1566–1569.

Gerson, F., & Huber, W. (2003). Electron spin resonance spectroscopy of organic radicals. Weinheim: Wiley-VCH.

Gould, K. A., & Wiehe, I. A. (2007). Natural hydrogen donors in petroleum resids†. Energy & Fuels, 21(3), 1199–1204.

Guo, A., Wang, Z., Zhang, H., Zhang, X., & Wang, Z. (2010). Hydrogen transfer and coking propensity of petroleum residues under thermal processing. Energy & Fuels, 24(5), 3093– 3100.

Gray, M. R., & Mccaffrey, W. C. (2002). Role of chain reactions and olefin formation in cracking, hydroconversion, and coking of petroleum and bitumen fractions. Energy & Fuels, 16(3), 756–766.

Hua, R., Wang, J., Kong, H., Liu, J., Lu, X., & Xu, G. (2004). Analysis of sulfur-containing compounds in crude oils by comprehensive two-dimensional gas chromatography with sulfur chemiluminescence detection. Journal of Separation Science, 27(9), 691–698.

Hayes, R. E., & Mmbaga, J. P. (2013). Introduction to chemical reactor analysis. Boca Raton: CRC Press.

Haji-Akbari, N., Teeraphapkul, P., & Fogler, H. S. (2014). Effect of Asphaltene concentration on the aggregation and precipitation tendency of asphaltenes. Energy & Fuels, 28(2), 909–919.

Haji-Akbari, N., Teeraphapkul, P., Balgoa, A. T., & Fogler, H. S. (2015). Effect of n-alkane precipitants on aggregation kinetics of asphaltenes. Energy & Fuels, 29(4), 2190–2196.

IP 143. (2016). Determination of asphaltenes (heptane insoluble) in crude petroleum and petroleum products. London, UK: Institute of Petroleum.

Kariznovi, M., Nourozieh, H., & Abedi, J. (2014). Measurement and correlation of viscosity and density for compressed Athabasca bitumen at temperatures up to 200ºC. Journal of Canadian Petroleum Technology, 53(06), 330–338.

Kaiser, M. J., De Klerk, A., Gary, J. H., & Handwerk, G. E. (2020). Petroleum refining: technology, economics, and markets. Boca Raton: CRC Press,Taylor & Francis Group.

Kapoor, M. P.; Kothiyal, V.; Singh, I. D. (1993). Compositional and structural studies of visbroken residues. Fuel Sci. Technol. Int.Fuels, 11 (7), 975-989.

Kapadia, P. R., Kallos, M. S., & Gates, I. D. (2012). A new kinetic model for pyrolysis of Athabasca bitumen. The Canadian Journal of Chemical Engineering, 91(5), 889–901.

Kalichevsky, V. A., & Kobe, K. A. (1956). Petroleum refining with chemicals. Amsterdam: Elsevier Pub. Co, p.24.

Kenkel, J. (2014). Analytical chemistry for technicians. Boca Raton, FL: CRC.

Mirshamsi, S., Yan, Y., Kamal, S., Yasemi, A.-A., Gupta, R., De Klerk, A., & Prado, G. H. C. (2019). Thermal behaviour of nitrogen oxides relevant to oxidative denitrogenation. The Journal of Chemical Thermodynamics, 136, 28–43.

Maurer, C. A. (1983). Electron spin resonance spectroscopy: a potential technique for dating ancient ceramics. Ann Arbor, MI: Univ. Microfilms Intern.

Mullins, O. C., & Sheu, E. Y. (1995). Asphaltenes: fundamentals and applications. New York: Plenum Press., p. 97-130.

Naghizada, N., Prado, G. H. C., & Klerk, A. D. (2017). Uncatalyzed hydrogen transfer during 100–250 °C conversion of asphaltenes. Energy & Fuels, 31(7), 6800–6811.

Manning, F. A., & Thompson, R. (1995). Oilfield processing of petroleum. - 2: Crude oil. Tulsa: PennWell.

Payan, F., & De Klerk, A. (2018). Hydrogen transfer in asphaltenes and bitumen at 250 °C. Energy & Fuels, 32(9), 9340–9348.

Rahmani, S., Mccaffrey, W. C., Dettman, H. D., & Gray, M. R. (2003). Coking kinetics of asphaltenes as a function of chemical structure. Energy & Fuels, 17(4), 1048–1056.

Rogel, E. (1997). Theoretical estimation of the solubility parameter distributions of asphaltenes, resins, and oils from crude oils and related materials. Energy & Fuels, 11(4), 920–925.

Ramakrishna, S. A., & Grzegorczyk, T. M. (2009). Physics and applications of negative refractive index materials. Bellingham: SPIE Press.

Rahmani, S., McCaffrey, W., & Gray, M. R. (2002). Kinetics of solvent interactions with asphaltenes during coke formation. Energy & Fuels, 16(1), 148–154.

Rahimi, P. M., Teclemariam, A., Taylor, E., Debruijn, T., & Wiehe, I. A. (2005). Thermal processing limits of Athabasca bitumen during visbreaking using solubility parameters. ACS Symposium Series Heavy Hydrocarbon Resources, 183–196.

Rahimi, P. M., & Gentzis, T. (2003). Thermal hydrocracking of Cold Lake vacuum bottoms asphaltenes and their subcomponents. Fuel Processing Technology, 80(1), 69–79.

Ryan, L. (2015). Advanced chemistry for you. Oxford, United Kingdom: Oxford University

Speight, J. G. (2007). The chemistry and technology of petroleum. Boca Raton: CRC Press/Taylor & Francis.

Speight, J. (2012). Visbreaking: A technology of the past and the future. Scientia Iranica, 19(3), 569–573.

Strausz, O. P. (2003). The chemistry of Alberta oil sands, bitumens and heavy oils. Calgary: Alberta Energy Research Institute.

Speight, J. G., Long, R. B., & Trowbridge, T. D. (1984). Factors influencing the separation of asphaltenes from heavy petroleum feedstocks. Fuel, 63(5), 616–620.

Subramanian, H., Landais,Y., Sibi, M. P. (2014). Radical addition reactions. Comprehensive organic synthesis. Amsterdam: Elsevier.

Schultz, K. F.; Selucky, M. L. (1981). ESR measurements on asphaltene and resin fractions from various separation methods. Fuel, 60(10), 951-956.

Speight, J. G., & Özüm, B. (2002). Petroleum refining processes. New York: Marcel Dekker.

Speight, J. G. (2015). Handbook of petroleum product analysis (2nd ed.). Laramie, Wyoming: Wiley.

Stratiev, D., Shishkova, I., Tsaneva, T., Mitkova, M., & Yordanov, D. (2016). Investigation of relations between properties of vacuum residual oils from different origin, and of their deasphalted and asphaltene fractions. Fuel, 170, 115–129.

Siskin, M., Kelemen, S. R., Eppig, C. P., Brown, L. D., & Afeworki, M. (2006). Asphaltene molecular structure and chemical influences on the morphology of coke produced in delayed coking. Energy & Fuels, 20(3), 1227–1234.

Sachanen, A. N. (1948). Conversion of Petroleum; Production of motor fuels by thermal and catalytic processes. New York, Reinhold Pub. Corp.

Stratiev, D., Nedelchev, A., Shishkova, I., Ivanov, A., Sharafutdinov, I., Nikolova, R., … Atanassov, K. (2015). Dependence of visbroken residue viscosity and vacuum residue conversion in a commercial visbreaker unit on feedstock quality. Fuel Processing Technology, 138, 595–604.

SG, C., & M., D. (1992). Resid and heavy oil processing. Paris, Editions Technip

Singh, J., Kumar, S., & Garg, M. O. (2012). Kinetic modelling of thermal cracking of petroleum residues: A critique. Fuel Processing Technology, 94(1), 131–144.

Singh, I., Kothiyal, V., Ramaswamy, V., & Krishna, R. (1990). Characteristic changes of asphaltenes during visbreaking of North Gujarat short residue. Fuel, 69(3), 289–292.

Savvidis, T. G., Fenistein, D., Barré, L., & Béhar, E. (2001). Aggregated structure of flocculated asphaltenes. AIChE Journal, 47(1), 206–211.

Sirota, E. B. (2005). Physical structure of asphaltenes†. Energy & Fuels, 19(4), 1290–1296. Synapse Information Resources, Inc. (n.d.). Handbook of Solvents (2nd Edition). S.l.

Tannous, J. H., & Klerk, A. D. (2019). Quantification of the free radical content of oilsands bitumen fractions. Energy & Fuels, 33(8), 7083–7093.

Tavakkoli, M., Grimes, M. R., Liu, X., Garcia, C. K., Correa, S. C., Cox, Q. J., & Vargas, F. M. (2015). Indirect method: a novel technique for experimental determination of asphaltene precipitation. Energy & Fuels, 29(5), 2890–2900.

Wiehe, I. A. (1992). A solvent-resid phase diagram for tracking resid conversion. Industrial & Engineering Chemistry Research, 31(2), 530–536.

Wang, S., Chung, K., Masliyah, J. H., & Gray, M. R. (1998). Toluene-insoluble fraction from thermal cracking of Athabasca gas oil: formation of a liquid-in-oil emulsion that wets hydrophobic dispersed solids. Fuel, 77(14), 1647–1653.

Wiehe, I. A. (1993). A phase-separation kinetic model for coke formation. Industrial & Engineering Chemistry Research, 32(11), 2447–2454.

Wang, L., Zachariah, A., Yang, S., Prasad, V., & Klerk, A. D. (2014). Visbreaking oilsands-derived bitumen in the temperature range of 340–400 °C. Energy & Fuels, 28(8), 5014–5022.

Yan, T. (1990). Characterization of visbreaker feeds. Fuel, 69(8), 1062–1064.

Yan, Y.; De Klerk, A.; Prado, G. H. C. (2020) Visbreaking of vacuum residue deasphalted oil: New asphaltenes formation. Energy Fuels, 34, in press (9b03465).

Zhang, N., Zhao, S., Sun, X., Xu, Z., & Xu, C. (2010). Storage stability of the visbreaking product from Venezuela heavy oil. Energy & Fuels, 24(7), 3970–3976.

Zirrahi, M., Hassanzadeh, H., Abedi, J., Moshfeghian, M. (2014). Prediction of solubility of CH4, C2H6, CO2, N2, and CO in bitumen. The Canadian Journal of Chemical Engineering, 92, 563-572.

Zhao, B., & Shaw, J. M. (2007). Composition and size distribution of coherent nanostructures in Athabasca bitumen and Maya crude oil. Energy & Fuels, 21(5), 2795–2804.

Zachariah, A., & De Klerk, A. (2017). Partial upgrading of bitumen: Impact of solvent deasphalting and visbreaking sequence. Energy & Fuels, 31(9), 9374–9380.

Appendicess

Appendix A. Supporting information for Chapter 3

Table A1. *n*-Pentane insoluble content (wt%) of liquid products at different reaction conditions[a]

Description	Reaction conditions		*n*-pentane insoluble (wt%)	
	Temperature (°C)	time (min)[b]	x	*u*
Control	417	0	10.4	1.9
	425	0	10.9	1.0
	438	0	24.4	0.8
Regular reactions	417	30	14.6	0.9
	425	20	20.1	2.3
	438	10	22.7	1.4

[a] Average (x) and standard uncertainty (*u*) of analyses in triplicate;

[b] Reactions time exclude any heat-up and cool-down periods

Table A2. Mineral matter free basis MCR of visbroken products and their corresponding *n*-pentane insoluble[a]

Description	Reaction conditions		Mineral matter free basis MCR of visbroken products		Mineral matter free basis MCR of *n*-pentane insolubles	
	Temperature (°C)	time (min)[b]	x	*u*	x	*u*
Control	417	0	8.5	1.4	42.4	4.3
	425	0	10.6	4.2	42.1	1.5
	438	0	20.9	5.2	58.1	1.3
Regular reactions	417	30	15.5	6.0	52.8	3.9
	425	20	26.0	0.7	54.6	1.0
	438	10	27.1	5.5	60.8	1.6

[a] Average (x) and standard uncertainty (*u*) of analyses in triplicate;

[b] Reactions time exclude any heat-up and cool-down periods

Table A3. Refractive index of visbroken products[a]

Description	Reaction conditions		Refractive index					
			20 °C		40 °C		60 °C	
	Temperature (°C)	time (min)[b]	x	u	x	u	x	u
Control	417	0	1.5933	0.0005	1.5857	0.0006	1.5782	0.0007
	425	0	1.5928	0.0006	1.5848	0.0006	1.5771	0.0005
	438	0	1.6028	0.0019	1.5938	0.0017	1.5807	0.0026
Regular reactions	417	30	1.5987	0.0044	1.5904	0.0042	1.5815	0.0032
	425	20	1.6056	0.0026	1.5969	0.0027	1.5877	0.0024
	438	10	1.6031	0.0079	1.6000	0.0124	1.5922	0.0141

[a] Average (x) and standard uncertainty (*u*) of analyses in triplicate;

[b] Reactions time exclude any heat-up and cool-down periods

Table A4. Electron spin resonance (ESR) analysis of liquid products and their *n*-pentane insoluble[a]

Description	Reaction conditions		Free radical content (× 10^{18} spins/g) of visbroken products		Free radical content (× 10^{18} spins/g) of *n*-pentane insoluble	
	Temperature (°C)	time (min)[b]	x	*u*	x	*u*
Control	417	0	1.3	0.1	3.4	0.3
	425	0	1.2	0.0	3.8	0.3
	438	0	2.3	0.5	8.2	2.0
Regular reactions	417	30	1.8	0.5	5.1	1.1
	425	20	1.8	0.0	6.1	0.2
	438	10	2.5	0.6	6.8	0.4

[a] Average (x) and standard uncertainty (*u*) of analyses in triplicate;

[b] Reactions time exclude any heat-up and cool-down periods

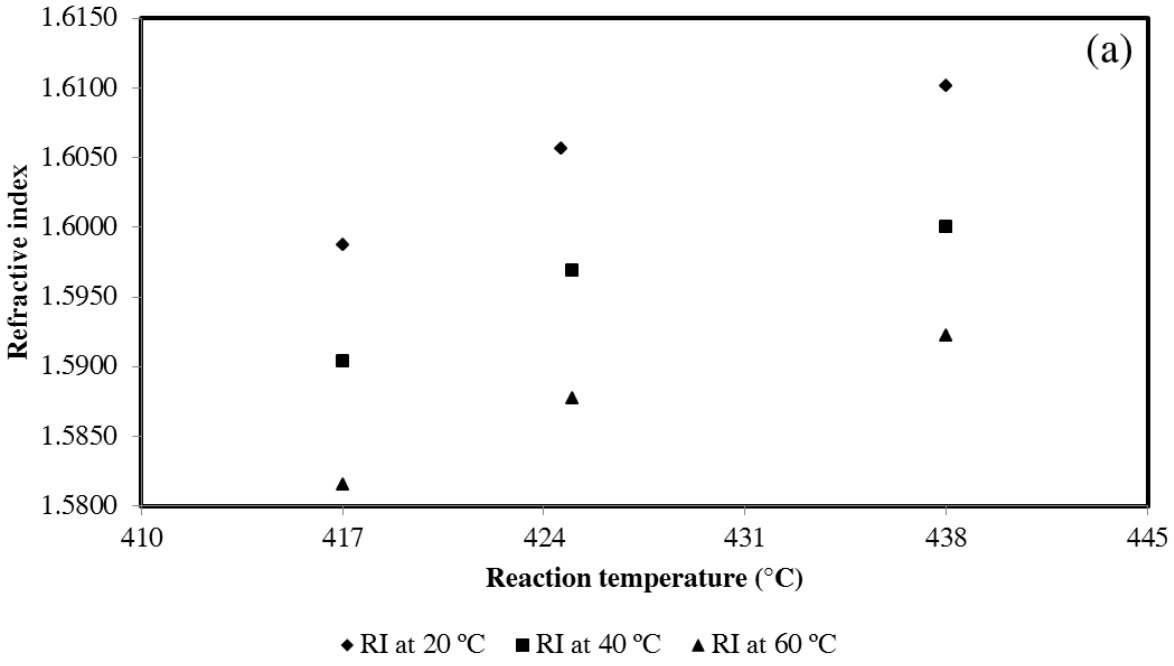

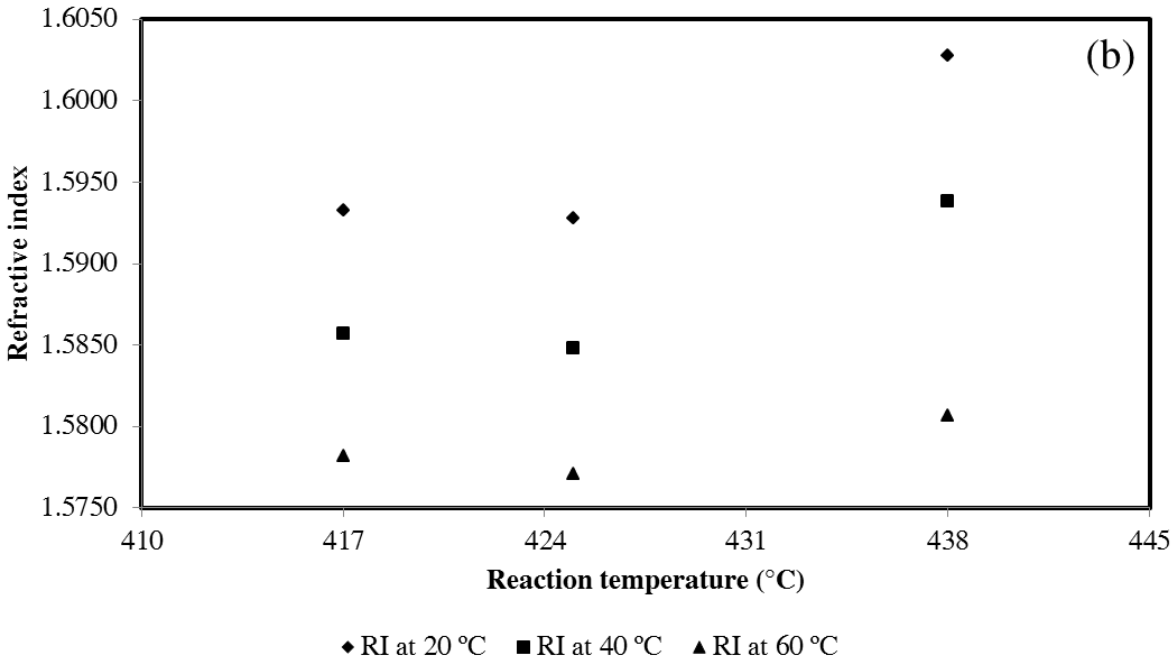

Figure A1. Refractive index of visbroken products from (a) regular reactions and (b) control

Appendix B. Supporting information for Chapter 5.

In Chapter 5, product A-α (visbroken product with 10 wt% of α-methylstyrene), product A-β (visbroken product with 10 wt% of dihydronaphthalene), and product A-γ (visbroken product with 10wt% of 9,10-dihydroanthracene) were quantitatively analyzed using a gas chromatograph with a flame ionization detector (GC-FID). During the analysis, weight of product, internal standard (biphenyl) and solvent (methanol) were recorded. Calculations were performed using gas chromatography. Sample calculation of the products A-α were:

Weight of α-methylstyrene = wight of products A-α×10 wt%

$$wt\%\ of\ sample = \frac{\text{weight of } \alpha - \text{methylstyrene}}{\text{weight of } \alpha - \text{methylstyrene} + \text{weight of internal standard} + \text{weight of solvent}}$$

$$wt\%\ of\ internal\ standard = \frac{\text{weight of internal standard}}{\text{weight of } \alpha - \text{methylstyrene} + \text{weight of internal standard} + \text{weight of solvent}}$$

RRF (Relative Response Factor)= $\frac{weight\ of sample/\ weight\ of\ internal\ standard}{Area\ of sample/Area\ of\ internal\ standard}$

$$Final\ concentration = \frac{Area\ of\ sample}{Area\ of\ internal\ standard} \times \frac{wt\%\ of\ internal\ standard}{RRF}$$

Sample converted = wt% of sample- final concentration

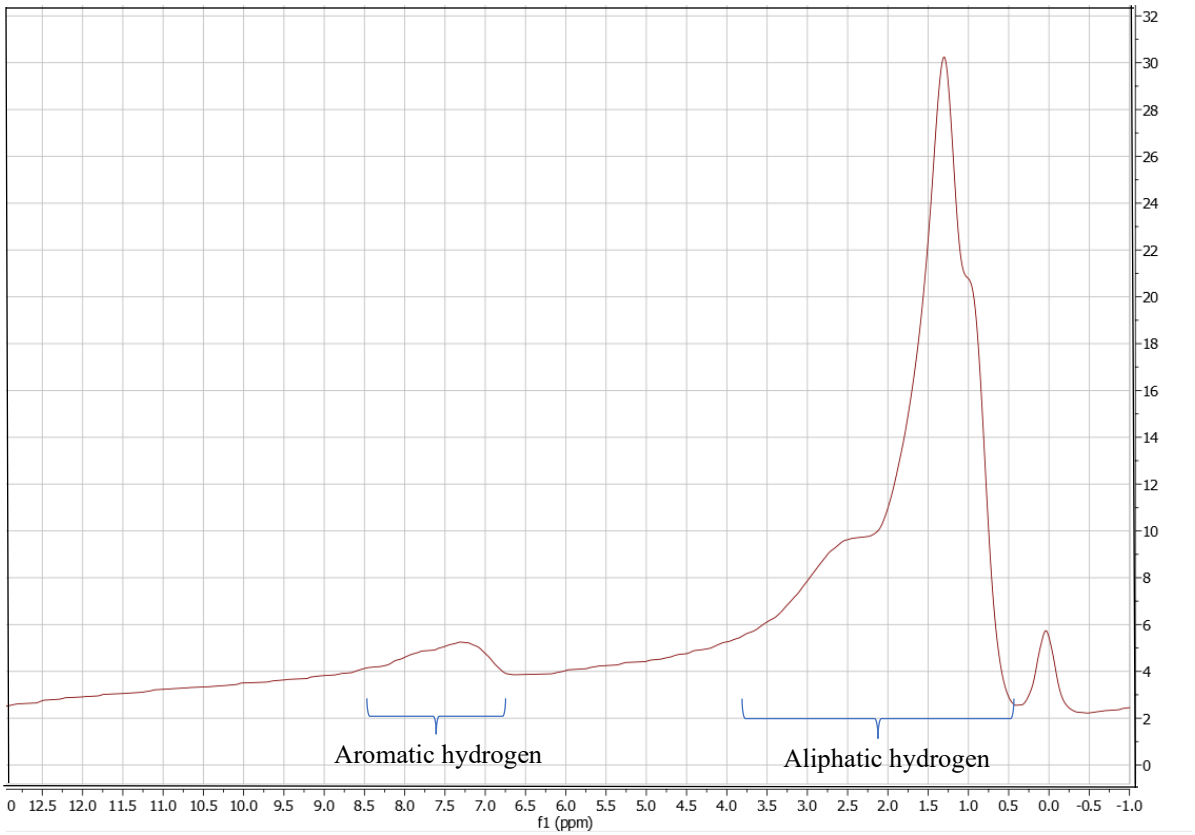

Figure B1. Sample proton NMR results for bitumen obtained from the Athabasca region.

Table B1. Density of visbroken product A at 20 °C, 40 °C and 60 °C measured at different storage time[a]

Measured Time	Density (kg/m^3) at 20 ºC		Density (kg/m^3) at 40 ºC		Density (kg/m^3) at 60 ºC	
	x	u	x	u	x	u
First measurement	986.6	0.0	974.0	0.0	959.3	0.0
After 2 weeks	991.5	0.1	977.9	0.0	963.0	0.1
After 4 weeks	993.5	0.1	979.9	0.0	966.2	0.0
After 8 weeks	997.1	0.0	983.7	0.1	970.1	0.0
After 12 weeks	998.9	0.0	985.7	0.0	972.6	0.0

[a] Average (x) and standard uncertainty (*u*) of analyses in triplicate;

Table B2. At 20 ºC with shear rate equal to 10 1/s and 5 1/s, viscosity of product A measured at different storage time[a]

Measured Time	**Viscosity (Pas) at shear rate = 10 s^{-1}**		**Viscosity (Pas) at shear rate = 5 s^{-1}**	
	x	**u**	**x**	**u**
First measurement	0.1	0.02	b	b
After 2 weeks	0.9	0.01	0.9	0.01
After 4 weeks	1.0	0.02	1.0	0.01
After 8 weeks	1.5	0.01	1.3	0.03
After 12 weeks	2.2	0.01	2.1	0.02

[a] Average (x) and standard uncertainty (u) of analyses in 10 measured points.

[b]Inaccurate viscosity results measured at 1 1/s shear rate.

Table B3. Asphaltenes content of product A measured at different storage time[a]

Measured Time	Asphaltenes content (wt%)	
	x	u
First Measurement	18.3	0.59
Affter 2 weeks	19.8	0.12
After 4 weeks	20.3	1.01
After 8 weeks	21.0	0.09
After 12 weeks	22.0	0.55

[a] Average (x) and standard uncertainty (u) of analyses in duplicate

Table B4. Electron spin resonance (ESR) analysis of liquid products and their *n*-pentane insoluble at different storage time[a]

Time	Free radical content of liquid product ($\times 10^{18}$ spins/g of liquid product A)		Free radical content of Asphaltenes ($\times 10^{18}$ spins/g of Asphaltenes)	
	x	u	x	u
First measurement	1.9	0.3	7.3	0.3
After 2 weeks	2.2	0.1	6.4	0.1
After 4 weeks	2.1	0.4	6.9	2.4
After 8 weeks	1.6	0.02	4.9	0.3
After 12 weeks	1.7	0.07	7.5	0.01

[a] Average (x) and standard uncertainty (*u*) of analyses in triplicate

Table B5. Refractive index (RI) of product measured at different storage time at 20, 40 and 60 ^{o}C[a]

Measured Time	RI at 20		RI at 40		RI at 60	
	x	u	x	u	x	u
First Measurement	1.5749	0.0013	1.5674	0.0016	1.5601	0.0018
After 2 weeks	1.5755	0.0000	1.5675	0.0001	1.5597	0.0001
After 4 weeks	1.5760	0.0003	1.5675	0.0001	1.5606	0.0002
After 8 weeks	1.5774	0.0000	1.5689	0.0000	1.5610	0.0000
After 12 weeks	1.5797	0.0000	1.5712	0.0001	1.5624	0.0003

[a] Average (x) and standard uncertainty (*u*) of analyses in triplicate

Table B6. H:C, N:C and S:C ratio of asphaltenes from product A at different storage time[a]

Measured Time	H:C		N:C		S:C	
	x	u	x	u	x	u
First Measurement	0.921	0.002	0.017	0.000	0.033	0.001
After 2 weeks	0.949	0.002	0.016	0.000	0.034	0.001
After 4 weeks	0.948	0.003	0.016	0.000	0.033	0.000
After 8 weeks	0.953	0.004	0.015	0.000	0.032	0.001
After 12 weeks	0.967	0.002	0.016	0.000	0.033	0.000

[a] Average (x) and standard uncertainty (*u*) of analyses in triplicate

Table B7. Average and standard deviation of MCR of product measured at different storage time[a]

Measured time	MCR (wt%)		Mineral Matter (wt%)	
	x	u	x	u
First Measurement	13	0.4	2.1	0.3
After 2 weeks	17	1.6	4.3	2.4
After 4 weeks	18	1.5	3.3	1.4
After 8 weeks	17	1.1	5.6	4.7
After 12 weeks	18	3.1	7.2	0.9

[a] Average (x) and standard uncertainty (*u*) of analyses in duplicate

Table B8. [1]H-NMR results of product A at different storage time[a]

Measured time	liquid product			
	aromatic		saturate	
	x	u	x	u
First measurement	14.3	b	85.7	b
After 2 week	13.3	0.4	86.7	0.4
After 4 week	14.8	0.0	85.2	0.0
After 8 week	12.1	1.3	87.9	1.3
After 12 week	7.6	0.1	92.4	0.1

[a] Average (x) and standard uncertainty (*u*) of analyses in duplicate

[b]Only one run was performed once

Table B9. [1]H-NMR results of asphaltenes from product A at different storage time[a]

Measured time	Asphaltenes			
	aromatic		Saturate	
	x	u	x	u
First measurement	23.0	b	77.0	b
After 2 week	19.6	1.4	80.4	1.4
After 4 week	19.1	1.1	80.9	1.1
After 8 week	21.5	1.3	78.5	1.3
After 12 week	18.8	1.7	81.2	1.7

[a] Average (x) and standard uncertainty (*u*) of analyses in duplicate

[b]Only one run was performed once